Edinburgh Wave Power Project

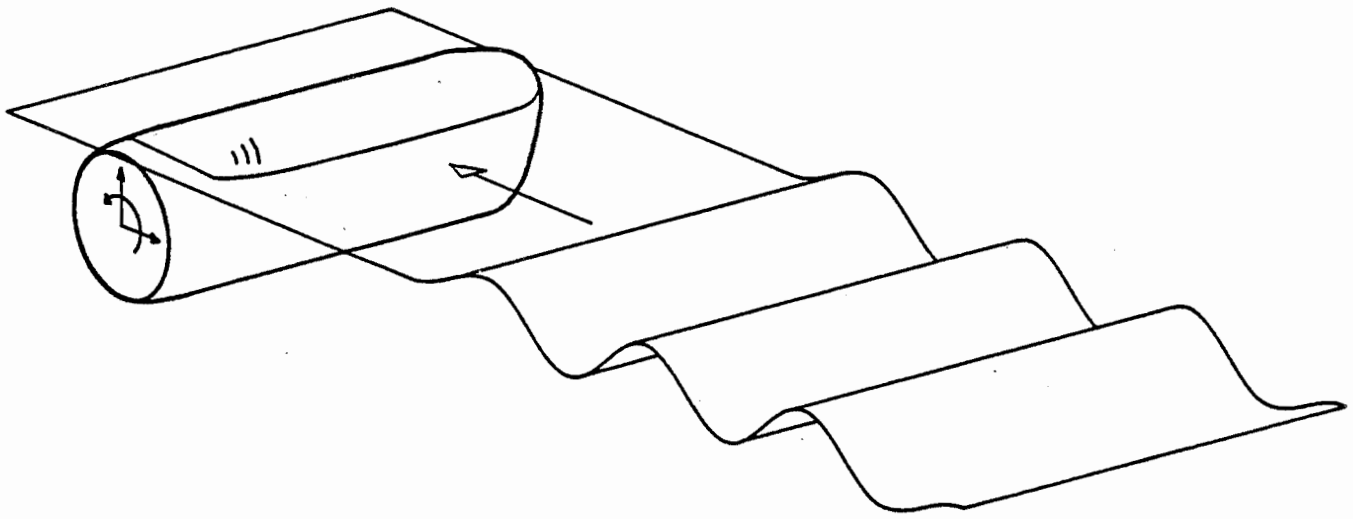

Solo Duck Linear Analysis

1987

SOLO DUCK LINEAR ANALYSIS

A report to the Wave Energy Steering Committee

covering work supported by the United Kingdom Department of Energy

EDINBURGH UNIVERSITY WAVE POWER PROJECT

University of Edinburgh

Mayfield Road

Edinburgh EH9 3JL

031 667 1081 x 3276

Abstract

The motion of a single duck wave energy converter in the presence of waves is described by a linear matrix equation, formulated in the frequency domain. An equation for the extracted power in spectra is derived for any linear controller. The parameters in the equation of motion, namely, the radiation impedance and wave force coefficients, are found from a model by experiment in a wave tank. Predictions for the absorbed power are compared against further measurements made in the tank when the duck's motion is governed by a simple linear controller, implemented on a digital computer.

CONTENTS

LIST OF FIGURES

Introduction

The duck is a partially submerged rigid body which extracts power from water waves through its motion. The design considered here is intended to be a single unit which would operate in ocean waves and generate electricity. We investigated the absorption characteristics of a particular solo duck, with the ultimate aim of optimising its design from productivity and cost constraints.

There are two areas to be explored when designing a device of this type, the shape and the motion control for maximum power.

We took two approaches to the appraisal of shape. In one, a scale model of the duck was tested in a 3D wave tank with its motion governed by a particular linear controller. In the other, a minimal set of equations was sought which would describe the motion given some assumptions about the physics.

Model testing under simulated operating conditions has the advantage of differing from the final device only in scale. As a result some non-linearities are built in correctly, although others do not scale properly. The method is one of trial and error with a great many parameters, but with the possibility of discovering some empirical rules. One drawback of this approach is that device shape and motion control remain completely intertwined.

The most fundamental equations would describe the motion of the water in the presence of a general boundary. The duck moves as a result of the pressure distribution on its surface due to the water, and since it is a rigid body this distribution can be integrated over the surface to yield forces and torques.

Newman (1976) starts from hydrodynamic theory, forms surface integrals and obtain impedances which describe the net effect of the pressure distribution on the rigid body due to its motion and the waves. This approach leads to two important theoretical results which are used here, the symmetry of the impedances and the upper limit on capture width as the device width tends to zero. It also provides a way to calculate the

impedances from the device shape, analytically if the integrals are of a simple form or else by finite element techniques. In principle, an equation for the optimal duck shape could be derived using this route.

We follow the phenomenological approach described by Falnes (1980) and Evans (1979). Equations are written down and impedances defined without explicit reference to the hydrodynamics. The impedances are available through the measurement of a model in a wave tank.

The equations are formulated in the frequency domain and, inevitably, restricted to the linear case. Fourier analysis offers the possibility of identifying non-linearities through the harmonics when the effects are small. Where appropriate, equations are written in matrix form with the intention of increasing ease of manipulation, readability and generalisation.

Linear equations of motion and control are defined, then combined to give the velocities and forces acting on the duck as a function of the control parameters. Equations for the extracted power and efficiency are derived and control parameters which maximise them are given.

Experiments are carried out to determine the parameters in the equation of motion for a particular duck shape. After further processing the parameters are used to predict efficiencies under a limited set of wave and control conditions. The predictions are then tested against measurements made under those conditions.

The effect of control parameters on efficiency is discussed further by evaluation of the efficiency function. The mathematical model allows linear controllers to be tested without being implemented. Finally, some remarks are made about full scale applications and possible reasons for departure from linearity noted.

Mathematical model

The duck's motion is assumed to be linear so that solutions for the motion can be superposed. All quantities are defined in the frequency domain. Mechanical impedance is strictly the ratio of force to velocity, but is used as general term covering the ratio of force to wave amplitude as well.

Definition of the variables

a) The state of the duck motion is represented by a force and a velocity vector.

b) The incident waves are represented by a distribution of amplitudes in frequency and angle.

Definition of the impedances

c) The interaction of the duck motion and the water is represented by a radiation impedance matrix.

d) The diffraction of incident waves is described by a force coefficient vector with wave angle dependence.

e) The restraining forces are made functions of the motion by a defined control matrix.

Derived quantities

f) The extracted power depends on the three impedances listed above.

g) A maximum for the absorbed power occurs when the control matrix is the complex conjugate of the radiation impedance.

Definition of efficiency

h) Efficiency is the absorbed power divided by the power incident per metre and the duck width.

Experimental model

A physical model was used to determine the impedances and to measure efficiencies when controlled by a computer.

Physical model

i) The duck is represented by a scale model in a wave tank with three degrees of freedom: pitch, heave and surge.

j) Measurements can be made of the torque and 2 forces acting on the duck, its velocities and the wave heights in the tank.

k) Each of the duck motions can be driven by a motor.

Measurement of efficiency

l) The duck's motion is controlled by a digital computer which calculates the force drive requirements from measurements of velocity.

m) Absorbed power is calculated by integrating the instantaneous power over a whole number of cycles.

Main conclusions

Measurement of the impedances

1) The measured radiation impedance matrix, shown in figure 3.1, has a high degree of symmetry about the leading diagonal, in agreement with theory, giving confidence in the experimental method.

2) The force coefficient vector can be determined from any linear motion in incident waves.

3) Reflections from the wave tank walls cause most of the experimental noise.

Comparisons between predicted and measured efficiency

4) Using the measured impedances the efficiency can be predicted within the limits of tank repeatability for regular waves and small mixed seas.

5) The maximum efficiency for a controller with four terms can be predicted accurately in regular waves.

Predictions from the impedances for small waves

6) In regular waves a capture width 1.6 times the duck width is achievable when the wavelength is about 15 duck diameters. For longer waves the capture width falls away from the small device limit.

7) In regular waves the duck with a four term controller can almost reach the maximum power absorption obtainable when the controller is the complex conjugate of the radiation impedance.

8) In mixed spectra a controller with four terms achieves about half the efficiency of the complex conjugate controller if it does not have the correct frequency dependence.

General experimental description

The set of experiments described in this report were carried out in the wide tank of the Edinburgh University Wave Power Project. For those not familar with this facility some background information about the tank, the apparatus and the experimental methodology is given.

In the wide tank we can generate regular waves with chosen height, frequency and angle or a mixed spectrum comprising many such components. Under computer control the outputs from an instrumented model can be sampled as the wave conditions are varied. Alternatively, a model may be driven directly in the absence of waves. Experiments consist of many automated test runs, usually with systematic changes between each test, but all with the same physical arrangement.

The duck was originally intended to extract power from the incident waves through the induced pitching motion. After years of testing in a narrow wave tank the shape evolved from a plane flap into an asymmetric cam with rounded corners, which moved in heave and surge as well as pitch. The duck model used for this set of experiments had the same cross-section as the last in that generation.

The duck model was supported and its motion controlled through a rig which was suspended from bridges above the water surface. The rig was originally designed to straddle the parallel walls of the narrow wave tank in which the duck model was almost as wide as the tank. As a result only motion in pitch, heave and surge was possible, although this is not thought to be an important restriction.

The forces and velocities measured at the duck axis were available for sampling by the overseeing computer. In addition the velocities were used by a BBC microcomputer to calculate force requirements for the rig's drive motors. The particular control functions of spring and damping implemented on the BBC controller should be thought of as being a subset of the complete linear controller described in the text.

In most experiments the duck was driven sinusoidally either directly or by the waves. After a minute's settling time the motion was steady and sampling was carried out for a whole number of cycles. Other experiments were conducted in pseudo-random spectra, again ensuring that the sampling time equalled the repeat time of the wave sequence.

The long-term repeatability of wave amplitude was around 4% for the small waves used. Short term repeatability was better at about 2%. When appropriate, we relied on good repeatability over a few hours by replacing the duck model with a wavegauge and rerunning the wave conditions. The tank transfer function was used to set up the waves, but measurement at the model position also allowed the amplitude and phase of the wave to be determined more accurately.

Two types of wavegauge were used. The heaving float gauge measures the movement of a float on the water surface. It is best suited to the measurement of parallel waves, but was used as the standard throughout with an angle correction where necessary. The wire wavegauge measures the conductance between two half immersed rods, providing wave measurement in a much smaller area.

1) Mathematical description of the system

The interaction of the duck motion and the incident waves is described by a linear equation. A control equation of similar form is written down and expressions derived for the extracted power and efficiency.

Definition of the variables

In three dimensions a rigid body can move with six degrees of freedom, which comprise a rotational and a translational mode for each dimension. However, the duck model is constrained to move in a vertical plane with just three of these modes, known as pitch, heave and surge. The state of the duck may be represented by six functions of time **t**, chosen to be three forces acting on the axis and three velocities measured at the axis. The incoming wave is a function of position $\underline{r}$ as well as time.

$\tau(t)$	torque acting in pitch	$\dot{\theta}(t)$	angular velocity in pitch
$F_z(t)$	force acting in heave	$\dot{z}(t)$	velocity in heave
$F_x(t)$	force acting in surge	$\dot{x}(t)$	velocity in surge

$\Phi(t,\underline{r})$ incoming wave field

The same symbols are used to represent the variable and its Fourier Transform. When the functional dependence is not explicit the Fourier Transform is to be assumed.

$$f(\omega) = \frac{2}{T}\int_0^T f(t)e^{-i\omega t}dt \qquad (1.1)$$

$$f(t) = \frac{1}{2}\sum_{n=-\infty}^{\infty} f(\omega)e^{i\omega t} \qquad (1.2)$$

Where T is the sampling period and is always a whole number of cycles

ω is the angular frequency and $\omega_n = 2\pi n/T$

Note that $f(t)$ is real and therefore $f(\omega) = f^*(-\omega)$

Since the equations for each degree of freedom take on a similar form it is convenient to define two vectors :

$$\underline{F} = \begin{bmatrix} \tau \\ F_z \\ F_x \end{bmatrix} \qquad \underline{u} = \begin{bmatrix} \dot{\theta} \\ \dot{z} \\ \dot{x} \end{bmatrix} \qquad (1.3)$$

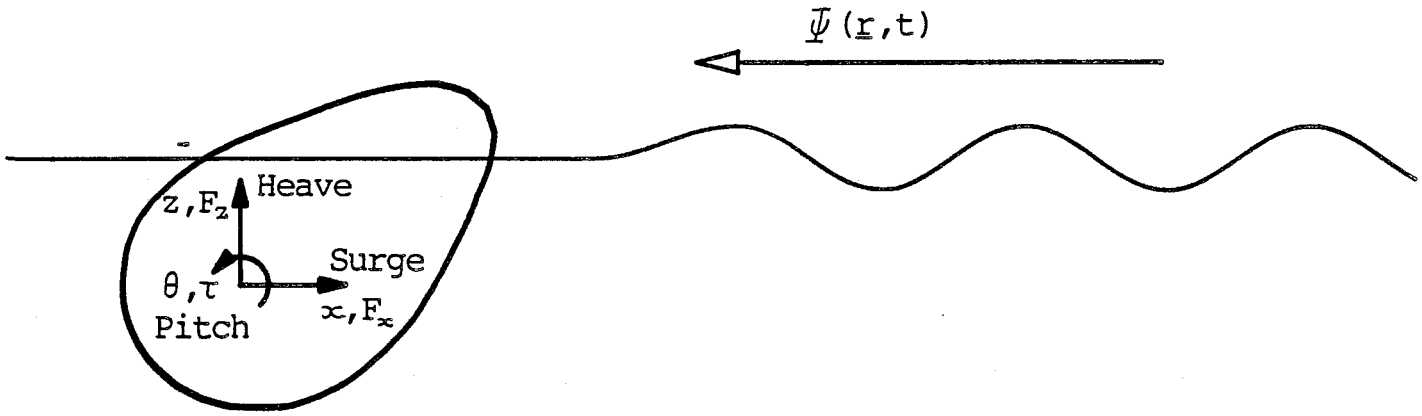

Displacements and forces

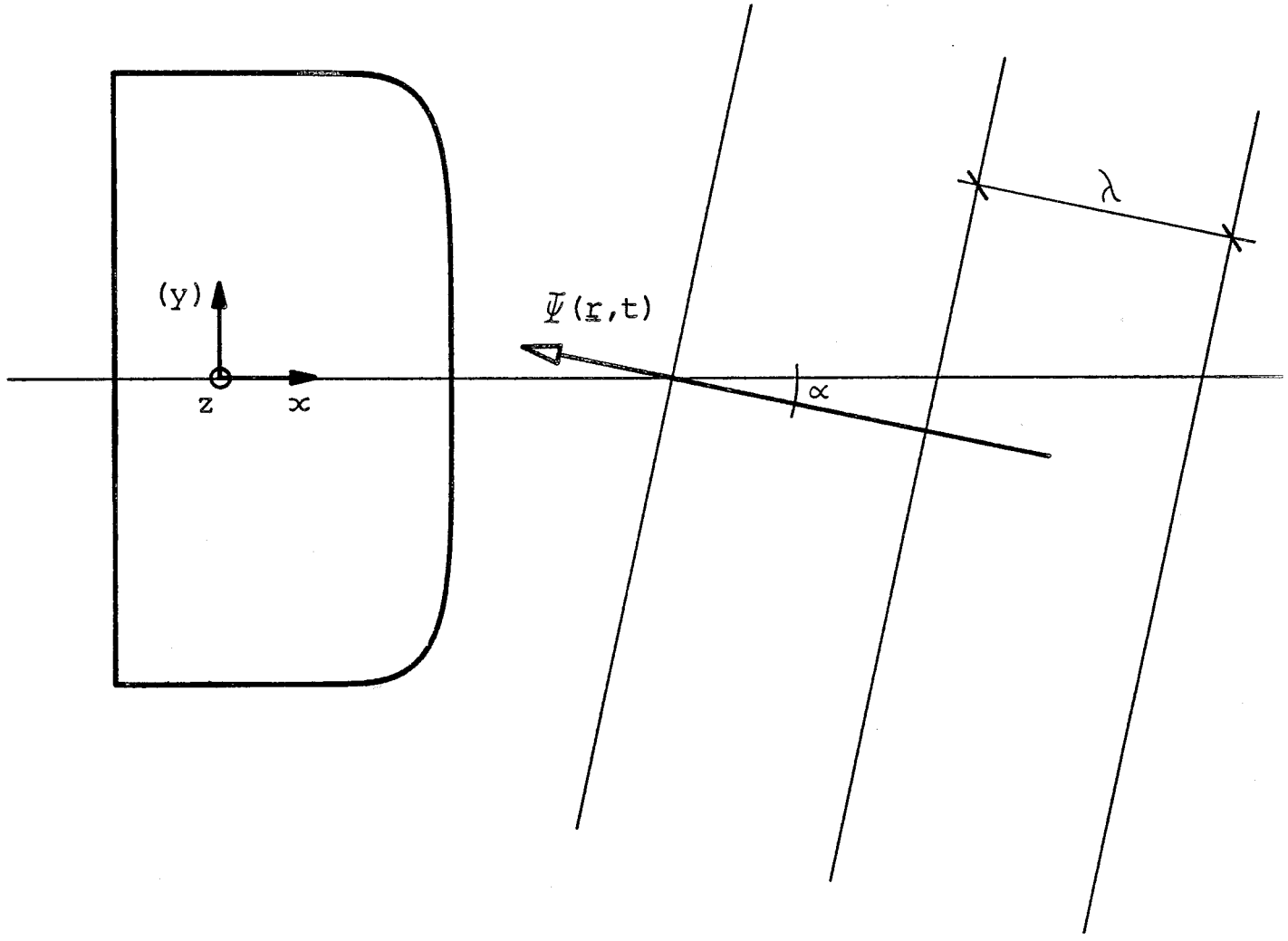

Figure 1.1 Definition of the variables

An individual wave front $\psi(t,x,y)$ is represented by

$$\psi(t,x,y) = \mathrm{Re}\ \{\ a\ e^{ikx\cos\alpha\ +\ iky\sin\alpha\ +\ i\omega t}\ \} \qquad (1.4)$$

Where a is the complex amplitude $a = Ae^{i\phi}$

ω is the angular frequency $\omega = 2\pi\nu$

α is the angle of incidence

k is the wave number $k(\omega) = 2\pi/\lambda$

Equation of motion

The linear relationship of the variables can be expressed in an equation of motion. Following Evans (1979) the external forces are equated to the hydrodynamic forces which are separated into two parts, corresponding to radiated and incident waves.

$$\underline{F}(t) = \underline{F}_R(t) + \underline{F}_W(t) \qquad \text{or} \qquad \underline{F}(\omega) = \underline{F}_R(\omega) + \underline{F}_W(\omega) \qquad (1.5)$$

Where $\underline{F}_R$ are the forces due to the motion of the duck in the water and are linearly dependent on $\underline{u}$ only.

$\underline{F}_W$ are the forces due to the incident wave and are linearly dependent on a only.

Hence the equation of motion in the presence of waves can be written as

$$\underline{F}(\omega) = \underline{\underline{Z}}(\omega).\underline{u}(\omega) + \underline{W}(\omega,\alpha)\ a(\omega) \qquad (1.6)$$

Where $\underline{\underline{Z}}$ is the complex radiation impedance matrix

$\underline{W}$ is the complex force coefficient vector

The equation of motion gives the duck velocities resulting from the external forces and the wave forces. The matrix multiplication is necessary because the velocity in each mode depends on all the forces acting. The incident wave amplitude might be responsible for the exciting term with the external forces functions of the motion. Alternatively, the external forces could be generated in the absence of waves. The equation covers all linear possibilities and is written most simply as

$$\boxed{\underline{F} = \underline{\underline{Z}}.\underline{u} + \underline{W}\ a} \qquad (1.7)$$

$\underline{\underline{Z}}$ is a frequency dependent 3x3 complex matrix whose terms give the magnitude and phase of the force acting in one direction due to unit velocity in another. It is dimensionally inhomogeneous because of the definitions of $\underline{F}$ and $\underline{u}$.

$$\underline{\underline{Z}}(\omega) = \begin{bmatrix} Z_{00} & Z_{01} & Z_{02} \\ Z_{10} & Z_{11} & Z_{12} \\ Z_{20} & Z_{21} & Z_{22} \end{bmatrix} = \begin{bmatrix} \frac{\text{pitch torque}}{\text{pitch velocity}} & \frac{\text{pitch torque}}{\text{heave velocity}} & \frac{\text{pitch torque}}{\text{surge velocity}} \\ \frac{\text{heave force}}{\text{pitch velocity}} & \frac{\text{heave force}}{\text{heave velocity}} & \frac{\text{heave force}}{\text{surge velocity}} \\ \frac{\text{surge force}}{\text{pitch velocity}} & \frac{\text{surge force}}{\text{heave velocity}} & \frac{\text{surge force}}{\text{surge velocity}} \end{bmatrix}$$

The real part of the radiation impedance matrix is often known as the 'added damping' because energy is radiated from the duck when there is a component of force in phase with the velocity. The imaginary part is due to the effects of hydrostatic spring, duck inertia and the 'added mass' of the water around the duck.

Making use of the equivalence $\frac{d}{dt} = i\omega$ the matrix can be split up into these four parts

$$\underline{\underline{Z}}(\omega) = \underline{\underline{D}}_A(\omega) + i\omega\underline{\underline{M}}_A(\omega) + i\omega\underline{\underline{\mu}} + \frac{1}{i\omega}\underline{\underline{\sigma}} \qquad (1.8)$$

Where $\underline{\underline{D}}_A$ is the real, frequency dependent added damping matrix

$\underline{\underline{M}}_A$ is the real, frequency dependent added mass matrix

$\underline{\underline{\mu}}$ is the duck inertia matrix

$\underline{\underline{\sigma}}$ is the hydrostatic spring matrix

Newman (1976) shows that the radiation impedance matrix is symmetric about the leading diagonal.

$\underline{W}$ gives the forces required to hold the duck still when a wave of unit amplitude is incident. The force phase is given relative to the phase of the wave at the origin.

$$\underline{W}(\omega,\alpha) = \begin{bmatrix} W_0 \\ W_1 \\ W_2 \end{bmatrix} = \begin{bmatrix} \frac{\text{pitch torque}}{\text{wave amplitude}} \\ \frac{\text{heave force}}{\text{wave amplitude}} \\ \frac{\text{surge force}}{\text{wave amplitude}} \end{bmatrix}$$

Control equation

In order to extract power from the system the motion of the duck must be controlled. This could be achieved in any manner, but here the forces $\underline{F}$ are made linear functions of the velocities $\underline{u}$. In matrix form

$$\boxed{\underline{F} = -\underline{\underline{A}}.\underline{u}} \qquad (1.9)$$

$\mathbf{A}(\omega)$ is a frequency dependent 3x3 complex matrix, the control matrix. Its terms may represent simple springs and dampers or other linear filter functions. For example

A constant damping is to be applied in pitch	$\tau = -d\dot{\theta}$
A spring force is to be applied in heave	$F_z = -sz = -s\dot{z}/i\omega$
An inertia term is to be applied from surge to pitch	$\tau = -m\ddot{x} = -i\omega m\dot{x}$
A general filter function is to be applied to surge	$F_x = -g(\omega)\dot{x}$

Giving

$$\underline{\underline{A}} = \begin{bmatrix} d & 0 & i\omega m \\ 0 & \frac{s}{i\omega} & 0 \\ 0 & 0 & g(\omega) \end{bmatrix}$$

The motion of the duck is now dependent on the parameters of $\underline{\underline{A}}$. Combining (1.7) and (1.9)

$$-\underline{\underline{A}}.\underline{u} = \underline{\underline{Z}}.\underline{u} + \underline{W}\, a$$

$$\rightarrow \quad \boxed{\underline{u} = -(\underline{\underline{A}}+\underline{\underline{Z}})^{-1}.\underline{W}\, a} \qquad (1.10)$$

Substituting for $\underline{u}$ in (1.9)

$$\boxed{\underline{F} = \underline{\underline{A}}.(\underline{\underline{A}}+\underline{\underline{Z}})^{-1}.\underline{W}\, a} \qquad (1.11)$$

Extraction of power

In the time domain the average power P passing through the duck axis is given by

$$P = \frac{1}{T}\int_0^T \tau(t)\dot{\theta}(t) + F_z(t)\dot{z}(t) + F_x(t)\dot{x}(t)\, dt$$

$$P = \frac{1}{T}\int_0^T \underline{F}(t).\underline{u}(t)\, dt \qquad (1.12)$$

Note that the definitions of $\underline{F}$ and $\underline{u}$ lead to P being negative when power is extracted.

By taking the Fourier Transform of equation (1.12) it is shown in appendix B that in the frequency domain

$$P = \frac{1}{4} \sum_{n=1}^{\infty} \underline{F}(\omega_n).\underline{u}^*(\omega_n) + \underline{F}^*(\omega_n).\underline{u}(\omega_n) \tag{1.13}$$

Where $\omega_n = 2\pi n/T$

For a particular frequency $\omega = \omega_n$

$$P = \frac{1}{4} \left[\underline{F}.\underline{u}^* + \underline{F}^*.\underline{u}\right] \tag{1.14}$$

$$= \frac{1}{2} \mathrm{Re}\{\underline{F}.\underline{u}^*\} \tag{1.15}$$

or $$\boxed{P = \frac{1}{2} \left[\mathrm{Re}\{\underline{F}\}.\mathrm{Re}\{\underline{u}\} + \mathrm{Im}\{\underline{F}\}.\mathrm{Im}\{\underline{u}\}\right]} \tag{1.16}$$

This result may also be obtained by viewing each pair F_j , u_j as rotating vectors in the complex plane.

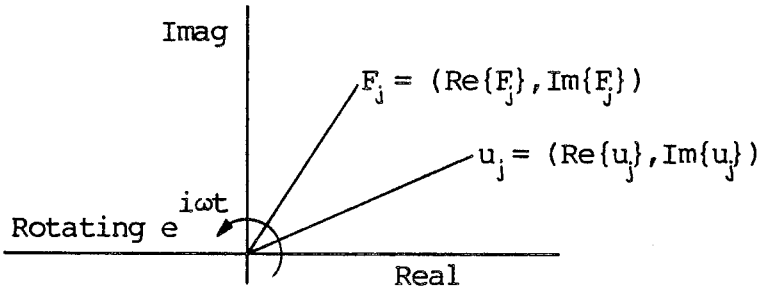

For each mode the amplitude of the extracted power is given by the scalar product of the rotating vectors. The factor of a half appears because of the time average and the total power is the sum of the three modes.

If the duck is driven in calm water it can be shown from (1.7) and (1.14) and the symmetry of $\underline{\underline{Z}}$ that

$$P = \frac{1}{2} \underline{u}^*.\mathrm{Re}\{\underline{\underline{Z}}\}.\underline{u} \tag{1.17}$$

Since power must be put in under these circumstances the equation has to be positive for all $\underline{u}$, placing the condition on $\underline{\underline{Z}}$ that it is positive definite. In other words, the duck cannot absorb energy from calm water.

Maximisation of the extracted power

Substitution from equations (1.10) and (1.11) into (1.15) gives P as a function of $\underline{\underline{A}}$

$$P = -\frac{1}{2} \mathrm{Re}\{(\underline{\underline{A}}.(\underline{\underline{A}}+\underline{\underline{Z}})^{-1}.\underline{W}).((\underline{\underline{A}}+\underline{\underline{Z}})^{-1}.\underline{W})^{*}\} \ |a|^{2} \qquad (1.18)$$

Differentiation of this equation is carried out in Appendix C, and it is found that a maximum for the extracted power, minimum for P, occurs when

$$\boxed{\underline{\underline{A}}(\omega) = \underline{\underline{Z}}^{*\tau}(\omega)} \qquad (1.19)$$

Where τ denotes the transpose

$\underline{\underline{Z}}$ is symmetric and by substitution the maximum power is

$$\boxed{P = -\frac{1}{8} \underline{W}^{*}.(\mathrm{Re}\{\underline{\underline{Z}}\})^{-1}.\underline{W} \ |a|^{2}} \qquad (1.20)$$

The control matrix given by equation (1.19) will be known as the 'complex conjugate controller'. An electrical analogy is extracting the most power from a battery by connecting a load whose resistance is equal to the internal resistance of the battery. Any reactance should be negated in the load so that the battery 'sees' only resistance, corresponding to the conjugation in equation (1.19).

Efficiency

Following on from earlier work efficiency is defined

$$\eta = \frac{\text{capture width}}{\text{duck width}} \qquad (1.21)$$

With capture width being defined as

$$C = \frac{\text{power absorbed}}{\text{power incident per metre}} \qquad (1.22)$$

Newman (1976), Evans (1976) and Budal (1977) show that the theoretical upper limit for the capture width of a device with two degrees of freedom as the width tends to zero is

$$C_{m} = \lambda/\pi \qquad (1.23)$$

Below some frequency the capture width of the 'point absorber' will be greater than the duck width, making its 'efficiency' greater than one.

Efficiency function

Equation (1.18) gives an expression for power in terms of the control matrix and other parameters. In spectra the total power can be found by superposition of the contributions from each frequency. Thus a function for efficiency in regular waves or pseudo-random spectra is obtained.

$$\eta = \frac{\text{Power extracted}}{\text{Width x Power incident per metre}} \qquad (1.24)$$

$$\eta = \frac{-\sum_{n=1}^{\infty} \mathrm{Re}\{(\underline{\underline{A}}(\omega_n).(\underline{\underline{A}}(\omega_n)+\underline{\underline{Z}}(\omega_n)).\underline{W}(\omega_n,\alpha_n))^{-1}.((\underline{\underline{A}}(\omega_n)+\underline{\underline{Z}}(\omega_n)).\underline{W}(\omega_n,\alpha_n))^{*}\}}{2 \times \text{width} \times \sum_{n=1} \frac{\rho g^2}{4\omega} \tanh(k(\omega_n)h)\left(1+\frac{2k(\omega_n)h}{\sinh(2k(\omega_n)h)}\right)} \qquad (1.25)$$

Where ω_n = angular frequency of the nth front = $2\pi n/T$

a_n = complex amplitude of the nth front

α_n = angle of the nth front

Summary

The equation of motion contains parameters known as the radiation impedance matrix and the force coefficient vector. Both have frequency dependence and the vector has a wave angle dependence too.

The linear control equation contains a frequency dependent control matrix.

Force and velocities can be expressed in terms of the parameters of motion and control.

Mean power is obtained from the component of force, or torque, in phase with velocity.

The extracted power in a mixed spectrum is found by superposition.

The efficiency function is the ratio of the power extracted and the power incident in the duck width.

The extracted power is maximised when the control matrix is the complex conjugate of the radiation impedance matrix.

2) Physical description of the system

Duck model description

A small model of the duck was made out of sealed expanded polystyrene with width 290mm and cross sectional diameter between 100mm and 180mm. Figure 2.1 contains a side view of the duck along with a list of its main physical attributes.

Part of the duck mass does not rotate in pitch and is supported by an external spring acting on the axis. The rotating mass is centred just below the centre of buoyancy and is nearly balanced by it.

Hydrostatic spring matrix

The first order hydrostatic spring matrix $\underline{\underline{c}}$ contains the linear coefficients in the Taylor series expansion of $\underline{F}$ as a function of $\underline{X}$

$$\sigma_{ij} = \frac{\delta F_i}{\delta X_j} \qquad \text{with} \qquad \underline{X} = (\theta, z, x)$$

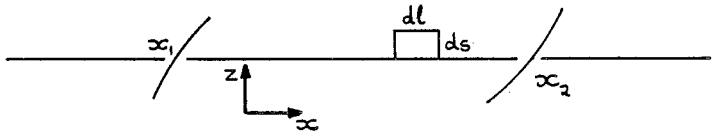

When a small element dl is raised a small distance ds above the waterlevel the restoring force is $w\rho g\ dl\ ds$.

Hence: $\frac{d\tau}{l} = w\rho g\ dl\ l\ d\theta$ $\qquad$ $\frac{d\tau}{l} = w\rho g\ dl\ dz$

$dF_z = w\rho g\ dl\ l\ d\theta$ $\qquad$ $dF_z = w\rho g\ dl\ dz$

By integrating over l between the limits x_1 and x_2, $\underline{\underline{c}}$ was found and evaluated using the measured values.

Inertia matrix

The inertia matrix $\underline{\underline{\mu}}$ contains cross terms between pitch and heave/surge because the centre of rotating mass is not at the origin.

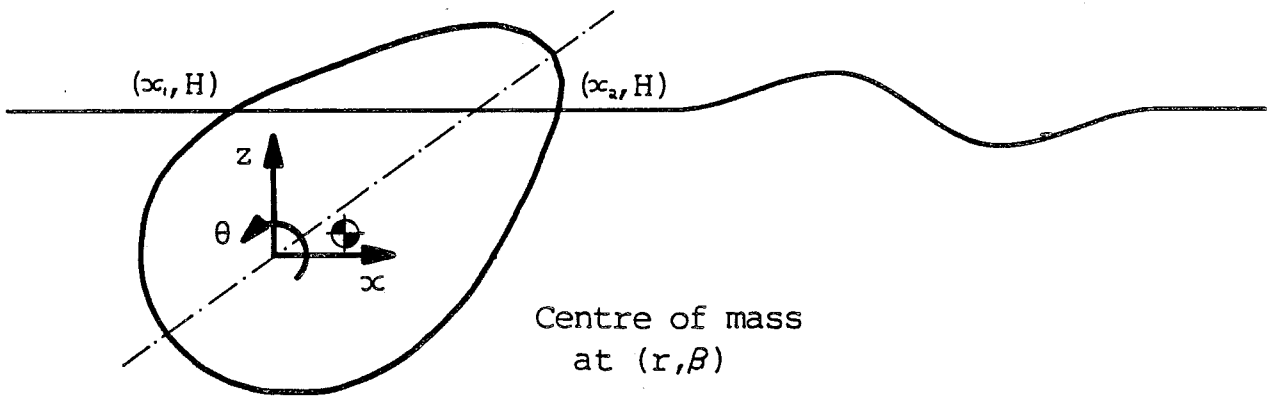

Figure 2.1 Duck model

Measured quantities

Total mass	M	= 4.31	kg
Rotating mass	m	= 2.63	kg
Mass moment	mr	= .0722	kg m
Beak angle	γ	= 36°	
Centre of mass angle	β	= 16°	
Waterline aft	x_1	= -.015	m
Waterline forward	x_2	= .107	m
Stern radius	s	= .05	m
Waterlevel	H	= .055	m
Width	w	= .29	m
Natural frequency	ν_o	= 1.68	Hz

Derived

$$I = \frac{(mr)g}{4\pi^2\nu_o^2} = .00636 \text{ kg m}^2$$

First order hydrostatic spring matrix

$$\underline{\underline{C}} = w\rho g \begin{bmatrix} (x_2^3 - x_1^3)/3 & (x_2^2 - x_1^2)/2 & 0 \\ (x_2^2 - x_1^2)/2 & (x_2 - x_1) & 0 \\ 0 & 0 & 0 \end{bmatrix} = \begin{bmatrix} 1.165 & 15.97 & 0 \\ 15.97 & 347.1 & 0 \\ 0 & 0 & 0 \end{bmatrix}$$

Inertia matrix

$$\underline{\underline{M}} = \begin{bmatrix} I & (mr)\cos\beta & -(mr)\sin\beta \\ (mr)\cos\beta & M & 0 \\ -(mr)\sin\beta & 0 & M \end{bmatrix} = \begin{bmatrix} .00636 & .0694 & -.0199 \\ .0694 & 4.31 & 0 \\ -.0199 & 0 & 4.31 \end{bmatrix}$$

The Pitch, Heave, Surge Rig

The duck model is supported and its motion measured and controlled through the rig shown schematically in figure 2.2. The rig and its associated electronics sub-divide into blocks which are described in outline, then in detail on the following pages.

The main linkage supporting the duck translates heave and surge motions into independent rotations inside the body of the rig. Deviations from linearity of about 1% are associated with 20mm movements of the duck axis in heave or surge because of this linkage. Duck pitching motion is measured directly at the axis.

Transducers measure the angular velocities of the three main rotation points, along with three associated torques. This set contains sufficient information to obtain the forces and velocities of the orthogonal pitch, heave, surge coordinate system.

The signals from the rig are conditioned then combined to form the orthogonal set. All heave and surge transducers are duplicated and these are first summed together. After combination the signals pass through 40Hz first-order low-pass filters, and calibration values are measured from this point in the circuitry.

The orthogonal set is available for sampling after first passing through low pass filters. The filters are second order with a 20Hz break point, and since sampling was carried out at 40Hz aliasing of frequencies is reduced.

The controller also has access to the signals. At present it is implemented on a BBC microcomputer along with some additional electronics. The BBC uses the velocity signals to calculate drive requirements for the rig's motors and updates them at 80Hz.

The drive requirements pass down to power amplifiers which provide the current to move the brushless torque motors. The current can be measured and because of the low losses this provides an excellent way of measuring the pitch torque.

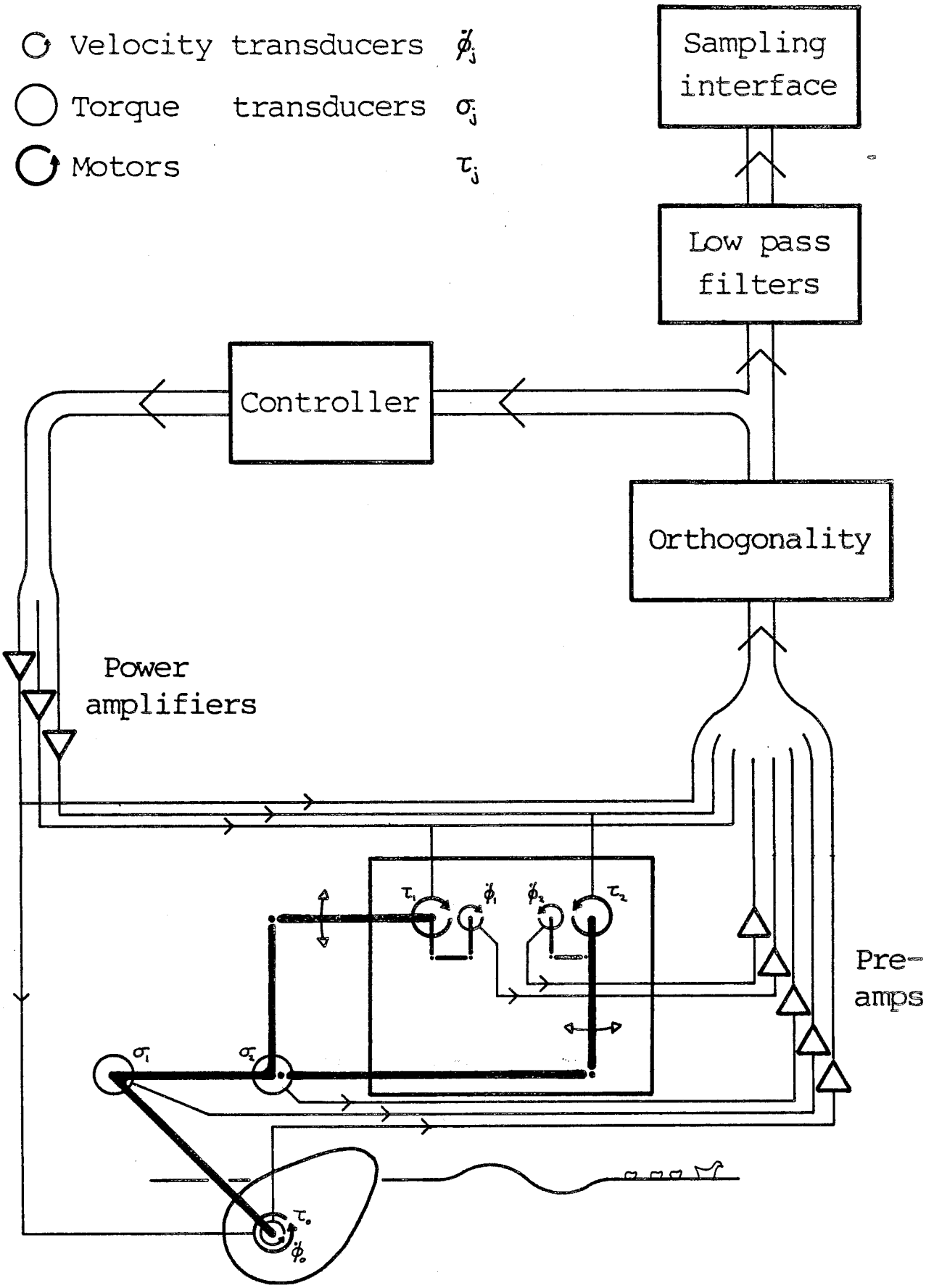

Figure 2.2 Pitch, heave, surge rig

Coordinate changes and orthogonality

There are three coordinate systems to consider. The duck's motion is described in the pitch, heave, surge system (PHS). However, the motors which drive it and the transducers which measure its motion each form slightly different systems. The means of converting between these two and PHS is discussed, assuming the linkage to be light and lossless.

Motor coordinate system

The most natural coordinates for the PHS rig are based on the three main rotation points. The torques are those delivered at the motors and the angular velocities those measured at the same points.

When changing coordinates to the PHS system most of the signals only have to be rescaled. One exception is surge force which has pitch torque subtracted because it passes through the surge motor. The second is pitch velocity which has a contribution from surge velocity taken away to account for the change of angle of its immediate support when surge motion occurs. These two correction terms complement each other.

$$\begin{aligned} \dot{\theta} &= \dot{\phi}_0 - \dot{\phi}_2 & \tau &= \tau_0 \\ \dot{z} &= a\,\dot{\phi}_1 & F_z &= \tau/a \\ \dot{x} &= a\,\dot{\phi}_2 & F_x &= (\tau_2 - \tau_0)/a \end{aligned} \qquad (2.1)$$

Where a is the distance of the duck axis from the rotation points (12")

Transducer coordinate system

In this system torques σ_1, σ_2 are measured in the linkage close to the duck's axis. It is the means of obtaining the heave and surge forces because the measurements are not affected by the inertia of the linkage or the friction in its joints.

$$\begin{aligned} \dot{\theta} &= \dot{\phi}_0 - \dot{\phi}_2 & \tau &= \tau_0 \\ \dot{z} &= a\,\dot{\phi}_1 & F_z &= (\sigma_1 - \sigma_2)/a \\ \dot{x} &= a\,\dot{\phi}_2 & F_x &= (\sigma_2 - \tau_0)/a \end{aligned} \qquad (2.2)$$

Calibration

The calibration procedure for the PHS rig falls into five main parts: checking the rig mechanics, checking the transducers, ensuring the six outputs are orthogonal, calibrating the outputs and calibrating the drive motors. The detailed procedure is described in separate documentation, but some important points are noted here.

If an output is a combination of more than one transducer fine adjustment of the balance is allowed by the inclusion of trimming potentiometers in the conditioning circuit. Heave and surge force come from the two torsional strain gauges and orthogonality is ensured by holding the axis, driving one mode and making the force reading on the other zero. By introducing a pitch torque in the absence of other forces the heave and surge force outputs can be made independent of pitch torque. Pitch velocity has a small contribution from surge velocity which can be set by moving the rig in surge while holding pitch still and adjusting the output to zero.

The torque and force outputs are calibrated with the aid of weights and and a weighing machine. Heave and surge velocities are measured while the axis is moved with a circular motion of known amplitude, and pitch velocity is measured by sinusoidal motion through a known angle. After also finding the frequency of motion the calibration factors may be calculated.

The calibration factors were measured before and after the set of experiments and are recorded here

	Calibration value	Units	Estimated error	Drift over two months
Pitch velocity	0.5735	rad s^{-1} / V	± 1 %	2.4 %
Heave velocity	0.02843	m s^{-1} / V	± 1 %	-0.6 %
Surge velocity	0.02888	m s^{-1} / V	± 1 %	-1.1 %
Pitch torque	0.08475	N m / V	± 1 %	0.4 %
Heave force	1.471	N / V	± 1 %	5.2 %
Surge force	1.440	N / V	± 1 %	1.9 %

Rig drive transfer function

The calibration values for the drive motors are measured in the absence of motion. However, in the case of heave and surge torsional springs and rotating inertias act in parallel with the motors. At the time of the set of experiments these quantities were measured to be as follows

Heave spring	S_z	120 ± 20	N m^{-1}
Surge spring	S_x	90 ± 10	N m^{-1}
Heave inertia	I_z	1.4 ± .1	kg m^2
Surge inertia	I_x	.5 ± .1	kg m^2

These mechanical controls should be added to any electronic control of the motors to obtain the overall control function.

$$\underline{\underline{A}} = \underline{\underline{A}}^{BBC} + \begin{bmatrix} 0 & 0 & 0 \\ 0 & \frac{S_z}{i\omega} + i\omega I_z & 0 \\ 0 & 0 & \frac{S_x}{i\omega} + i\omega I_x \end{bmatrix}$$

Where $\underline{\underline{A}}^{BBC}$ is the control matrix due to the BBC controller

Any pitch torque applied also produces some surge drive, as can be deduced from equations (2.1) in the description of the motor coordinate system. An attempt to remove this effect was made by introducing an appropriate cross term into the controller so that the surge motor would balance the pitch torque as well as fulfilling its own drive requirements.

In future it would be better to make the drive motors truly orthogonal by feedback of the measured forces. The equations (2.1) are inadequate because the linkage is assumed to be light with frictionless joints. Feedback, if implemented ideally, would remove all effects due to the linkage and it would not be necessary to know the exact values of the springs and inertias given above.

BBC controller transfer function

The digital controller takes the three velocities and calculates the motor drive requirements. At present the controller is implemented on a BBC computer and the control functions are limited to spring and damping for each mode.

The digital integration and small time delay inherent in the controller can be well accounted for in the pitch term since the motor and transducer are the same. However, in heave and surge these smalls effects are comparable with the friction in the joints of the linkage and other errors in the rig. In most cases power was not extracted from heave or surge and it was found that damping factors for these modes were best set to zero by adjustment until no power was absorbed from each.

In this report the BBC controller is the implementation of the four control functions

Pitch damping	D^{BBC}
Pitch spring	S^{BBC}
Heave spring	S^{BBC}
Surge spring	S^{BBC}

Corresponding to the control matrix

$$\underline{\underline{A}}^{BBC} = \begin{bmatrix} \left(D^{BBC} + \frac{S^{BBC}\delta t}{1 - \lambda e^{-i\omega\delta t}} \right) e^{-i\omega\delta t} & 0 & 0 \\ 0 & \frac{S^{BBC}}{i\omega} & 0 \\ 0 & 0 & \frac{S^{BBC}}{i\omega} \end{bmatrix}$$

Where $\lambda = 1 - 1/256$

$\delta t = 1/80$ s

Experimental environment

Figure 2.3 is a plan view of the wide tank. Waves are generated by a bank of 80 wavemakers and absorbed by expanded metal 'beaches' on two sides. The wavemakers themselves also absorb most reflected waves and a settling time of 50 seconds was found to be adequate for all the experiments conducted.

The beaches have nonlinear absorption characteristics. Reflection ratios are normally in the range 2% to 20% with the lowest values available at higher frequencies and larger amplitudes. The wavemaker absorption is good when they are also generating waves: reflection ratios of 10% to 20% are typical. However, because of stiction in the wavemaker motors, the very small waves generated when a model is driven in a still tank are not well absorbed.

Incident and reflected regular waves at the model position

The complex amplitudes of the incident and reflected waves at the model position were determined for the particular case of regular waves parallel to the wavemakers. Waves were generated with expected amplitude of 4mm over a range of frequencies and measurements made with a line of wire wave gauges. Assuming that only incident and reflected regular waves were present in the tank at each frequency, their amplitudes were calculated from a pair of readings. The experimental arrangement is sketched in figure 2.4 with the results in modulus form.

$\Psi(x,t) = \Psi_I(x,t) + \Psi_R(x,t)$

At position (0) measured amplitude $c = a + b$ a,b,c complex

At position (j) measured amplitude $c_j = ae^{ikd_j} + be^{-ikd_j}$ $j = 1,2,3$

$$\rightarrow \quad a = \frac{c_j - ce^{-ikd_j}}{2i \sin kd_j} \qquad b = \frac{ce^{ikd_j} - c_j}{2i \sin kd_j}$$

The separations must be chosen to avoid $kd_j = n\pi/2$, n integral
In this case the closest pair were chosen, such that $kd_j > \pi/4$

Freq range (Hz)	Separation (mm)	Pair
0.467 to 0.801	139 ± 1	0,1
0.820 to 1.211	309 ± 1	0,2
1.230 to 2.031	681 ± 1	0,3

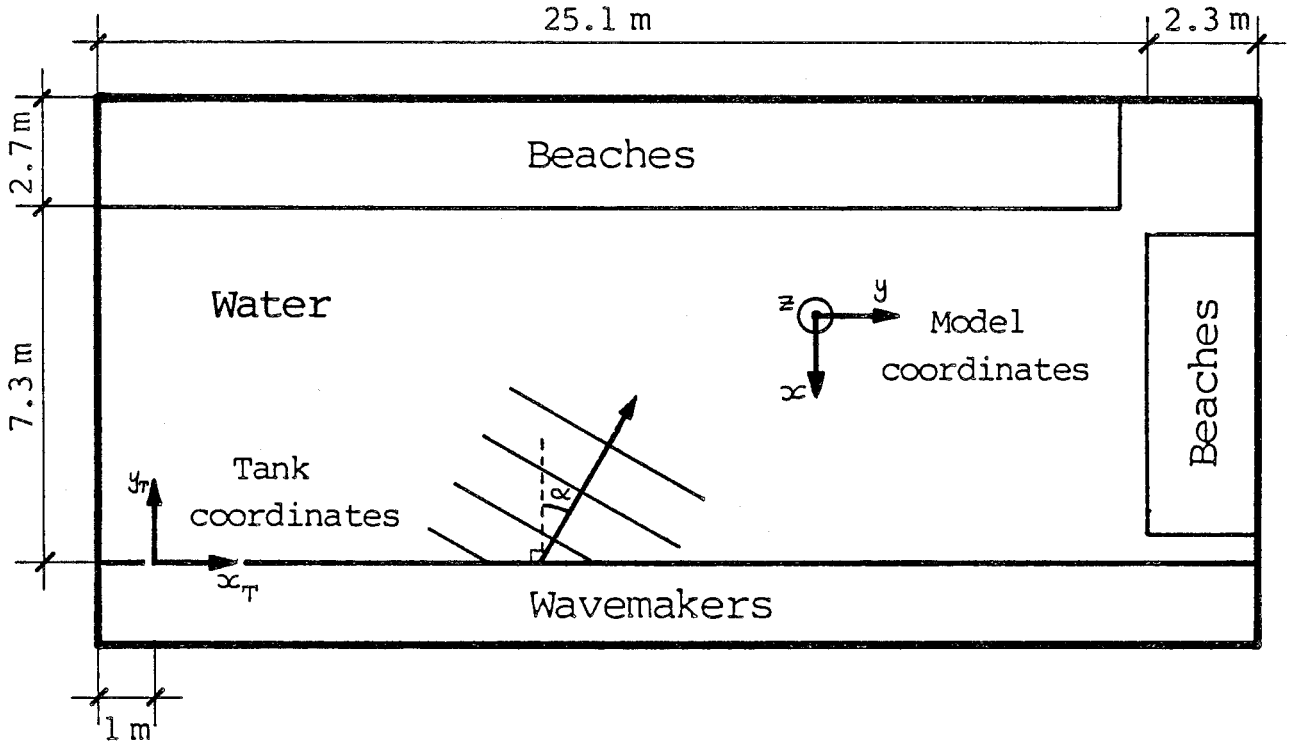

Figure 2.3 Wide tank plan

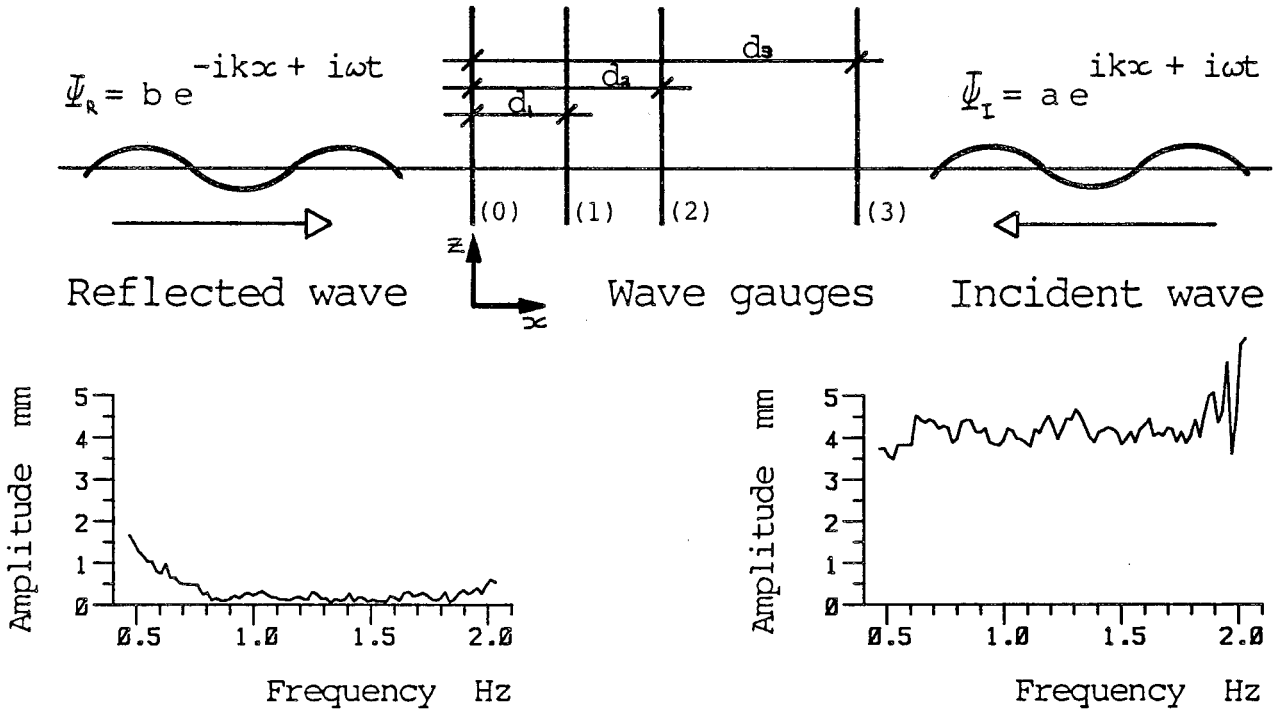

Figure 2.4 Reflected and incident regular waves

Sampling System

The sampling system consists of an overseeing computer, with direct memory access capability, a real time computer containing the master clock, and a sampling interface. The real time computer generates a set of waveforms to drive the wavemaker array, or a single signal suitable for directly driving the system under test. It also produces the sampling clock by dividing the master clock and delaying it for an exact period.

The sampling interface on receiving its clock signal, samples all the channels required by the overseeing computer and enters the results directly into its memory. Because signal generation and sampling are synchronised all the waveforms can be made repeatable within the sampling interval. Data collected in this way may be analysed without worrying about effects due to the ends of the sampling window.

A particularly important method of analysis is the Fast Fourier Transform (FFT) which is used most correctly when the boundary conditions are periodic. By choosing sinusoidal drive signals which fit into the sampling period an integral number of times, the response of the system at this particular frequency can be found and the harmonics identified. Figure 2.6 shows an FFT of a sampled signal obtained in this way and for comparison there is an FFT of a non-synchronised waveform.

Experiment specification

The following sampling parameters were used for all experiments described in this report

```
      Number of samples  :  2048
      Sampling rate      :    40 Hz
->    Sampling period    :  51.2 s
      Sampling delay     :  50.0 s
```

By only choosing freqencies at n/51.2 Hz with n integral the repeat time of the waves was made equal to the sampling time.

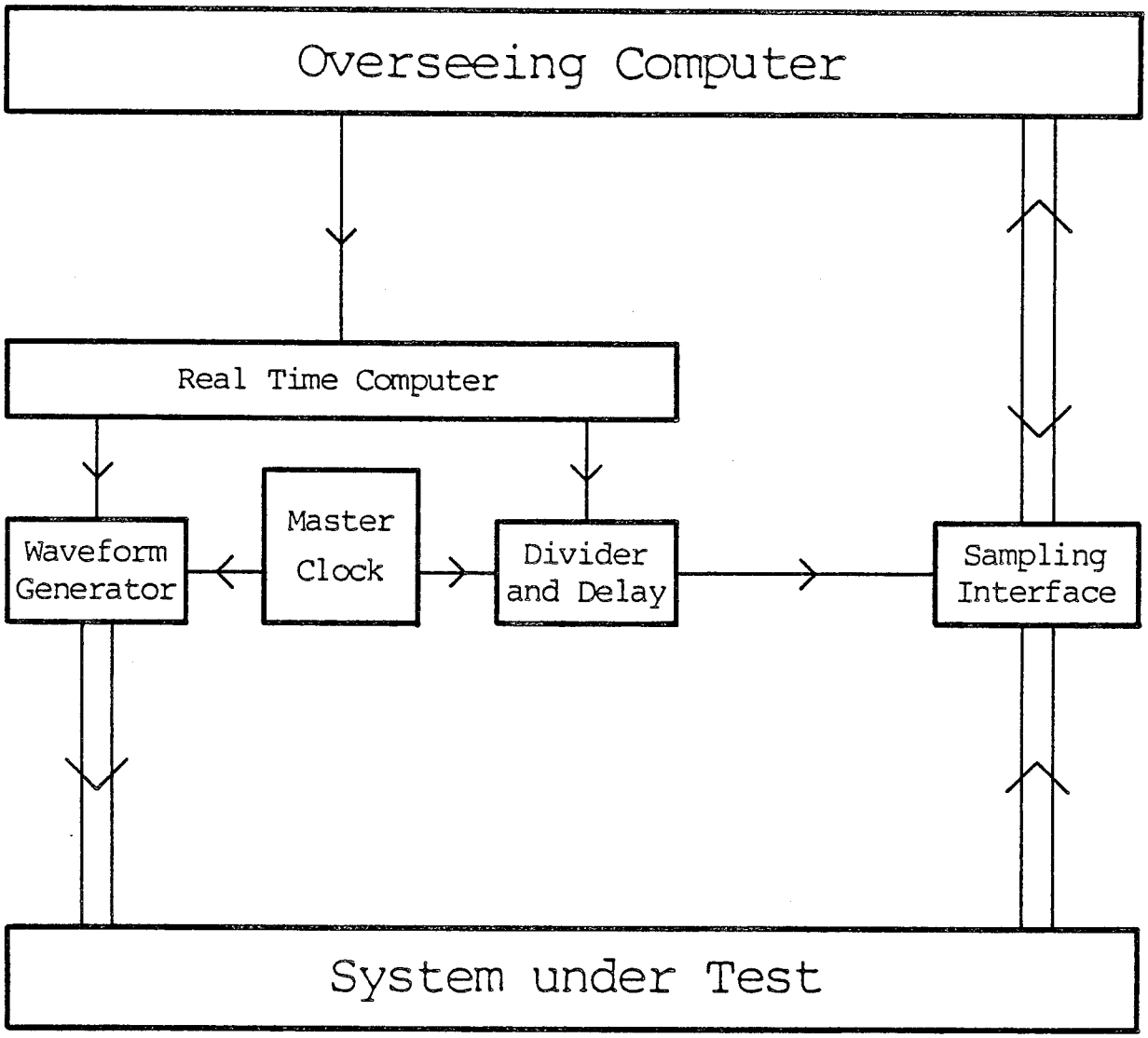

Figure 2.5 Wide tank sampling system

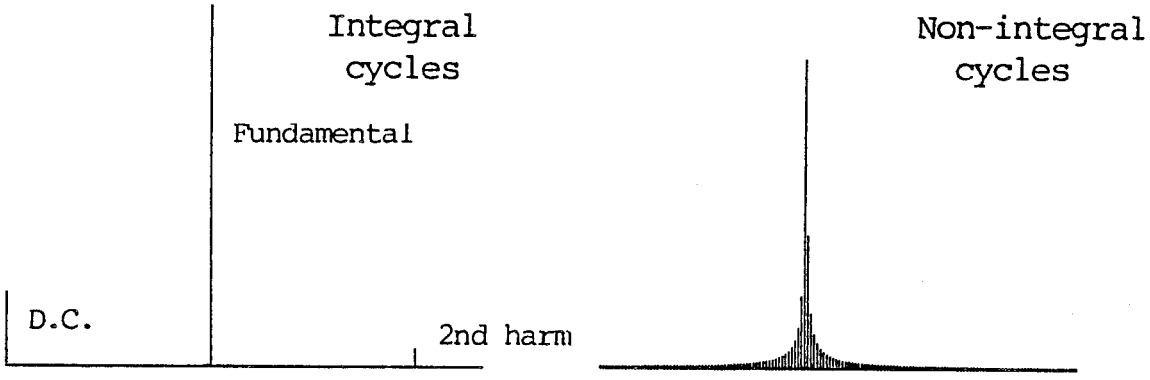

Figure 2.6 FFT of integral and non-integral cycles

Heaving float wave gauge

A 190mm long cylinder of expanded polystyrene floats on the water surface and its motion is translated by a linkage into a rotation. Two small meters act as velocity transducers and their outputs are pre-amplified then summed. The signal is then available as velocity or, after integration, as amplitude. The gain of the outputs can be adjusted during calibration.

Wave angle correction

For the float to work well the projected length in the direction the wave is travelling should be small compared to the wavelength. This can be assumed for parallel waves, corresponding to use in the narrow tank, but not for fronts with small wavelengths and large angles.

The heaving float gauge was used for angled waves, nevertheless. A formula for the resulting underreading can be derived by assuming that the wave height is averaged over the projected length of the float.

$$g = \frac{\sin\left(l_o \pi \sin\alpha / \lambda(\nu) \right)}{l_o \pi \sin\alpha / \lambda(\nu)} \qquad (2.3)$$

Where l_o is the float width

ν the wave frequency

α the wave angle

This equation was used to correct wave amplitudes measured in the tank. For all regular wave fronts which were used the correction to be made was less than 15%. The equation was checked for a few angles by rotating the gauge on a spot while sending monochromatic waves across the tank. Figure 2.8 contains the results of those measurements compared to the prediction from the formula.

Phase correction

The integrator introduces a phase error, removable by multiplying by $e^{i\phi}$ where

$$\phi = \tan\left(\frac{-1}{a(\nu/b - b/\nu)} \right) \qquad \text{with} \quad a = .74, \quad b = .158 \text{ Hz}$$

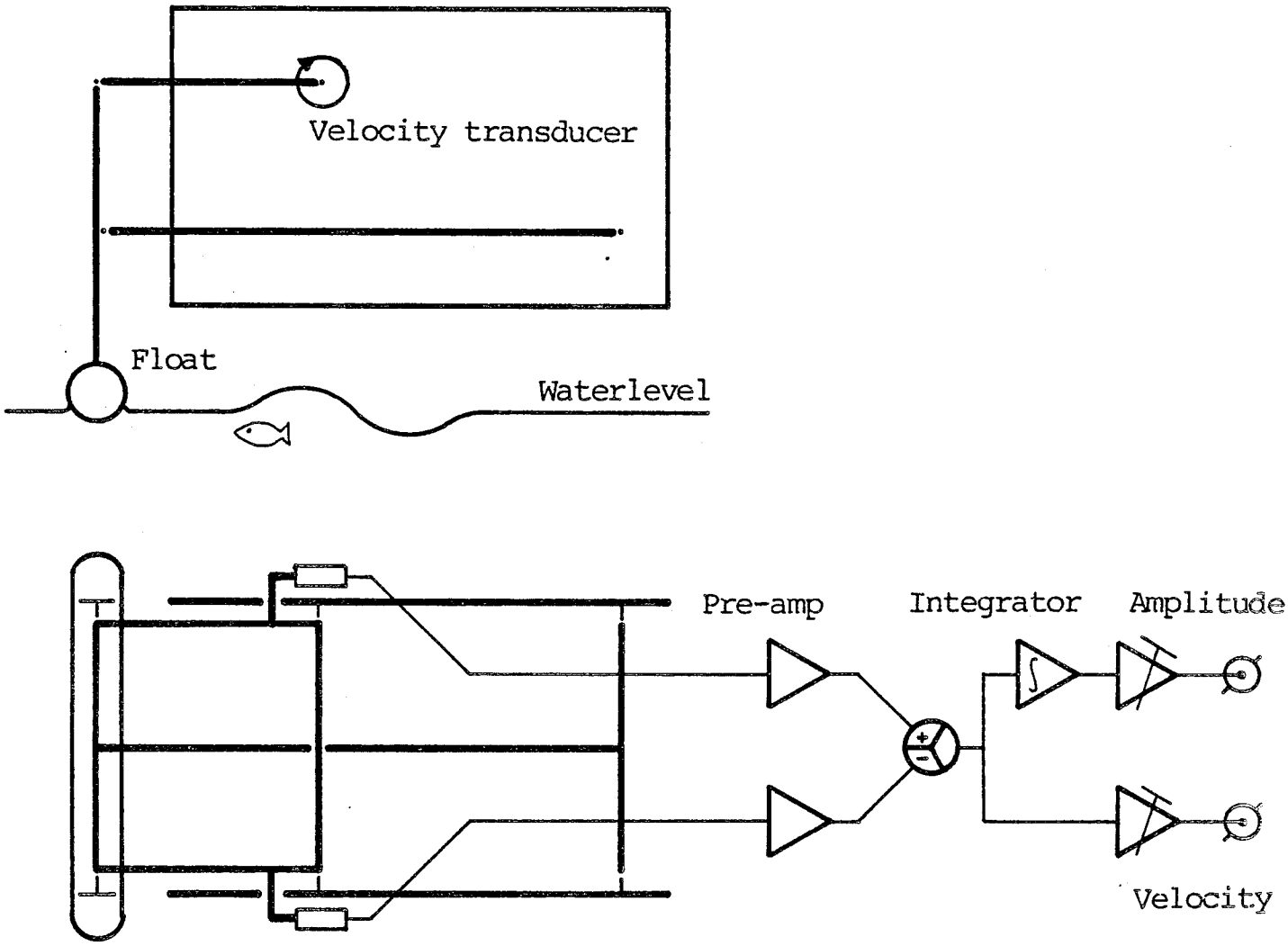

Figure 2.7 Heaving float wave gauge

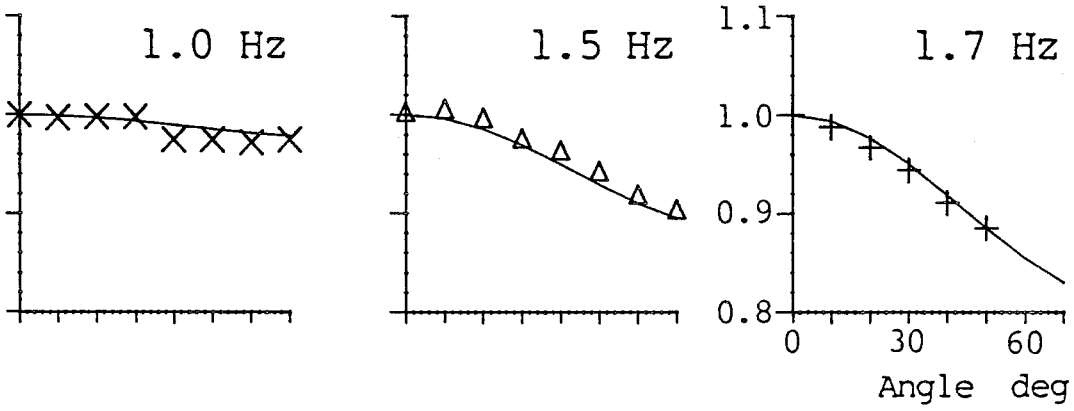

Figure 2.8 Heaving float angular correction

Wire wave gauge

The wire wave gauge consists of two parallel metal rods half immersed in the water. The circuitry shown in figure 2.9 is designed to measure the conduction between the rods. The conductance of the water is measured through a third wire and a compensation made for it.

This particular type of gauge was only used when the waves were to be measured in several places at once. The calibration value of the output was found before use by moving the gauge to known positions above and below the operating point and measuring the difference.

Small amplitude effects

If the gauges are cleaned before use then for most amplitudes the meniscus on the rods can be assumed to remain the same shape as the waves rise and fall. However, the curvature of the meniscus is reduced slightly as the water reaches its highest point creating noticable effects when the waves are very small.

An experiment was conducted to see how much the gauges would underread as the wave height became small. A gauge was attached near the pivoted end of a long lever and its end placed in water. By moving the free end of the lever through a known distance and moving the attachment point of the gauge different amplitudes of motion were obtained. In figure 2.10 the ratio of the actual and measured amplitudes are plotted, showing that underreading occurs when the waves are smaller than about 1mm.

Comparison between Wire and Heaving float gauges

Monochromatic waves were measured at the model position for a range of frequencies, first by the heaving float wave gauge then the wire gauge. The fundamental complex amplitudes were obtained by Fourier transforming the measurements from each experiment. Figure 2.11 contains graphs of the complex ratio in modulus/argument form. The gauges agree within the limits of tank repeatability at low frequency.

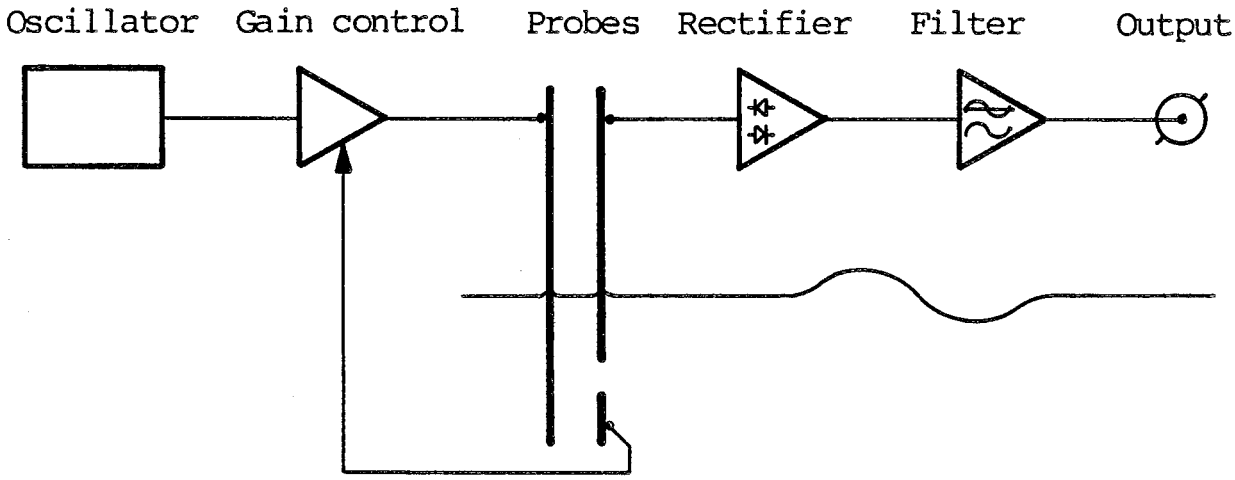

Figure 2.9 Wire wave gauge

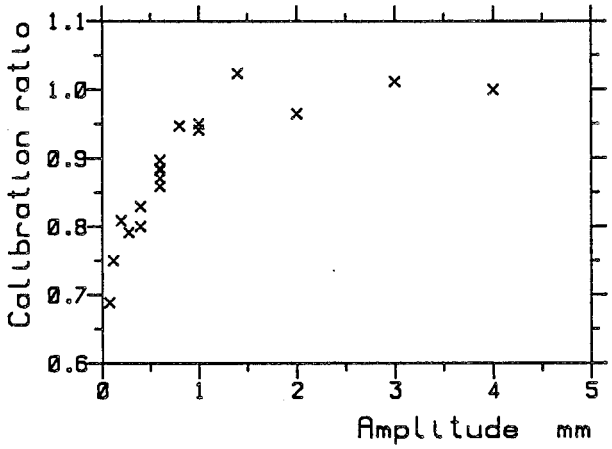

Figure 2.10 Wire wave gauge calibration curve

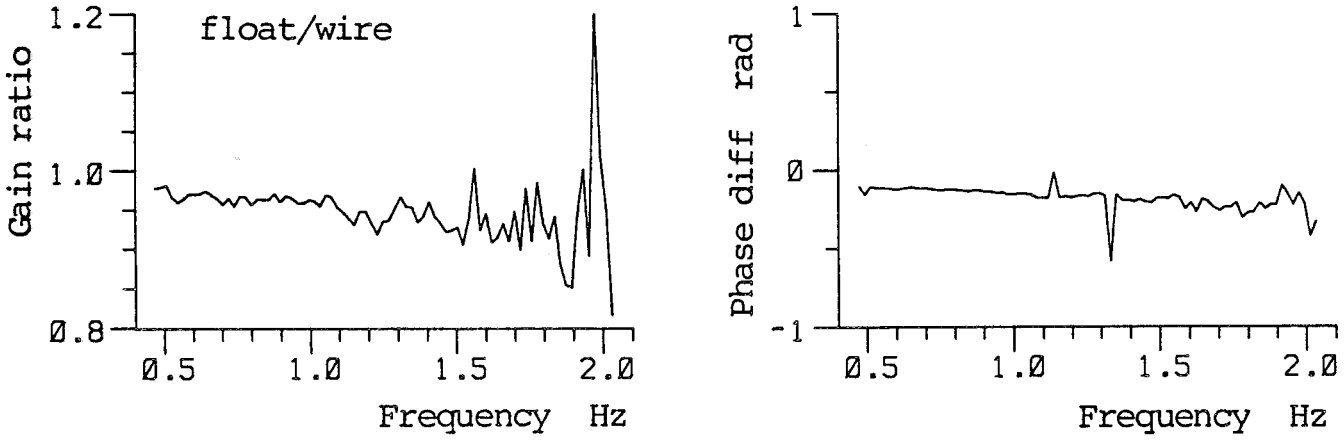

Figure 2.11 Comparison between heaving float and wire wave gauge

3) Experimental determination of the hydrodynamic parameters

Experiments were conducted to find the parameters in the equation of motion, and the radiation pattern when the duck is driven.

Radiation impedance tensor $\underline{\underline{Z}}(\omega)$

This relates the forces and velocities when the duck is driven in calm water. Recalling the equation of motion (1.7)

$$\underline{F} = \underline{\underline{Z}}.\underline{u} + \underline{W}\,a$$

In the absence of incident waves

$$\underline{F} = \underline{\underline{Z}}.\underline{u} \tag{3.1}$$

The above represents three complex equations, the unknowns being the nine complex terms which make up $\underline{\underline{Z}}$. In order to obtain enough equations so that $\underline{\underline{Z}}$ may be found, $\underline{F}$ and $\underline{u}$ need to be measured in three linearly independent experiments. It is not necessary to fix the modes which are not being driven, but only to ensure that the three motions measured are sufficiently independent to minimise the effect of noise.

For each frequency the following equations are constructed:

First experiment, driven in pitch $\quad {}^{\circ}\underline{F} = \underline{\underline{Z}}.{}^{\circ}\underline{u}$ (3.2)

Second experiment, driven in heave $\quad {}^{1}\underline{F} = \underline{\underline{Z}}.{}^{1}\underline{u}$ (3.3)

Third experiment, driven in surge $\quad {}^{2}\underline{F} = \underline{\underline{Z}}.{}^{2}\underline{u}$ (3.4)

The superscripts are indices

Equations (3.2),(3.3),(3.4) can be combined by defining matrices $\underline{\underline{\mathcal{F}}}, \underline{\underline{\mathcal{U}}}$ such that:

$$\underline{\underline{\mathcal{F}}} = ({}^{\circ}\underline{F}, {}^{1}\underline{F}, {}^{2}\underline{F}) \qquad \underline{\underline{\mathcal{U}}} = ({}^{\circ}\underline{u}, {}^{1}\underline{u}, {}^{2}\underline{u})$$

Then

$$\underline{\underline{\mathcal{F}}} = \underline{\underline{Z}}.\underline{\underline{\mathcal{U}}}$$

Postmultiplying by $\underline{\underline{\mathcal{U}}}^{-1}$, which will exist if the experiments are independent

$$\boxed{\underline{\underline{Z}} = \underline{\underline{\mathcal{F}}}.\underline{\underline{\mathcal{U}}}^{-1}} \tag{3.5}$$

The right hand side of this equation is composed entirely of measurable quantities and hence $\underline{\underline{Z}}$ can be determined.

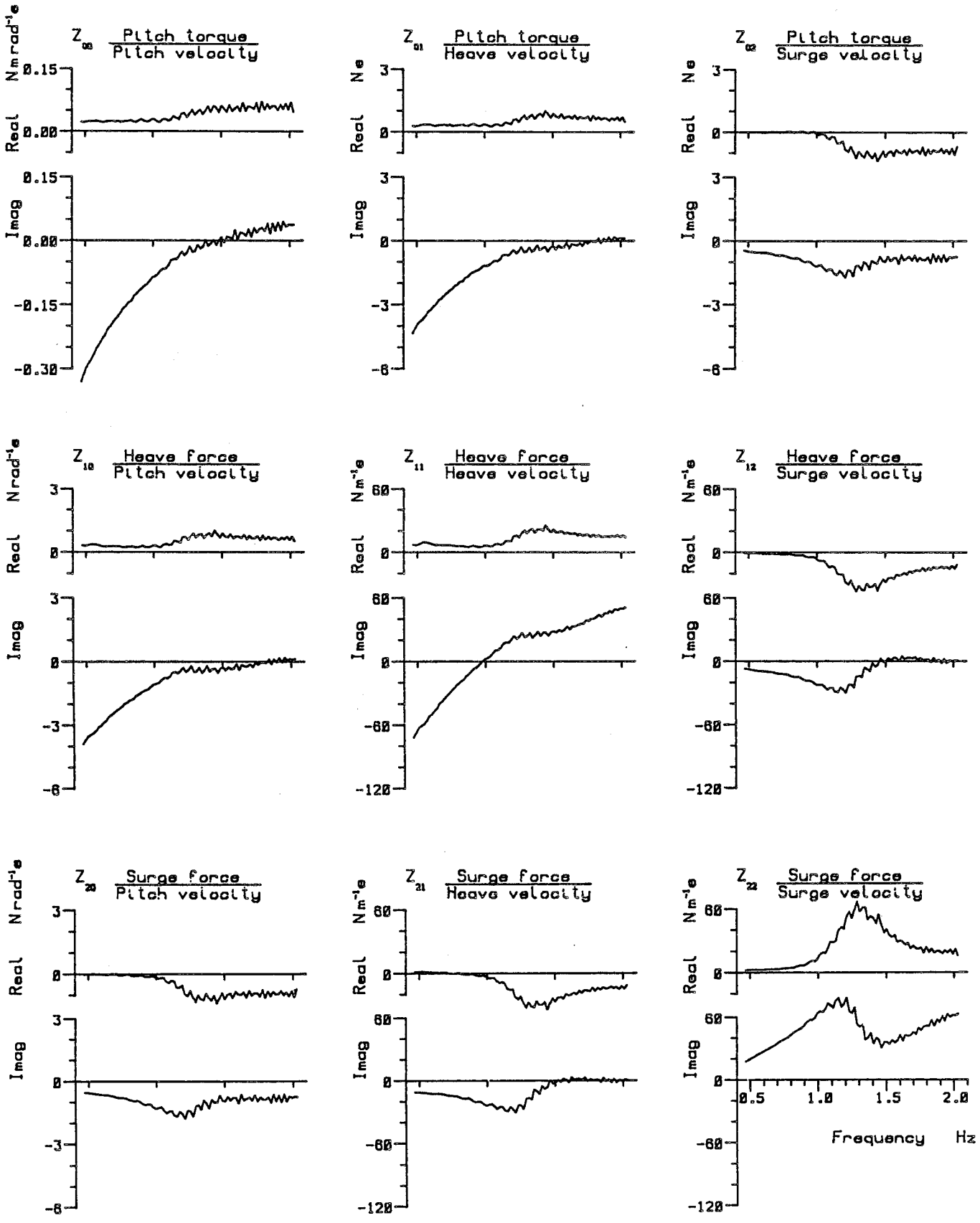

Figure 3.1 Radiation impedance matrix $\underline{\underline{Z}}(\omega)$

Impedance experiments

The results plotted in figure 3.1, and discussed in the next section, where obtained from three experiments in which each mode was driven for a range of frequencies while damping the others. The damping forces were chosen to limit resonances in the rig without making it unstable. By putting power into one mode and extracting some of it in the others a high degree of linear independence was expected between the three experiments.

The drive signal was taken from the filtered output of the wavemaking computer and the damping forces applied by the BBC controller. The usual set of frequencies was used

$$\nu = \frac{n}{51.2} \qquad n = 24,25,\ldots,104$$

The drive amplitudes were chosen such that the second harmonic of the velocity of the driven mode was less than 10% of the fundamental. This was taken to be a reasonable indicator of how linearly the duck was behaving since if the second harmonic of velocity and of force are both 10% of the fundamentals then the power in the second harmonic is only about 1%.

Figure 3.2 contains the harmonic amplitudes of the main velocity signals, with each column coming from a separate experiment. Only the responses of the modes being driven are shown. The drive amplitudes which produced these velocities are plotted in figure 3.3.

Non-linearities may arise for many different reasons. The change of waterline length with pitch angle and heave displacement leads to a strong second order term in the hydrostatic spring rates of each of these modes. Viscous damping can be expected to generate both fundamental and third harmonic. When non-linear effects are small, measurement of the harmonic response provides a starting point for identifying their origins and behaviour.

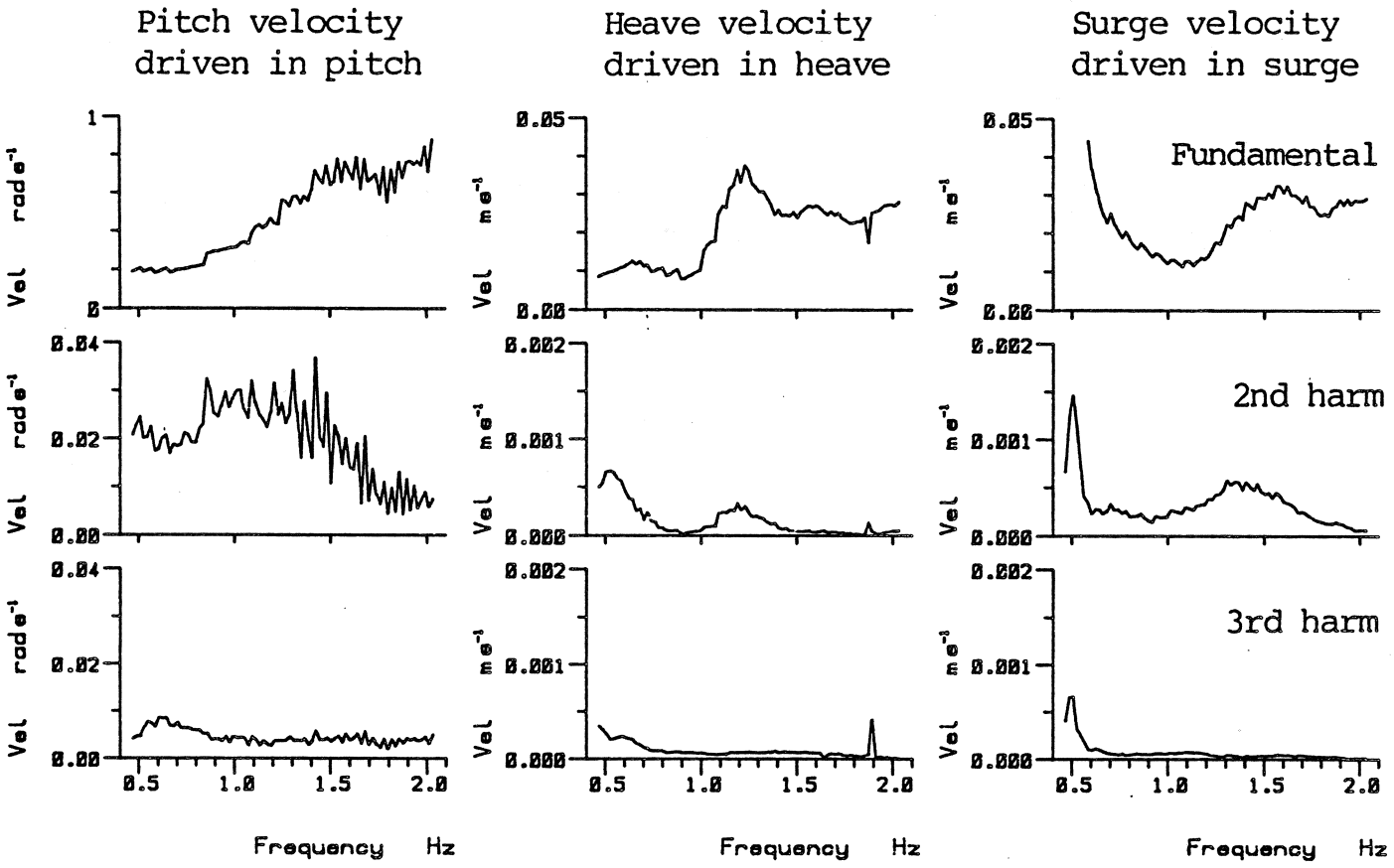

Figure 3.2 Velocity harmonics in the driven modes

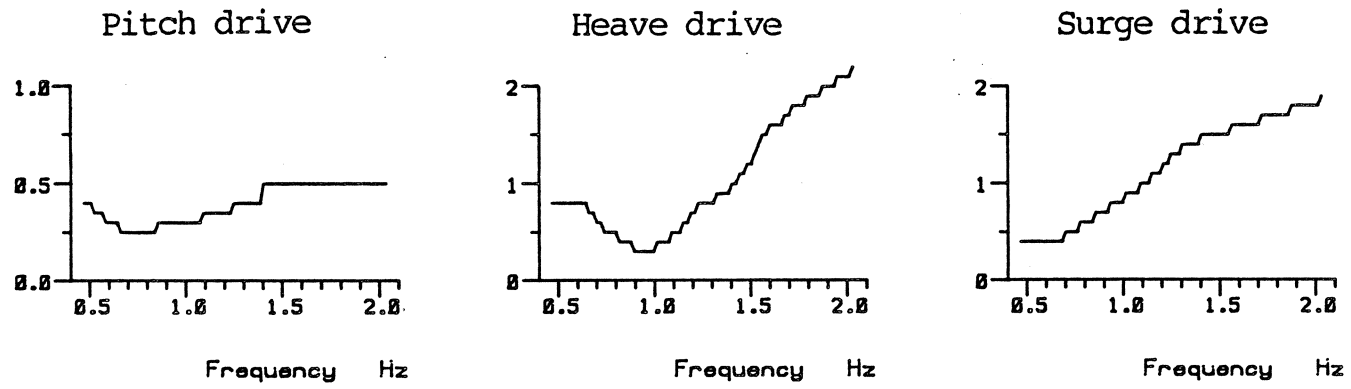

Figure 3.3 Drive signals

Radiation pattern vector $R(\omega,r,\alpha)$

When the duck is driven in still water a particular radiation pattern is set up on the water surface. The vector $\underline{R}$ links the wave amplitude at position r,α to the duck velocities.

$$a(r,\alpha) = \underline{R}(r,\alpha).\underline{u} \tag{3.6}$$

The components of $\underline{R}$ at a particular frequency and location may be discovered by driving the duck in three independent experiments, as for the radiation impedance, and measuring the wave height.

For each wave gauge and frequency the following are written down

First experiment, driven in pitch $\quad {}^{\circ}a = \underline{R}.{}^{\circ}\underline{u}$ (3.7)

Second experiment, driven in heave $\quad {}^{1}a = \underline{R}.{}^{1}\underline{u}$ (3.8)

Third experiment, driven in surge $\quad {}^{2}a = \underline{R}.{}^{2}\underline{u}$ (3.9)

Equations (3.7),(3.8) and (3.9) may be combined by defining

$$\underline{\mathcal{A}} = ({}^{\circ}a, {}^{1}a, {}^{2}a) \qquad \underline{\underline{\mathcal{U}}} = ({}^{\circ}\underline{u}, {}^{1}\underline{u}, {}^{2}\underline{u})$$

Then

$$\underline{\mathcal{A}} = \underline{R}.\underline{\underline{\mathcal{U}}}$$

Postmultiplying by $\underline{\underline{\mathcal{U}}}^{-1}$ which will exist if the experiments are independent

$$\boxed{\underline{R} = \underline{\mathcal{A}}.\underline{\underline{\mathcal{U}}}^{-1}} \tag{3.10}$$

Since all the quantities on the right hand side can be measured this equation provides the means to determine $\underline{R}$.

Radiation pattern experiments

In the experiments which produced the graphs shown in figure 3.4 twelve wire wave gauges were placed around the duck at 30° intervals and .92m radius. The model was driven in the same way as during the determination of the radiation impedance, the velocities and wave amplitudes measured and the fundamental component calculated. The modulus of the vector is plotted and only angles from 0° to 180° are shown since the results were very symmetric.

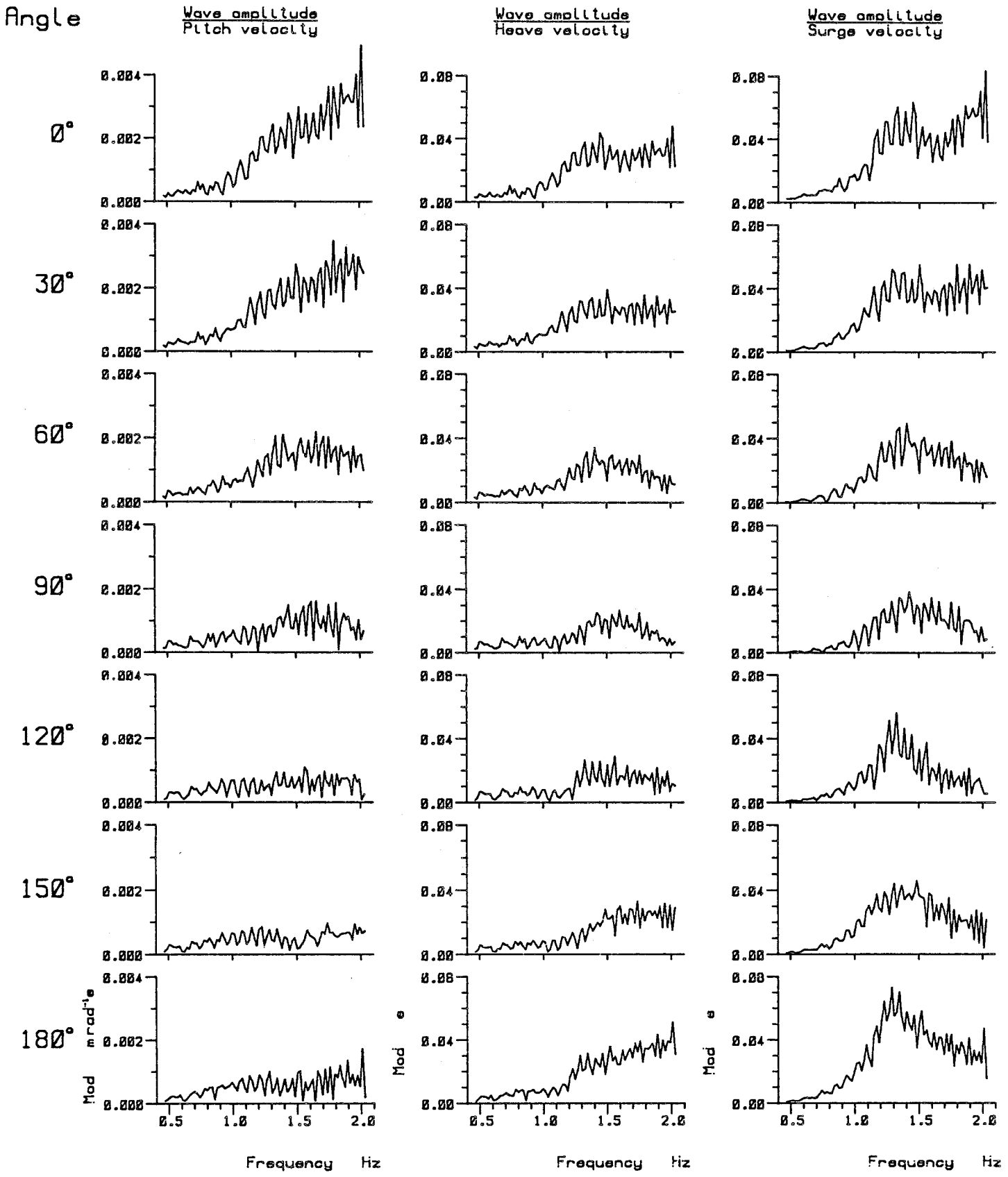

Figure 3.4 Radiation pattern vector $\underline{R}(\omega,r,\alpha)$

Modulus of measurements made at 0.92m radius

Force coefficient vector $\underline{W}(\omega,\alpha)$

This vector gives the forces required to hold the duck still when a wave of unit amplitude is incident. Its definition appears in the equation of motion (1.7) described previously.

$$\underline{F} = \underline{\underline{Z}}.\underline{u} + \underline{W}\,a$$

If the duck were fixed, $\underline{u}=0$, the vector $\underline{W}$ could be found without knowing the radiation impedance $\underline{\underline{Z}}$, but this is not necessary.

If it is assumed that $\underline{\underline{Z}}$ is known, then the three complex terms of the vector $\underline{W}$ may be determined by sending waves of small amplitude towards the duck at a range of frequencies and angles. The other quantities can be measured and $\underline{W}$ calculated directly.

Regular wave experiments

The graphs plotted in figure 3.5 were obtained with incident waves of nominal amplitude 4mm. This wave height was chosen to keep the harmonic content of the duck's motion small, while providing signals which were large enough to measure. The duck was fixed in surge, and its motion in pitch and heave damped. Other experiments were performed with different controls applied and similar results obtained.

For each angle α measurements of $\underline{F}$ and $\underline{u}$ were made at 81 frequencies in the range 0.469 to 2.031Hz. Wave fronts with high frequency and large angle produce extra 'ghost' fronts and tests were not conducted in these cases. The forward angles were regarded as the most important and measurements were made at 10° intervals up to 70°. Larger angles were obtained by placing the duck in two other orientations.

First experiment, with the duck in the model position $\alpha = 0^\circ, 10^\circ, \ldots, 70^\circ$
Second experiment, with the duck turned through 90° $\alpha = 90^\circ$
Third experiment, with the duck turned through 180° $\alpha = 120^\circ, 150^\circ, 180^\circ$

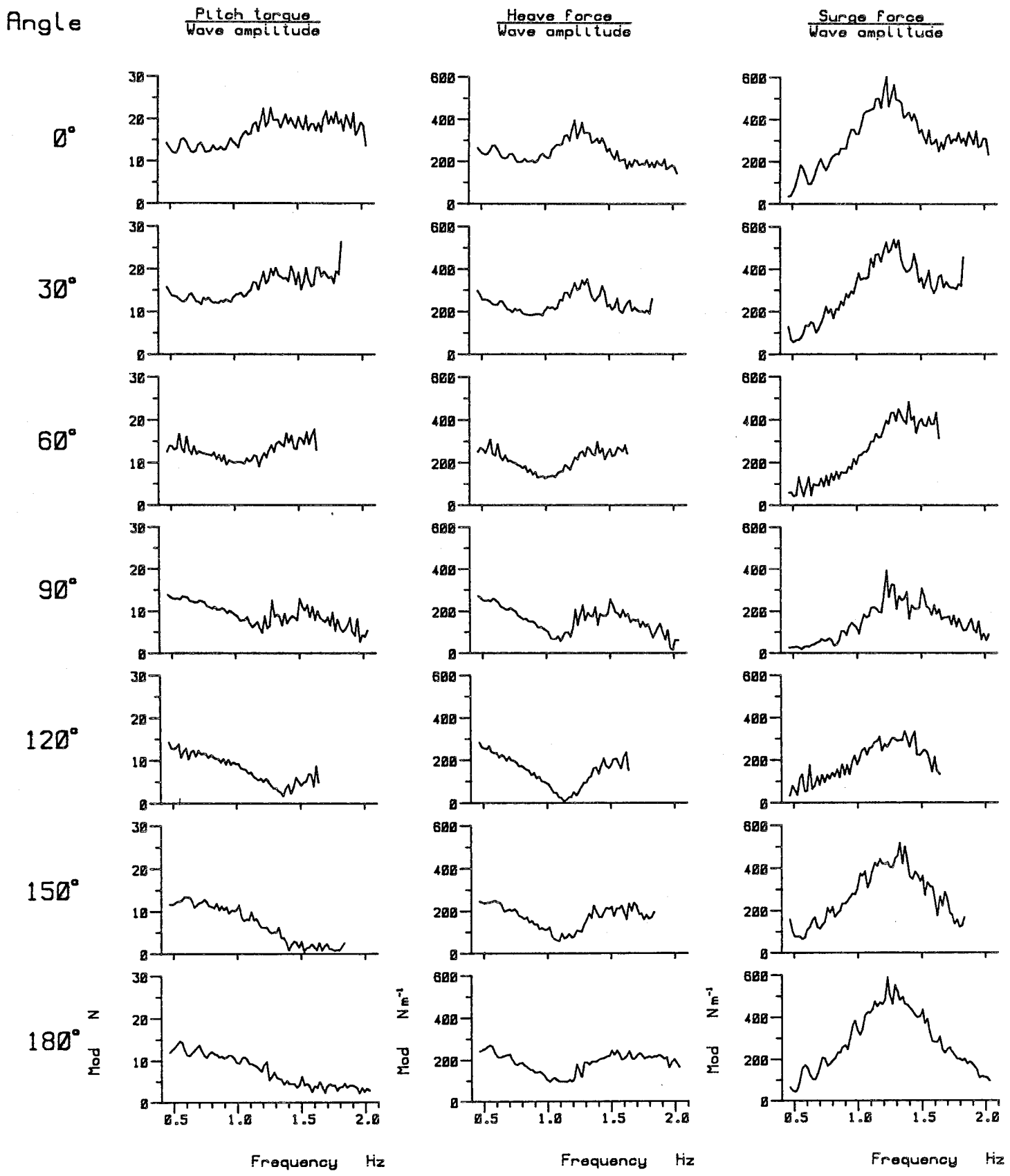

Figure 3.5 Force coefficient vector $\underline{W}(\omega,\alpha)$. Modulus

After each experiment was complete a wave gauge was placed in the model position, the wave conditions repeated and the wave height measured. For the results shown it was assumed that this amplitude was equal to the incident amplitude, although in truth the waves reflected from the beaches will interfere. For the case of $\alpha = 0^{\circ}$ the effect of the reflected wave may be calculated and removed. This is done in the next section.

The graphs plotted in figure 3.5 show the modulus of the terms of $\underline{\mathbf{W}}$ at 30° intervals while those in figure 3.6 show the phase for completeness.

When the frequency is low, the wavelength is much greater than the duck dimensions and the pitch and heave forces are π radians out of phase with the wave amplitude. This is expected since the duck has to be held down when the water rises. At these frequencies the phase difference between heave and surge is $\lambda/2$ radians, like the water motion.

Summary

The radiation impedance matrix and the radiation pattern are determined by driving the duck in calm water with three linearly independent motions.

The presence of harmonics provides a useful guide to the extent of linearity.

The force coefficient vector is found by measuring the duck motion in the presence of waves and knowing the radiation impedance matrix.

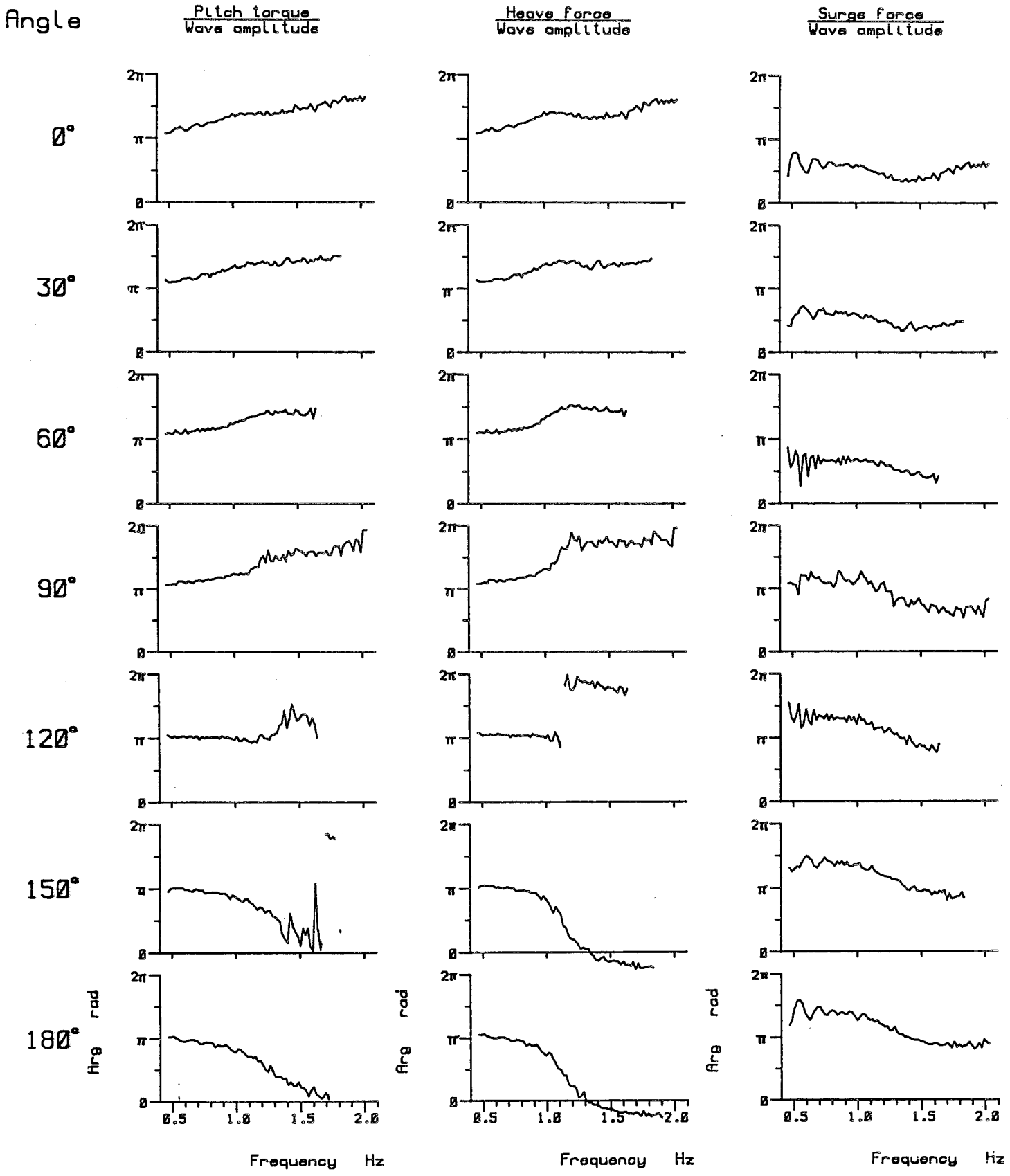

Figure 3.6 Force coefficient vector $\underline{W}(\omega,\alpha)$. Phase

4) Discussion and Further Processing of the Experimental Results

The composition of the imaginary part of the radiation impedance matrix is discussed and the real part related to the radiation pattern and the force coefficient vector. The reflection noise is removed from the impedance matrix by data processing and from the force coefficient vector by considering the beach reflections.

Radiation Impedance

The impedance tensor may be split into four parts up as described in Section 1

$$\underline{\underline{Z}}(\omega) = \underline{\underline{D}}_A(\omega) + i\omega\underline{\underline{M}}_A(\omega) + i\omega\underline{\underline{\mu}} + \frac{1}{i\omega}\underline{\underline{\sigma}}$$

Where $\underline{\underline{D}}_A$ is the real, frequency dependent added damping matrix
$\underline{\underline{M}}_A$ is the real, frequency dependent added mass matrix
$\underline{\underline{\mu}}$ is the duck inertia matrix
$\underline{\underline{\sigma}}$ is the hydrostatic spring matrix

In figure 4.1 curves for the predicted contributions of $\underline{\underline{\mu}}$ and $\underline{\underline{\sigma}}$ are plotted along with the imaginary part of $\underline{\underline{Z}}$ reproduced again for comparison. The graphs of $\underline{\underline{\mu}}$ and $\underline{\underline{\sigma}}$ are based on experimental values obtained for this particular duck model in Section 2 and are drawn having multiplied by $i\omega$ and $1/i\omega$ respectively.

The duck inertia $\underline{\underline{\mu}}$ should be removed from $\underline{\underline{Z}}(\omega)$ to leave values which depend only on the underwater shape of the duck. The particular values of $\underline{\underline{\mu}}$ are arbitary and could be different while maintaining the same underwater shape. However, it should be remembered that there are some constraints on $\underline{\underline{\mu}}$, notably that vector sum of weight, buoyancy and external static forces must be zero.

The hydrostatic spring matrix $\underline{\underline{\sigma}}$ depends on the shape of the duck around the waterline, and should be left in $\underline{\underline{Z}}$.

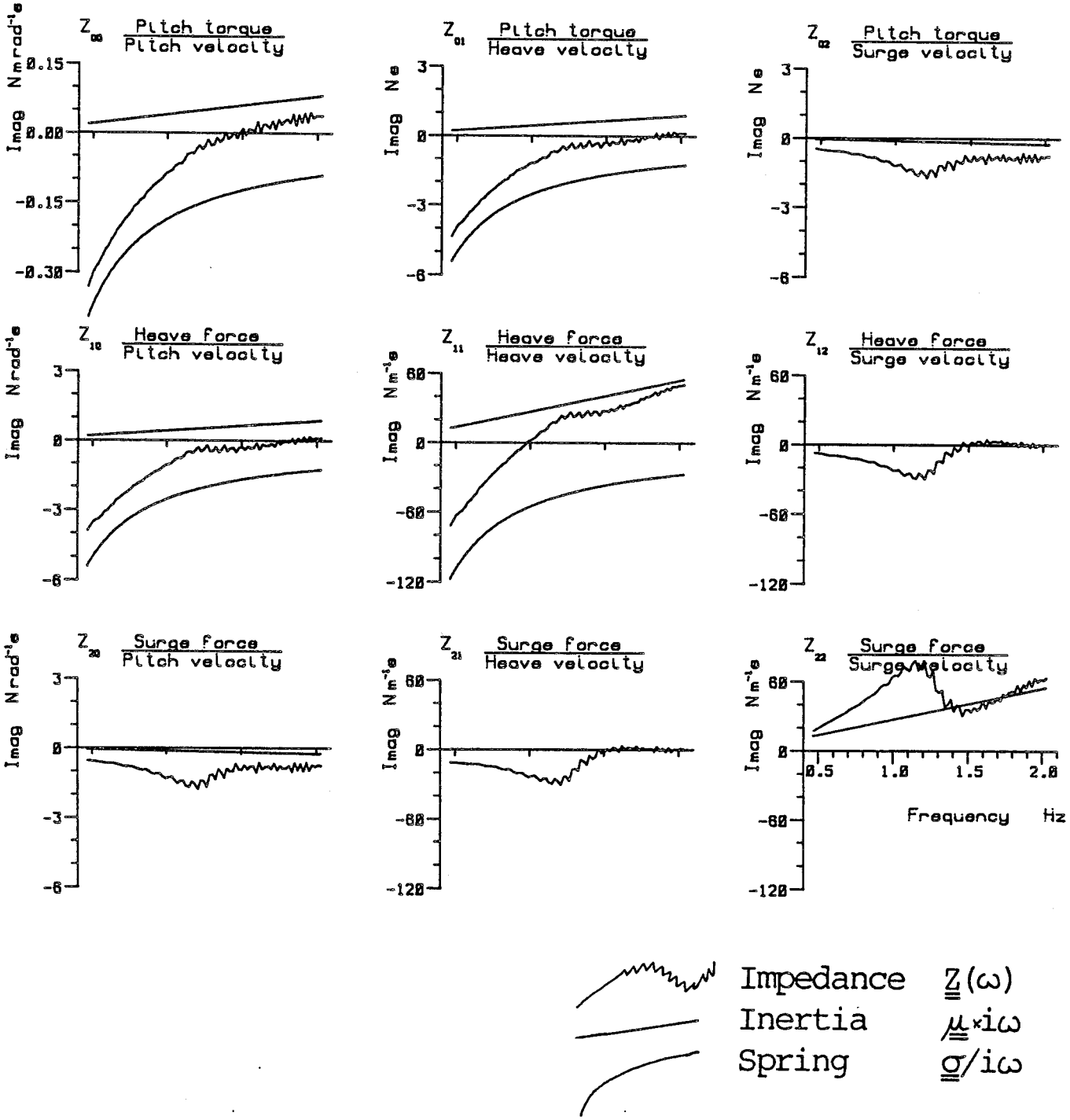

Figure 4.1 Comparison between duck inertia, hydrostatic spring and the imaginary part of the radiation impedance

Ripple noise

The ripple noise which appears on all experimental curves of $\underline{Z}$ is due to the radiated wave being reflected off the boundaries of the tank, returning to interfere with the motion of the duck. The ripple was found to be both highly repeatable and dependent on the position in the tank.

Figure 4.2 shows the imaginary surge component of the impedance matrix measured at the model position and about .25m further away from the wavemakers. This distance corresponds roughly to $\lambda/4$ at 1.2Hz and $\lambda/2$ at 1.8Hz. That the ripple is mainly due to reflection from the wave makers is confirmed because at these two frequencies the graphs are out of phase and in phase respectively.

An estimate for the effect of reflections can be obtained by combining the equation for the radiation pattern vector (3.6) with the equation of motion (1.7). The wave amplitude given by the radiation vector is assumed to propagate as a circular wave, reflect from the wavemakers as if emminating from the duck's mirror image and return to provide the incident wave in the equation of motion.

$$\begin{aligned} a' &= \underline{R}.\underline{u} \\ a &= a'\sqrt{\frac{r}{2d}}\, e^{ik(2d-r)} \\ \underline{F} &= \underline{Z}.\underline{u} + \underline{W}\, a \end{aligned} \qquad (4.1)$$

Where $\underline{R}$ was measured in front of the duck at radius r
d is the distance from the duck to the wave makers

By combining the three equation and estimate for the reflection noise is found

$$Z'_{jk} = Z_{jk} + W_j R_k \sqrt{\frac{r}{2d}}\, e^{ik(2d-r)} \qquad (4.2)$$

Figure 4.3 contains the predicted effect of reflection noise on the imaginary surge component of the radiation impedance. The general form of the curve corresponds well with with the observed ripple noise shown in the graph above.

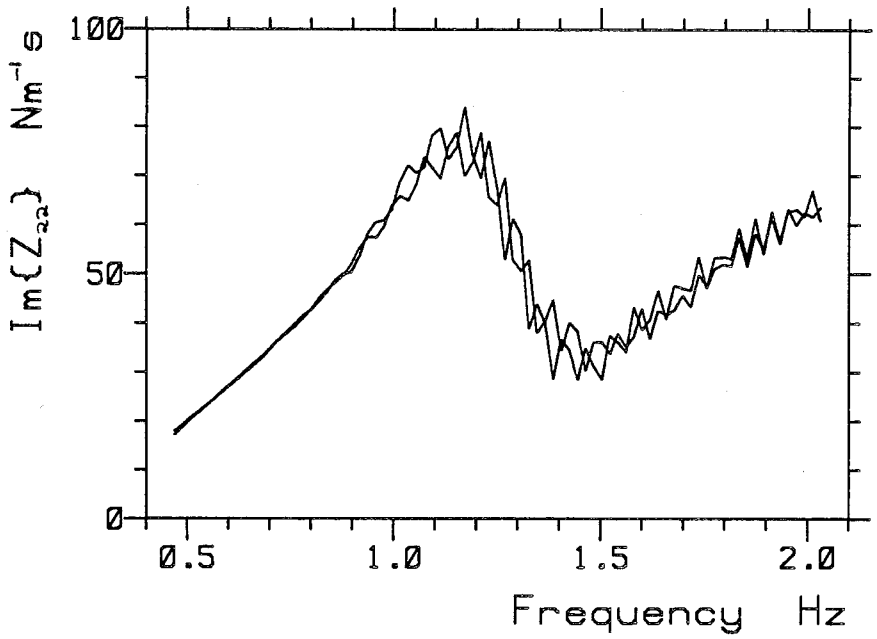

Figure 4.2 Imaginary part of surge impedance measured at two places

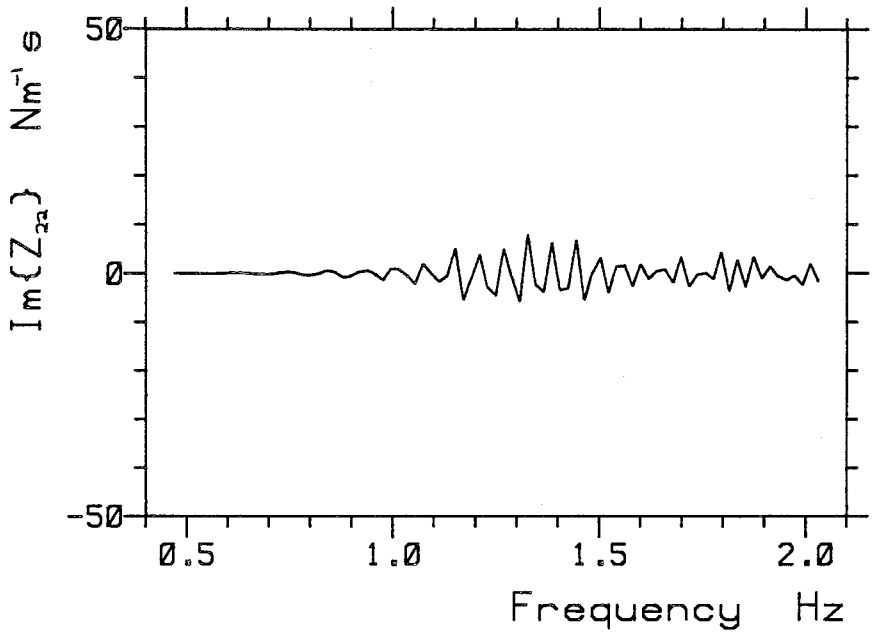

Figure 4.3 Estimate of reflection noise on imaginary surge impedance

Removal of ripple noise

The ripple is regarded as a non-linear characteristic of the tank. It occurs when the duck is driven in a still tank because the radiated waves are small and well reflected from all the boundaries, but would not be present if the duck was driven in the presence of incident waves when the wave makers and beaches absorb well. Our aim is to make predictions for its motion when waves are incident so the ripple has to be removed.

The method used to remove the ripple noise was first to subtract the matrices $\underline{\underline{\mu}}$ and $\underline{\underline{\sigma}}$, thus flattenning the ends of the curves. The spatial Fourier transform of each curve was taken, the higher frequency components removed and the inverse transform taken.

The radiation impedance

In figure 4.4 the radiation impedance curves are plotted with the ripple and duck inertia subtracted. They show the effect of the duck shape in an 'infinite' tank. The curves for surge, Z_{22}, resemble the characteristic shape for a wave maker flap, although its imaginary part never goes below zero (Hyun 1976). Pitch and heave show some similarities, with spring forces dominating both at low frequencies.

Note that the impedance matrix is very symmetric about the leading diagonal, as predicted by Newman (1976). For example, the heave force caused by unit pitch velocity is the same as the pitch torque caused by unit heave velocity. This is also apparent in the curves for the duck inertia and hydrostatic spring matrices.

The presence of strong symmetry shows that the calibration and the experimental method were good. Moreover, it provides the first indication that the linear analysis is a worthwhile exercise.

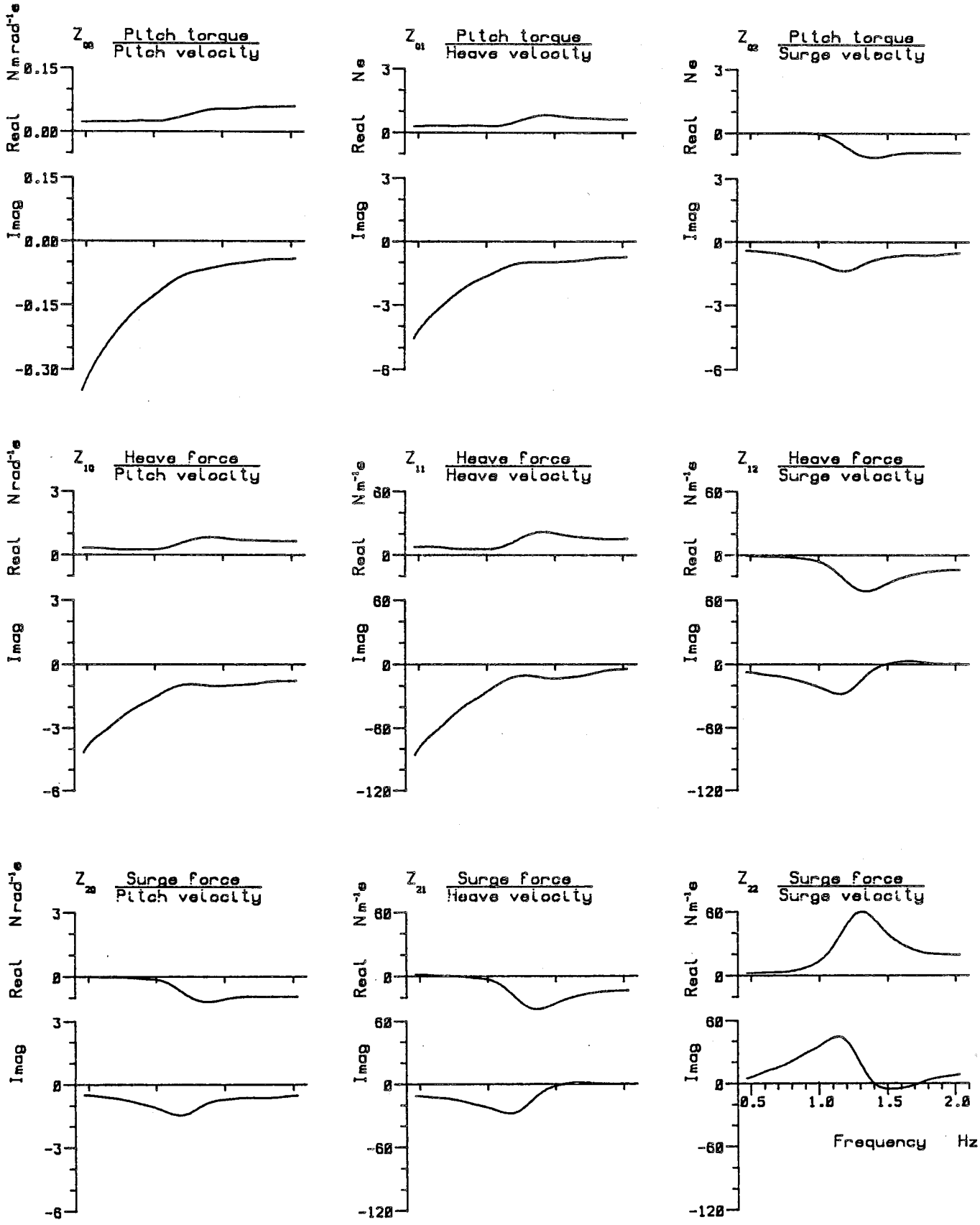

Figure 4.4 Radiation impedance without reflection noise and duck inertia

Conservation of energy in the radiated wave

If energy is only lost in the radiated wave, then in the steady state the power loss measured at the duck must equal the power flux through any surrounding boundary. This provides a way to link the radiation resistance, the real part of the impedance, to the radiated wave pattern.

The power lost by the duck in calm water, using the symmetry of $\underline{Z}$, was given in equation (1.17). Rewriting in suffix notation

$$P = \frac{1}{2} u_j^* \mathrm{Re}\{Z_{jk}\} u_k \tag{4.3}$$

An estimate for the power flux through a circular boundary, radius r, was obtained from the wave amplitudes at twelve equally spaced points on the boundary. The regular wave power formula was applied to each arc, assuming the power flowed radially, and the twelve contributions summed.

$$P = \sum_{n=0}^{11} C \, |a(\alpha_n)|^2 \, r \, \Delta\theta \tag{4.4}$$

$$\text{Where } C = \frac{\rho g^2}{4\omega} \tanh(kh)\left(1 + \frac{2kh}{\sinh(2kh)}\right) \tag{4.5}$$

Using the definition of $\underline{R}$ from equation (3.6) for a particular α

$$|a|^2 = a^* a = (R_j u_j)^* (R_k u_k) \tag{4.6}$$

Substituting for $|a|^2$ and $\Delta\theta = 2\pi/12$ into equation (4.4) and comparing with equation (4.3)

$$\mathrm{Re}\{Z_{jk}\} = \frac{\pi}{3} C \, r \sum_{n=0}^{11} R_j^*(\alpha_n) \, R_k(\alpha_n) \tag{4.7}$$

This equation was used to predict the radiation resistance from the radiation pattern and in figure 4.5 the predicted matrix is compared with the previous experimental results. The imaginary terms are also plotted on a single graph at the same scale as the corresponding real parts. The diagonal imaginary terms have to be zero, but the small size of the others indicates that the experimental values for $\underline{R}$ are good.

The predicted radiation resistance matrix differs significantly from that measured at low frequency. The wave height was small in these cases and this accounts for some of the discrepancy. Overall, the agreement is very good considering the approximations made.

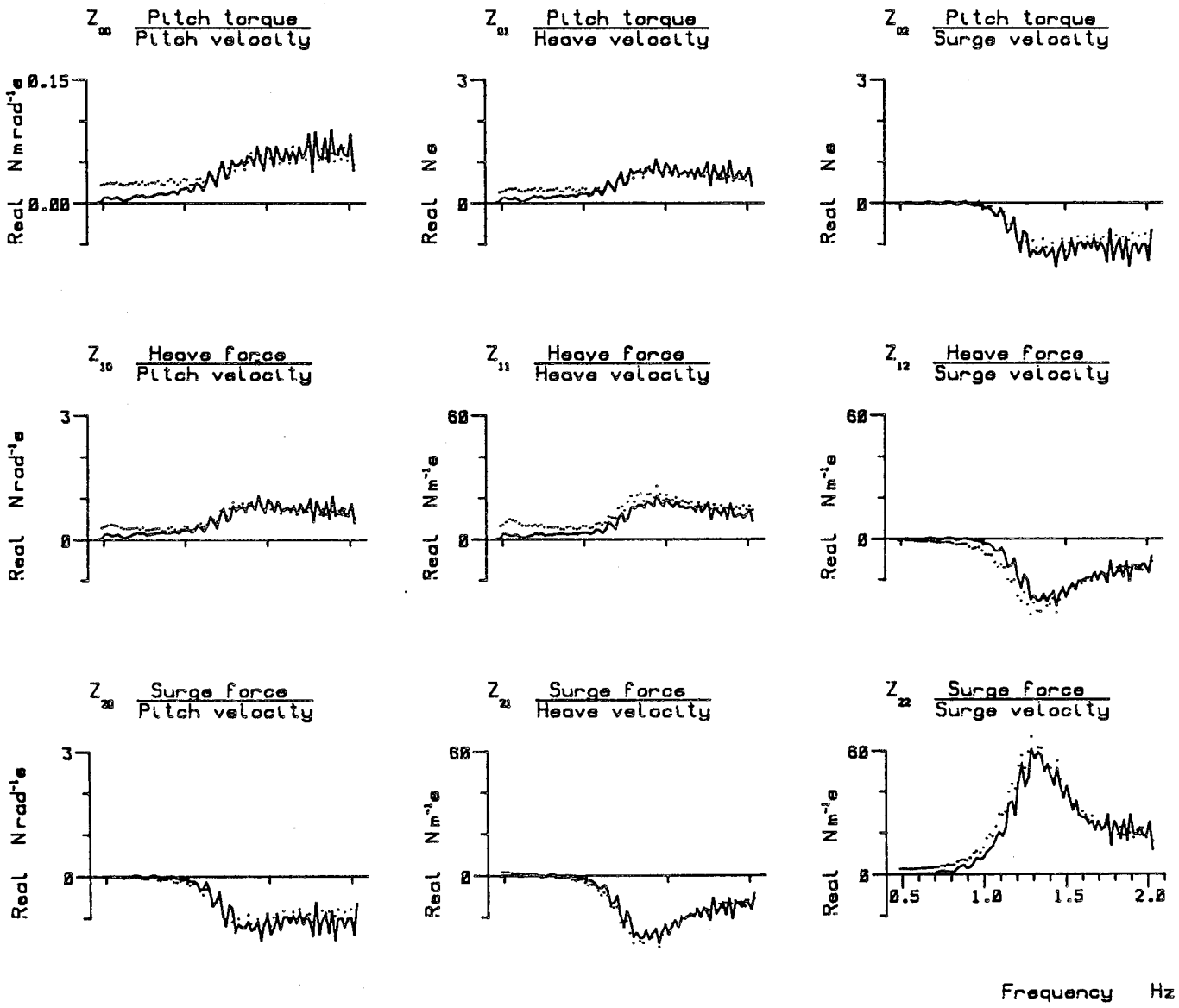

Prediction from radiated waves

Measured impedance

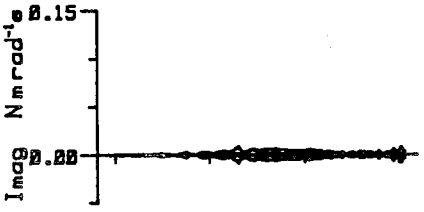

Figure 4.5 Predicted radiation resistance from radiation pattern vector

Radiation impedance and force coefficients

The real part of the radiation impedance matrix can be related to the force coefficient vector. Newman (1976) shows that

$$\mathrm{Re}\{Z_{jk}\} = \frac{1}{8\lambda P_w} \int_0^{2\pi} W_j^*(\alpha)\, W_k(\alpha)\, d\alpha \qquad (4.8)$$

Where P_w is the power in a wave of unit amplitude per metre

A prediction for the radiation resistance was made by approximating the integral in equation (4.8) with a summation. The experimental values for $\underline{W}$ found in Section 3 were used, with an appropriate weighting for the angular spread represented by each.

In figure 4.6 the predicted matrix is compared with that obtained by direct experiment. Also shown, on a single graph, are the imaginary contributions resulting from the calculation. These terms must be zero when the indices are equal, and should be zero when the indices are different if the equation is valid. The imaginary cross terms are close enough to zero to suggest that the experimental values for $\underline{W}$ are good.

The predicted and measured resistance matrices are similar, but the comparison is not exceptional at any frequency. Below 1.2Hz the prediction is consistently smaller. Above 1.5Hz the discrepancy is quite large, although in this region the wave tank was often close to its angular limits and $\underline{W}$ was not determined for some angles.

Comment

At low frequency the predicted maximum efficiency is much less than the point absorber limit (see figure 6.1), suggesting that the force coefficient vector could be larger or the radiation resistance smaller (see equation 1.20). It is in the same region that both predictions for the radiation resistance matrix are indeed always smaller than the values measured by direct experiment. This discrepancy could be due to a phase error in the measurement of the duck's motion. Alternatively it may result from other loss terms, perhaps acting in parallel with the hydrostatic spring, which do not produce radiated waves.

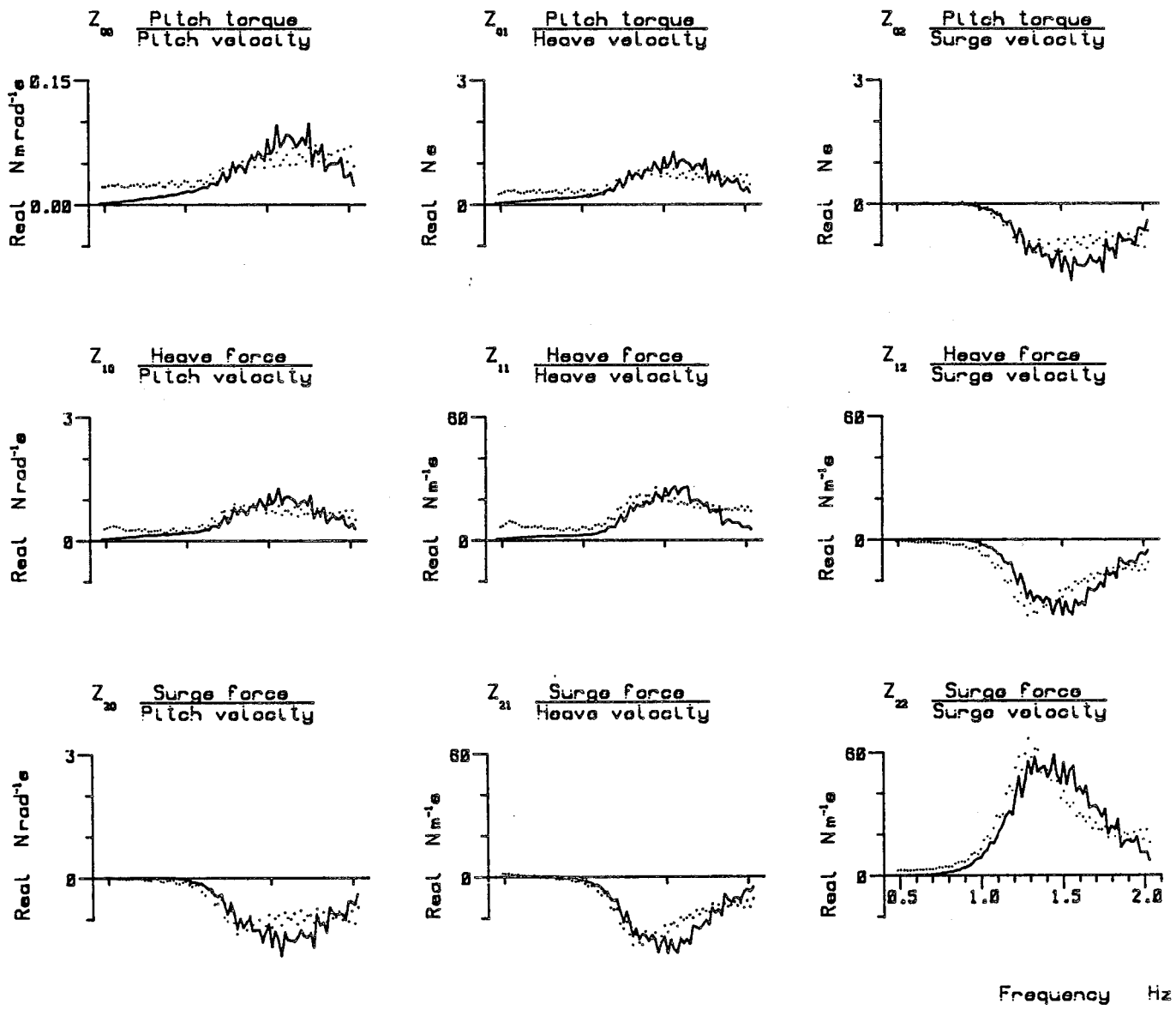

Figure 4.6 Predicted radiation resistance from force coefficient vector

Removal of reflection noise from the force coefficients

The force coefficient vector $\underline{W}(\omega,\alpha)$ was obtained by substituting experimental values into

$$\underline{F} = \underline{\underline{Z}}.\underline{u} + \underline{W}\, a$$

The matrix $\underline{\underline{Z}}$ was used with the ripple noise present and the amplitude a was assumed to be equal to the measured amplitude at the model position. These results are plotted again in the first row of graphs in figure 4.7 for the case of $\alpha = 0$.

When the tank is producing waves the smoothed values for $\underline{\underline{Z}}$ are appropriate and these are used to recalculate $\underline{W}$ with a as before. This set of curves is shown in the second row of figure 4.7

Next the true incident wave amplitude a is calculated from the measured amplitude c using the beach characteristic for parallel waves given in section 2.

$$a = (a'/c')\, c \qquad (4.8)$$

This value of a is now used in the calculation of $\underline{W}$ and the results plotted in the third row of figure 4.7. This set of values is the most appropriate to use when comparing predicted efficiencies with those measured in the tank.

When reflections from the beach are present not only is the wave height affected but also the forces felt by the duck. When the incident wave is at 0° and the reflected at 180° equation (1.7) can be extended

$$\underline{F} = \underline{\underline{Z}}.\underline{u} + \underline{W}(0)\, a + \underline{W}(\pi)\, b \qquad (4.9)$$

Similarly when the duck is turned through 180°.

$$\underline{F}' = \underline{\underline{Z}}.\underline{u}' + \underline{W}(\pi)\, a' + \underline{W}(0)\, b' \qquad (4.10)$$

a,b and a′,b′ are calculated from c and c′
$\underline{F},\underline{u}$ and $\underline{F}',\underline{u}'$ are measured and $\underline{\underline{Z}}$ is the smoothed impedance matrix

Equations (4.9) and (4.10) are solved for $\underline{W}(0)$ and $\underline{W}(\pi)$ and the resulting values for $\underline{W}(0)$ are shown in the fourth row of figure 4.7.

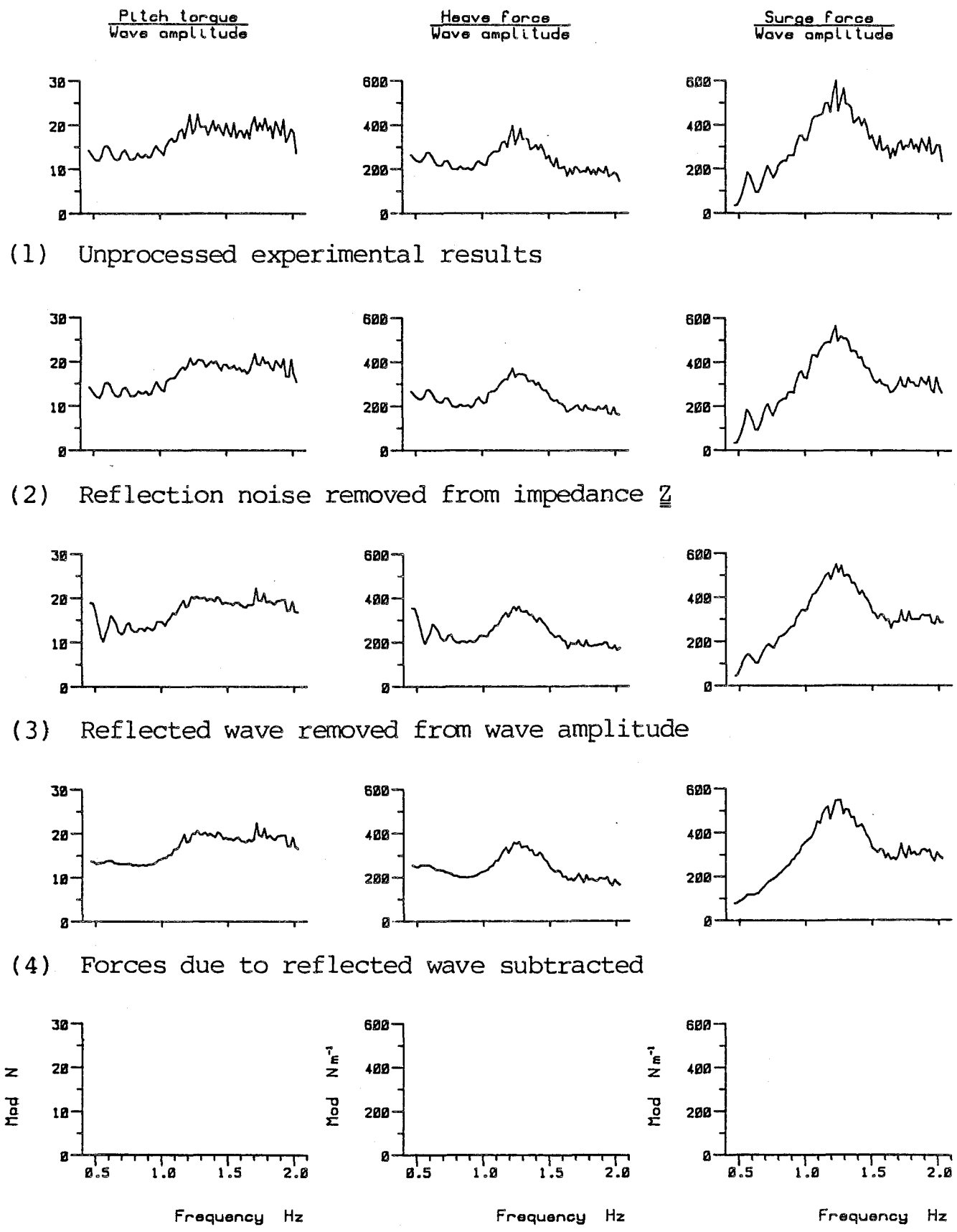

Figure 4.7 Force coefficient vector for regular waves. Removal of reflection noise

Force coefficient vector and the control matrix

In its definition the force coefficient vector $\underline{W}$ is independent of the way the duck is being controlled. Experiments were performed with different control parameters to judge the extent of this independance.

In figure 4.7 curves for the vector $\underline{W}$ are plotted from two separate experiments with different controllers. The measurements were made in regular parallel waves and the effect of beach reflections removed. In one case spring forces were applied in the surge direction allowing considerable motion, in the other the surge axis was fixed. The other control parameters were changed too and the sensitivity of the duck's motion to the parameters, particularly surge spring, can be judged by reference to Section 6.

The two sets of curves differ within the limits of tank repeatability, indicating that the separation of duck's behaviour into radiation impedance matrix, force coefficient vector and control matrix is valid.

Section summary

Tank noise reflections cause most of the experimental noise and are removed from the radiation impedance by a data processing method.

The radiation impedance matrix is very symmetric, showing that calibration and experimental are good, and suggesting that the linear approximation is valid.

The pattern of the radiated wave can be used to estimate the radiation resistance matrix with good agreement except at low frequency.

The force coefficient vector can be used to estimate the radiation resistance matrix with moderate agreement.

Reflection noise can be removed from the force coefficients by considering the beach reflections impinging on the rear of the duck.

The force coefficient vector can be found independent of the controller.

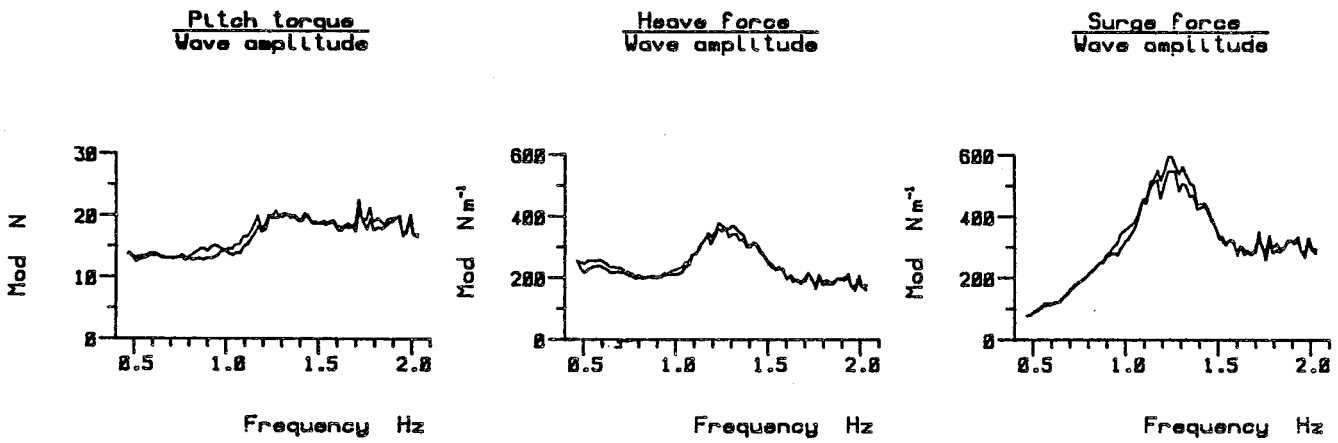

Figure 4.8 Force coefficient vector for regular waves

Modulus plotted

5) Comparison between measured and predicted efficiency

The accuracy of the mathematical model in the prediction of efficiency is checked under a range of conditions.

General remarks about the comparisons

There is a large amount of choice available when selecting the conditions under which to test prediction against measurement. The waves incident on the model were chosen to keep the motion linear and to cover a wide range of frequencies. The controller was implemented on the BBC computer and control values set so that efficiencies were fairly high. In all but one case power was extracted through pitch only.

Control functions

The control functions used on the BBC controller were

Pitch damping
Pitch spring
Heave spring
Surge spring

During the measurements the value for each was entered into the BBC by hand. Small amounts of heave and surge damping were also added or subtracted such that no power was extracted from these modes.

When a prediction is to be made the control function have to be converted into parameters of the control matrix $\underline{\underline{A}}$. Ideally this would be done by means of an equation of the type

$$\underline{\underline{A}} = \begin{bmatrix} D + \frac{S}{i\omega} & 0 & 0 \\ 0 & \frac{S}{i\omega} & 0 \\ 0 & 0 & \frac{S}{i\omega} \end{bmatrix}$$

However, there is a transfer function associated with both the BBC controller and the PHS rig mechanics, which is described in Section 2. This transfer function was used to modify $\underline{\underline{A}}$ before use. In addition the parameters of $\underline{\underline{A}}$ were also found by measurement in most cases.

Measurement of efficiency

The definition of efficiency given in Section 1, equation (1.24), is used here

$$\eta = \frac{\text{Power extracted}}{\text{Width x Power incident per metre}}$$

When measurements were carried out the mean power passing through the duck axis was calculated by approximating equation (1.12) with a sum

$$P = \frac{1}{m} \sum_{n=0}^{m-1} F(n).u(n) \qquad (5.1)$$

Where n is the sample number

m is the number of samples

The contribution due to the velocity offset was subtracted since this must have been introduced by the transducer or electronics.

The incident power was found by placing a wave gauge in the model position before or after the duck measurements. The heaving float gauge was used and its readings corrected using the angle and phase compensations described on page 29.

Prediction of efficiency

When predictions of efficiency were to be made the control matrix $\underline{\underline{A}}$ was first set up and then the efficiency function given in equation (1.25) used. This function should be thought of as a function of $\underline{\underline{A}}$, the appropriate radiation impedance matrices $\underline{\underline{Z}}$ and force coefficient vectors $\underline{W}$, and the sea state described as the superposition of a number of fronts.

$$\eta = \eta \left(\underline{\underline{A}}(\omega), \underline{\underline{Z}}(\omega), \underline{W}(\omega,\alpha), \text{sea} \right) \qquad (5.2)$$

Pitch efficiency in regular waves

Three small regular waves were chosen with low, middle and high frequency. The wave amplitude of 4mm was the same as that used in the determination of the force coefficientsand the wave angle 0°. In each of six cases one of the control functions was varied while the other three were held constant.

In figure 5.1 the crosses correspond to the measurements made in the tank. Since one frequency was being studied at a time the wave height was determined by placing two heaving float wave gauges a quarter wavelength apart. The incident wave height was taken as the mean.

The circles represent the prediction having determined the control matrix $\underline{\underline{A}}$ by measurement. The values in $\underline{\underline{A}}$ were found by dividing the fundamental force amplitudes by the fundamental velocity amplitudes. The predictions were made using the smoothed values of the impedance $\underline{\underline{Z}}$ and the values of the force vector $\underline{W}$ in the presence of beach relections.

The continuous curves were drawn by first calculating $\underline{\underline{A}}$ with the controller and rig transfer function, then evaluating the efficiency function.

The abcissa in each case is the measured control parameter as this is considered to be the most important.

The only major discrepancy between measurement and prediction occurs in the middle right graph, when the rig transfer function is inadequate not the mathematical model. Overall the efficiency function predicts very well under these conditions, within the limits of tank repeatability.

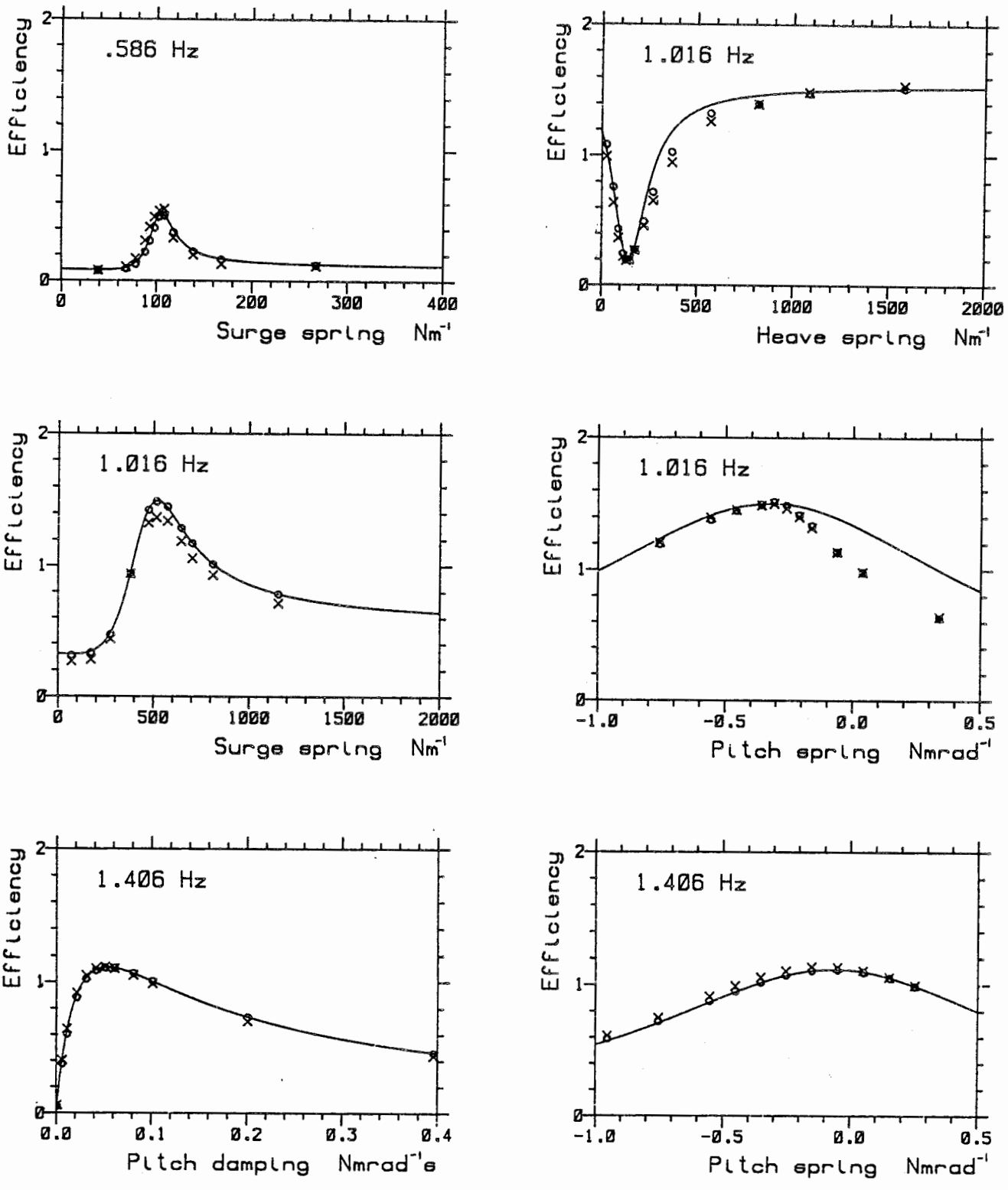

Figure 5.1 Pitch efficiency in regular waves
Prediction and measurement

Pitch efficiency in small mixed seas

Two Pierson-Moskowitz spectra with Mitsuyasu spreading were selected with the rms wave height much smaller than for the normal PM. In each of four cases one of the control functions was varied as the other four were held constant. The extra control function in these experiments was surge damping.

In figure 5.2 the crosses represent measurements made when the model was controlled in the appropriate test sea in the tank. The incident power was found by replacing the duck with a heaving float wave gauge, Fourier transforming the time series and calculating the power frequency by frequency. A predicted angle correction was applied to the sum and no account was taken of beach reflections.

The circles correspond to predictions made after detemining the control matrix $\underline{\underline{A}}$ from the measurements. The values of $\underline{\underline{A}}$ were found by dividing the force and velocity ampliudes at a central frequency. The experimental values for the impedance $\underline{\underline{Z}}$ and the force vector $\underline{W}$ from Section 2 were used with no further processing, $\underline{W}$ being available at ten degree intervals up to seventy degrees and found at intermediate angles by interpolation.

The smooth curves were plotted by first calculating $\underline{\underline{A}}$ at each frequency using the controller and rig transfer function and then evaluating the efficiency function.

The abcissa in all the graphs is the measured control parameter.

The predictions tend to be slighty greater than the measurements, but this is within the limits of tank repeatability and is not significant. Overall, the agreement is good, particularly in the positioning of peaks and troughs.

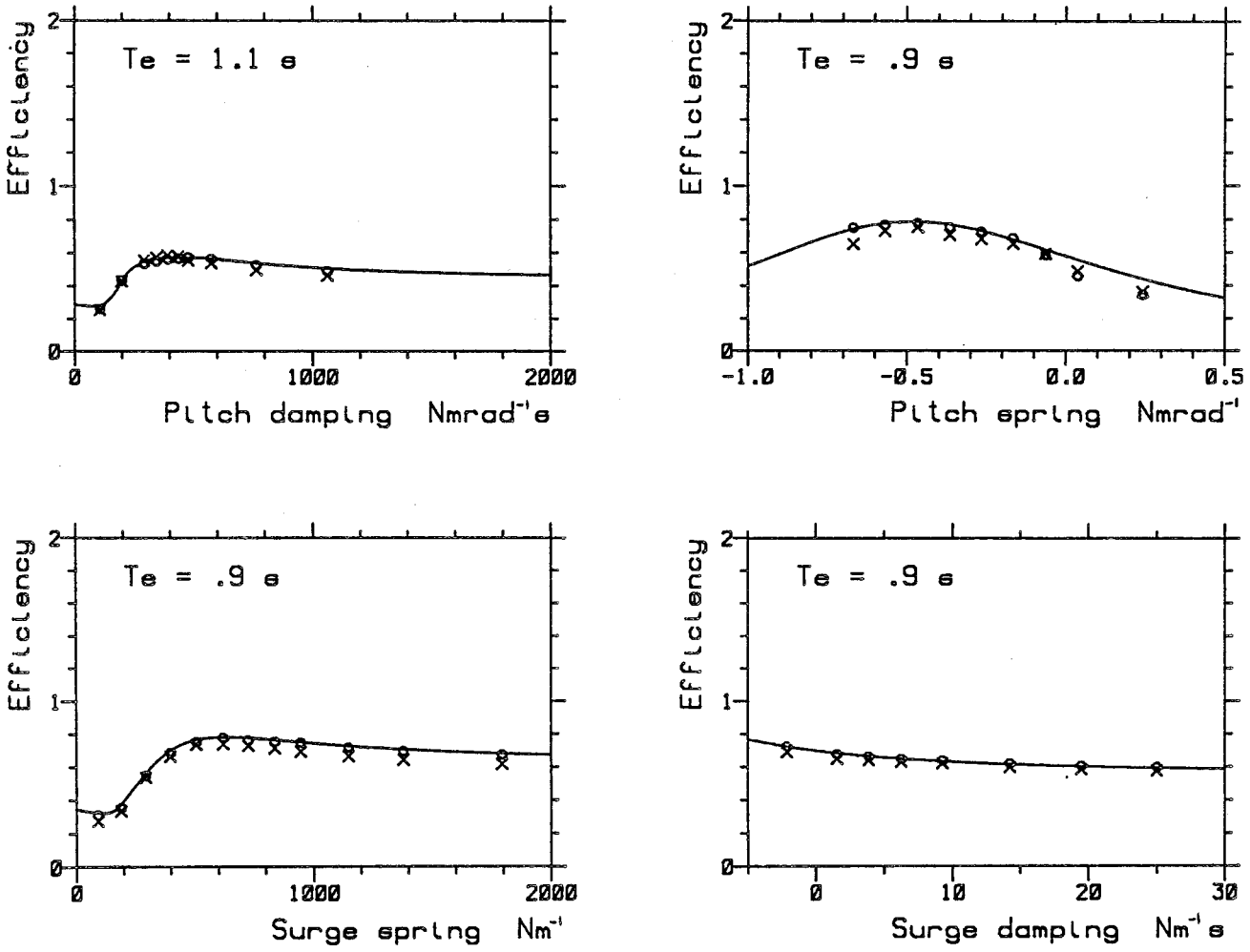

Figure 5.2 Pitch efficiency in small PM spectra
Prediction and measurement

Maximum pitch efficiency in regular waves

In previous work, the highest efficiencies found in small regular waves over a range of frequencies have been used to judge a shape's potential. In this comparison pitch efficiency was maximised in the tank and in the mathematical model. The method of optimisation was essentially the same in both cases.

Efficiency was maximised at each of 32 frequencies in the tank and 81 in the mathematical model. The wave height used was 4mm, the same as in the determination of the force coefficients. All four control functions were allowed to have variable settings.

The crosses in figure 5.3 show the highest efficiencies and best settings found when varying the control parameters by hand on the BBC controller. Initial values were set from experience and to save time most effort was concentrated on a few frequencies, the control values for the rest being found by interpolation. The wave amplitude was measured with the heaving float gauge placed in the model position, then corrected for beach relections using the beach characteristic described on page 25.

The circles correspond to the best efficiencies and control parameters predicted from the efficiency function. The starting values for each parameter were the same for each frequency and the optimum was found by the simplex method which was described by Nelder and Mead (1965). A maximum was reached in all cases but one.

The comparison for each control parameter is limited because the other parameters are not necessarily the same. The importance of any discrepancy between their values depends on the flatness of the efficiency response surface in that area.

The two methods produce very similar efficiency curves, well within the limits of wave repeatability, except at high frequency. The simplex maximisation the efficiency function is more reliable if many frequencies are to be optimised.

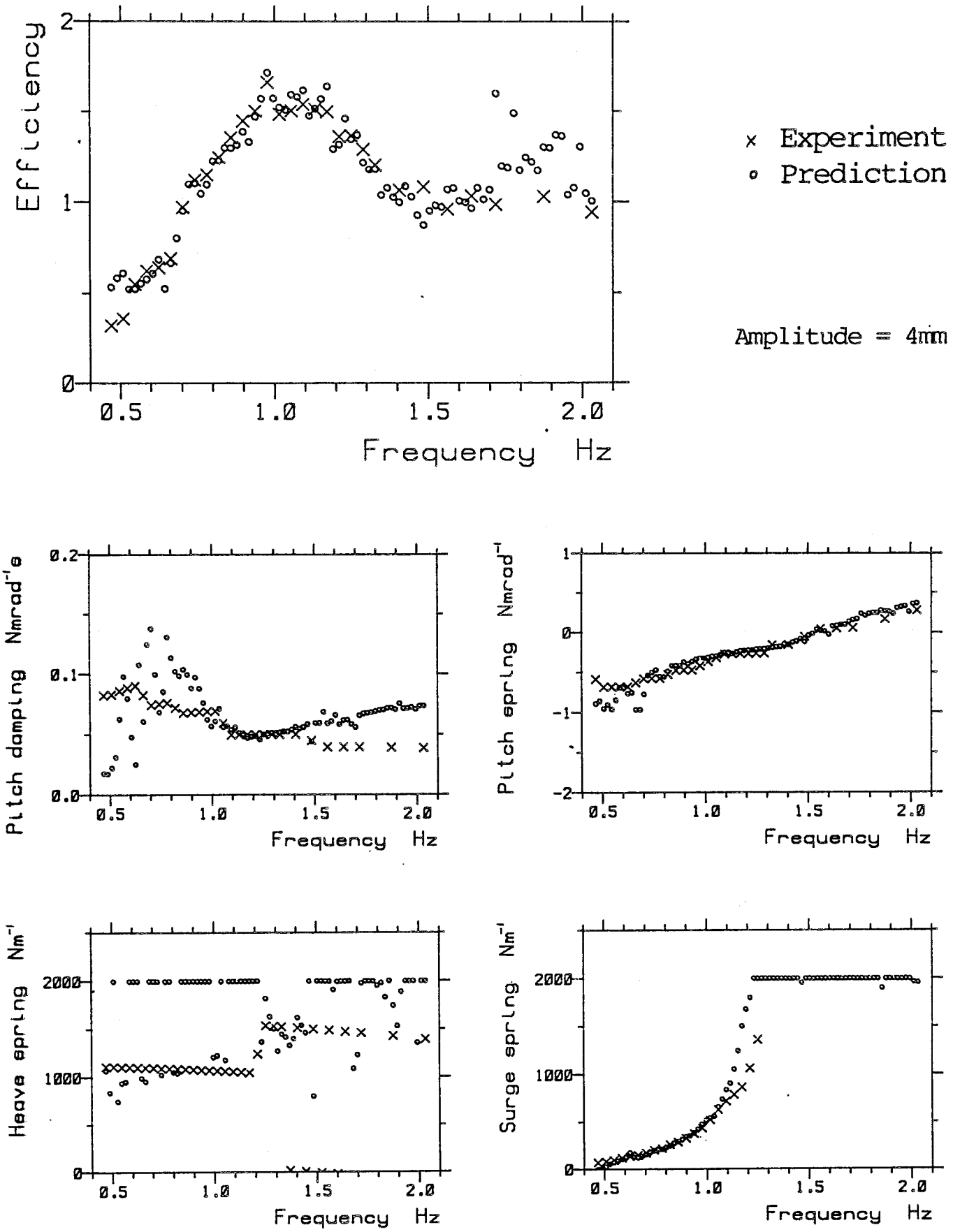

Figure 5.3 Maximum pitch efficiency and best control parameters in regular waves

Maximum pitch efficiency in small mixed seas

A set of reduced Pierson-Moskowitz seas were selected and efficiency maximised in the tank and with the mathematical model. The sea making parameters were chosen to make the waves small and so that there was only one front on each frequency.

Te	Hrms multiplier	Representation for Energy	Number of fronts	Repeat time
0.5	.7	.4	75	51.2
0.6	.6	.4	70	51.2
0.7	.5	.4	70	51.2
0.8	.4	.4	68	51.2
0.9	.3	.4	60	51.2
1.0	.3	.4	60	51.2
1.1	.2	.4	55	51.2
1.2	.15	.4	55	51.2
1.3	.1	.4	50	51.2

The crosses in figure 5.4 represent the highest efficiencies and best settings found while varying the BBC contol parameters. The incident power was calculated from a heaving float wave gauge placed in front of the model with an appropriate angular correction.

The circles show the best values obtained by optimising the efficiency function with the simplex method. The control parameters are predicted well, but the efficiency is consistently greater than that found in practice.

Summary

The shape of the efficiency surface can be predicted within the limits of tank repeatability for regular waves and small mixed seas.

The maximum possible efficiency using a simple controller with four parameters can be predicted well in regular waves, not so well in mixed seas.

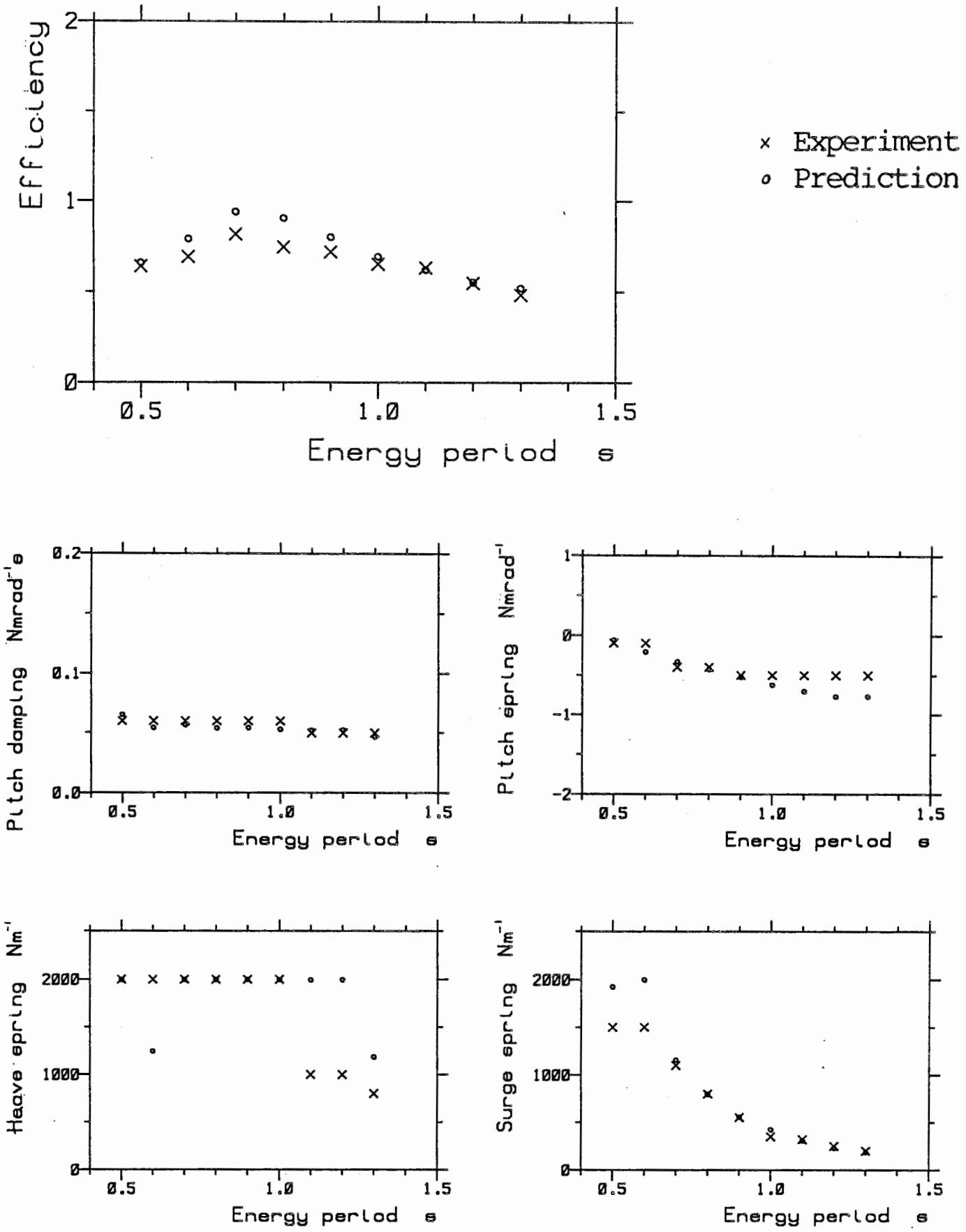

Figure 5.4 Maximum pitch efficiency and best control parameters in small PM spectra

6) Predictions from the efficiency function

The efficiency function defined in the first section and using radiation impedance and force coefficient measurements has been shown to predict selected parts of the response surface adequately for small amplitudes. Now it is used to make further predictions about the nature of the response surface.

Maximum efficiency in regular waves

Figure 6.1 contains predicted maximum efficiencies for the duck model in regular waves compared to the point absorber. The lower rough curve was obtained by varying pitch damping and pitch, heave, surge spring until a maximum was found. It was shown to be achievable on page 63. The upper rough curve assumes the complex conjugate controller with all eighteen control parameters and power extraction from each mode.

For comparison there are curves for a two degree of freedom point absorber and the 'sum' of the point absorber with a device which extracts all the energy in its own width. The latter is a guess at the advantage of finite width.

Maximum efficiency in Pierson-Moskowitz spectra

The efficiency function was maximised for a range of PM spectra with Mitsuyasu spreading by summing the contributions of each frequency. The curves plotted against the energy period Te in figure 6.2 are the best predicted for two controllers along with two theoretical predictions, the order of the curves being the same as above. The curve corresponding to the complex conjugate controller does not reach the same maximum as for the regular wave case because the efficiency drops with angle and the frequency convolution smoothes out the peaks. The discrepancy between this curve and that for the 'springs and damper' controller is increased since the latter controller's frequency dependence is not the best possible.

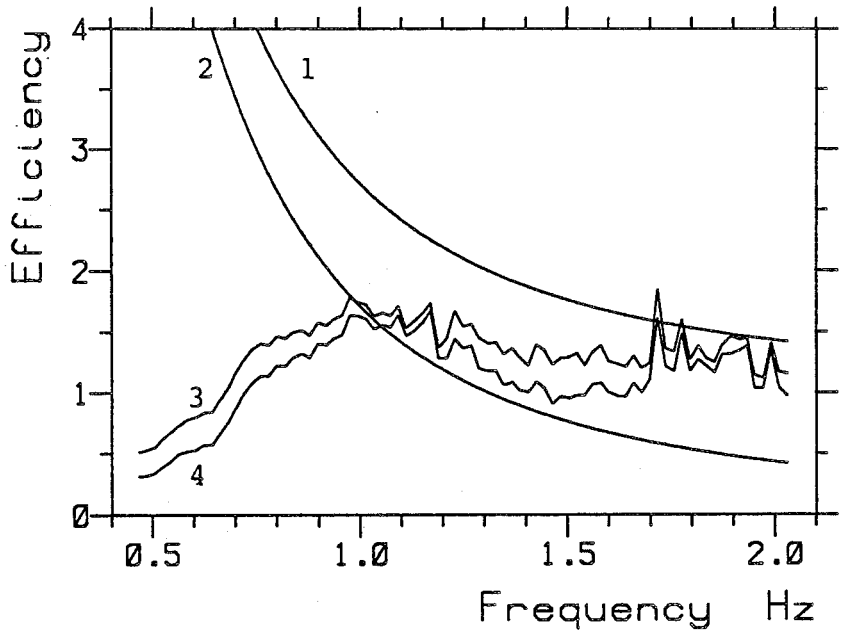

Order of curves

1) Point absorber
2) Point absorber '+' 1
3) Duck with complex conjugate controller
4) Duck with 4 term controller

Figure 6.1 Maximum efficiency in regular waves

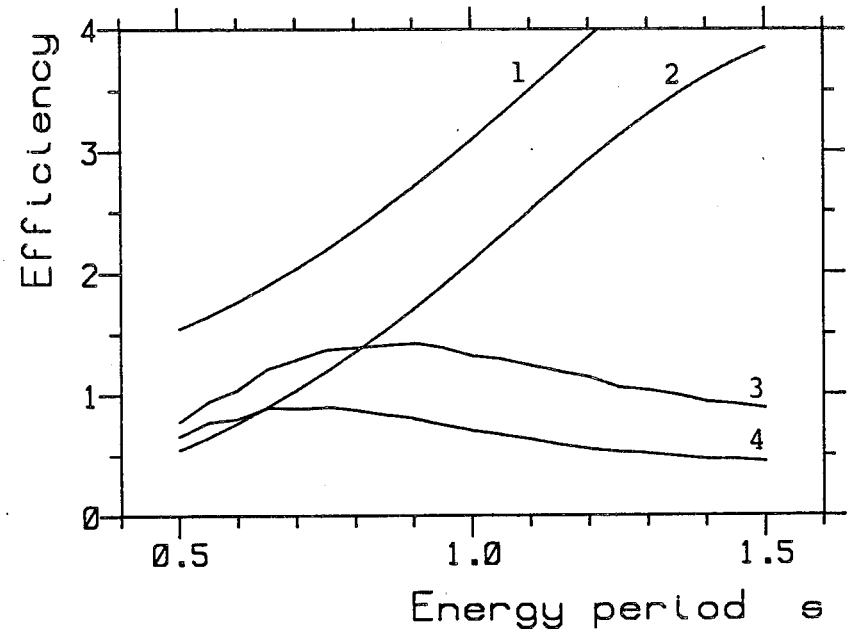

Order of curves

1) Point absorber
2) Point absorber '+' 1
3) Duck with complex conjugate controller
4) Duck with 4 term controller

Figure 6.2 Maximum efficiency in small PM spectra

Maximum efficiency in angled regular waves

The efficiency function was set up using the force coefficents for angled waves shown in figure 3.5. No attempt was made to remove reflection noise as this can only be achieved satisfactorily for waves parallel to the wave makers. The maximum of the function was found for the complete controller and for two reduced cases.

In the left hand column of figure 6.3 the maximum total efficiency predicted for the complex conjugate controller is plotted. The middle column contains the maximum obtained when the controller was constrained to have just four terms, pitch damping and pitch, heave, surge spring rates. On the right is the maximum efficiency for the controller with pitch damping and spring only, the other modes being fixed.

When waves are incident from the front the complete controller with eighteen terms performs only slightly better than that with four. The controller with just two terms compares badly in the region 0.7Hz to 1.2Hz, because the duck cannot move in surge. The advantage of surge motion at these frequencies can either be thought of as the transfer of power through the water from the surging motion to pitch, or further cancellation of the incident wave by the radiated wave due to surge.

For angles above 90° the amount that can be absorbed by pitch alone is small, whereas the complex conjugate controller can extract about as much as from in front.

It is useful to consider the duck's radiation as a combination of two waves, one circularly symmetric and the other with opposite sign in front and behind, with power being absorbed when the radiated wave interferes with the incident wave. It follows that the maximum absorption should be the same at 0° and 180° and should be reduced at 90° when only the circular wave has effect. This ignores the diffraction of the incident wave which will change with angle.

When power is absorbed through all the modes, the symmetry of the maximum efficiency curves for waves incident from the front or rear is an indication that subtle shape variations are not very important.

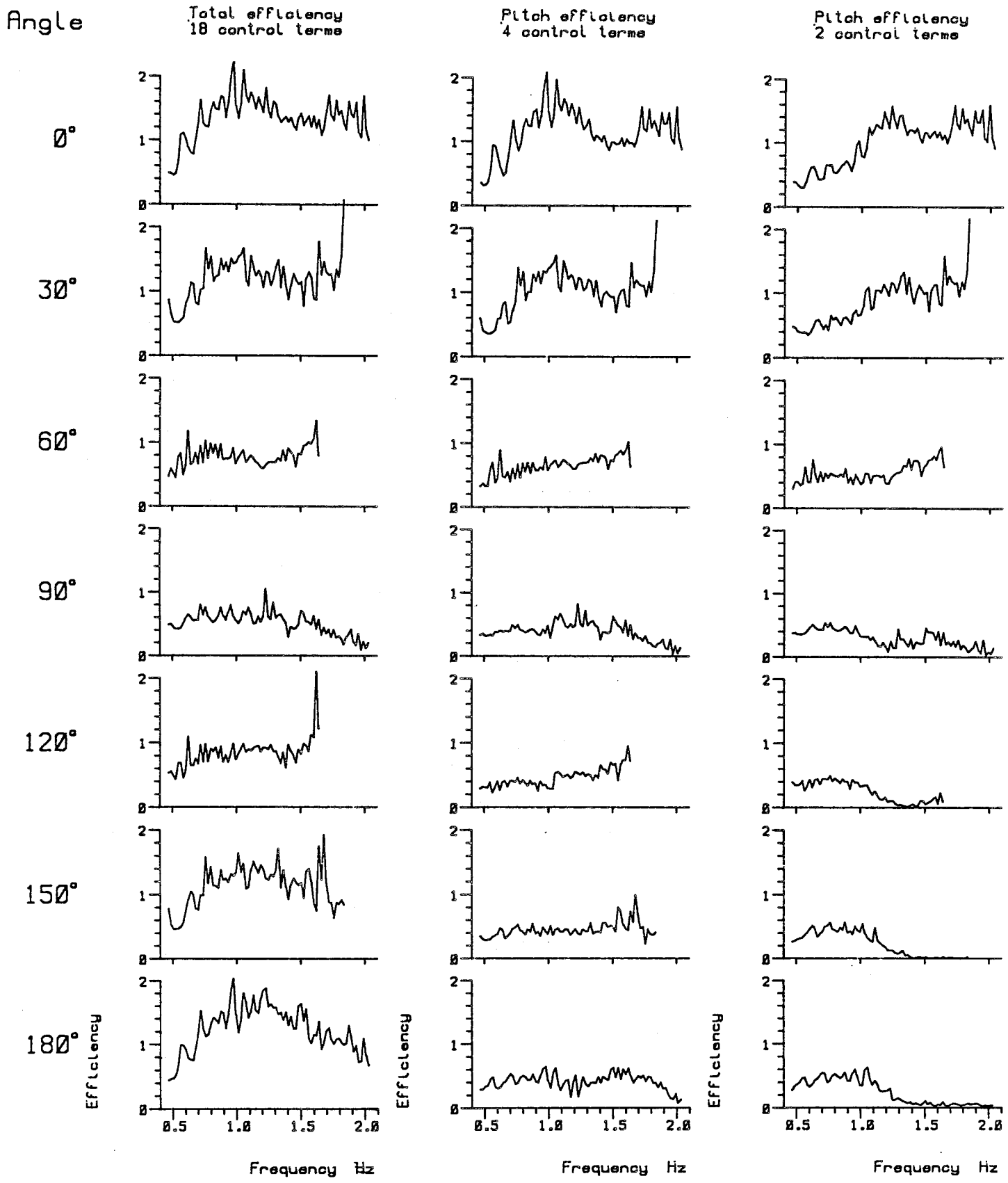

Figure 6.3 Maximum efficiency in angled regular waves

Deviations from maximum efficiency in regular waves

It is not possible represent the 18 dimensional efficiency surface graphically, even at one frequency. However, some of the control parameters have characteristic effects which are noted here.

The parameters of pitch damping and pitch, heave and surge spring which maximised efficiency at 1 Hz were found. Figure 6.4 shows the effect of varying each of the control values away from this set. The parameters are varied in pairs, real and imaginary, with each pair corresponding to one term of the control matrix $\underline{\underline{A}}$. Note that in the optimisation only four of the diagonal components were allowed to vary, the rest being left at zero.

Where the efficiency drops below zero it is plotted as zero. The real part of each control term corresponds to damping and the imaginary part to inertia or negative spring. To convert from the imaginary part to inertia or spring multiplication by or division by negative is required respectively.

The pitch surface shows the characteristic form in the imaginary part with the peak occuring in the region of negative spring. This peak is quite senstitive to frequency because of the frequency dependence of the corresponding component in the impedance matrix. In the direction of the real part the curve rises sharply then falls slowly, the maximum being fairly insensitive to frequency.

The surface has a minimum, nearly zero, at a low value of heave spring and maxima when the heave spring rate is very high or the inertia large. Conversely, the surface shows maximum for a finite value of surge spring tailing off to a constant value as the spring rate increases. The effect of these two parameters is of the same form at most frequencies.

The other curves are draw for completeness although in this part of the space it seems that the best values on each are at zero.

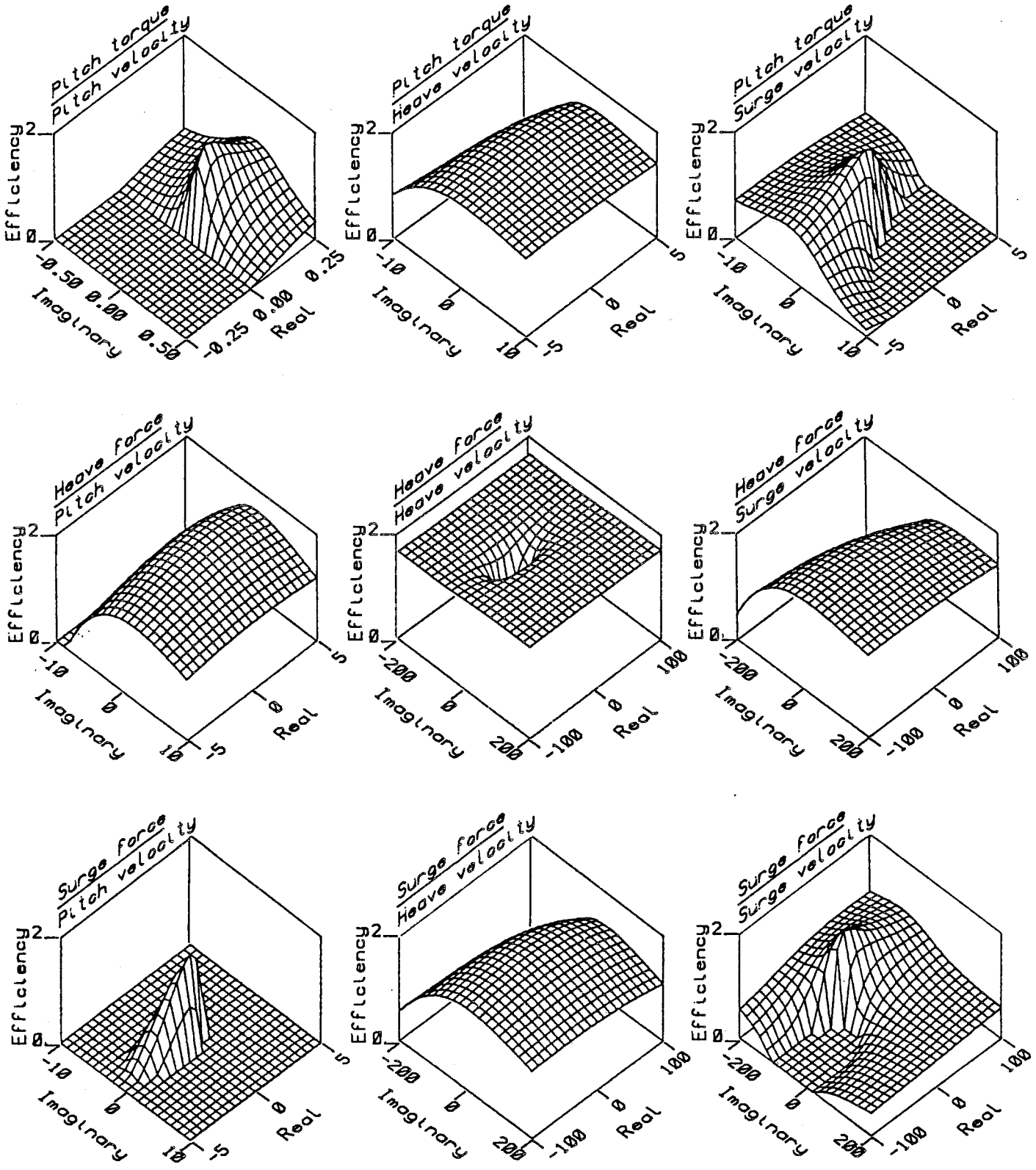

Figure 6.4 Efficiency surfaces for a 1Hz regular wave

Sensitivity of control parameters to frequency

Perhaps the most important consideration when designing a controller is the effect of frequency. It is relatively easy to achieve high efficiencies at an individual frequency, but settings which yield good results at one may perform badly at another. In a mixed spectrum the aim is to extract the available power at all the frequencies simultaneously.

An example of a control function which does not transfer well to mixed spectra is surge spring. Figure 6.5 shows how the efficiency surface varies with frequency and surge spring rate. The other control functions of pitch damping, pitch spring and heave spring are not being held constant, but set to their best values for each frequency.

The left hand portion of the surface is the most important, particularly the ridge which runs up the page. The aim in a mixed sea is to be on the top of this ridge throughout the spectrum. Clearly this is not possible for surge spring and when the best efficiencies are found in spectra considerable blurring of the ridge occurs.

Figure 6.6 contains the best efficiency surface plotted for PM spectra against energy period and surge spring rate. The reduction of the peak occurs mainly for the reason described, partly because of similar effects with other parameters and also because of reduction in efficiency with angle.

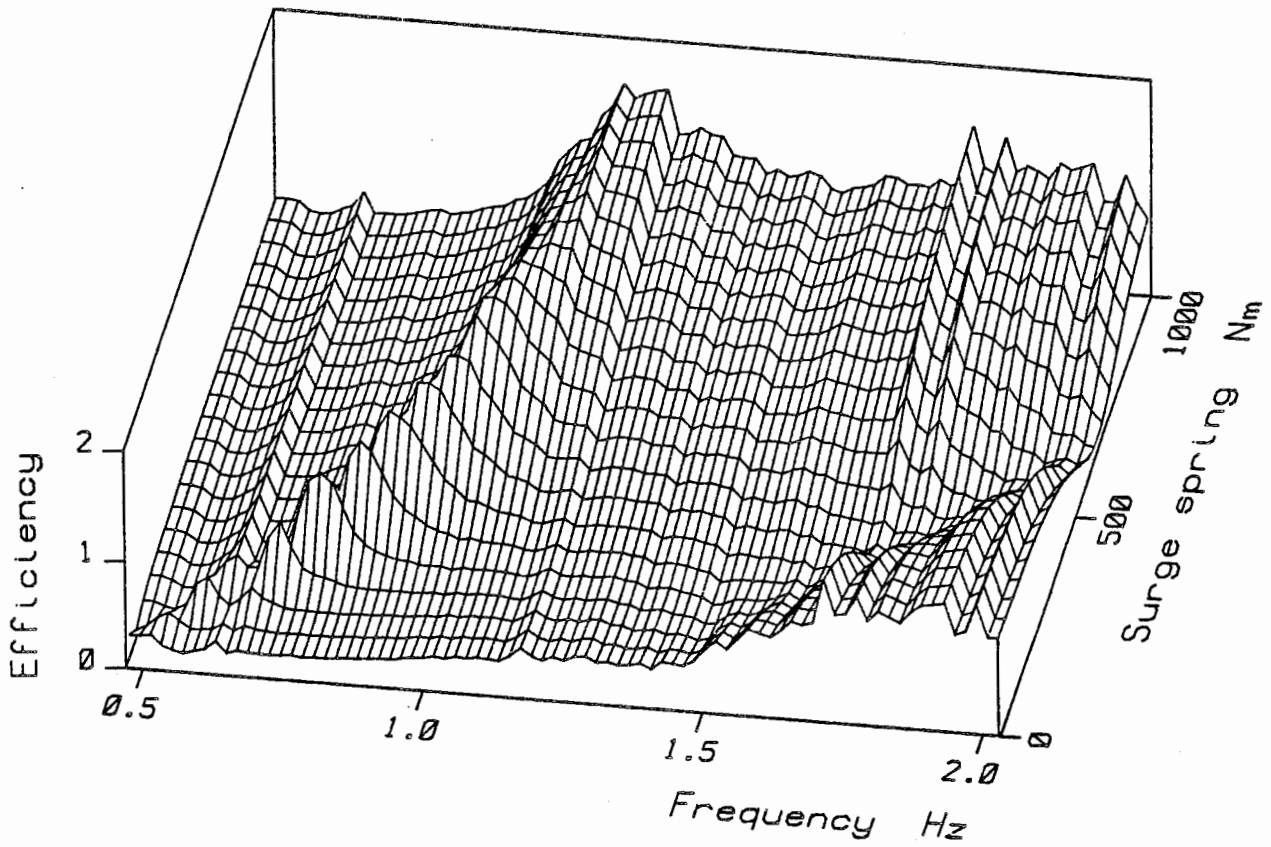

Figure 6.5 Efficiency surface in regular waves versus surge spring

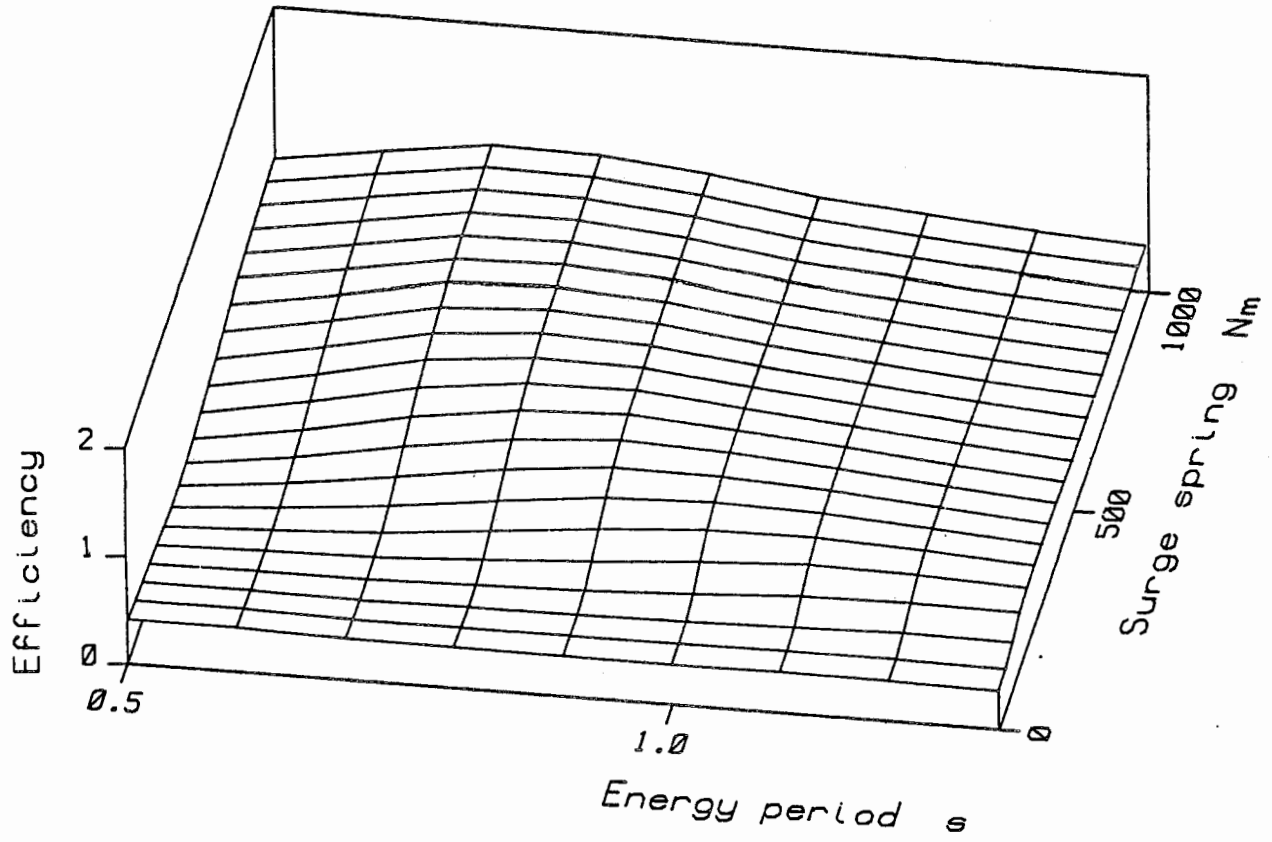

Figure 6.6 Efficiency surface in small PM spectrum versus surge spring

Rotation of coordinate system

The coordinate system chosen for model testing is not necessarily the most appropriate at full scale. In particular the duck may be moored by lines to the sea bed, perhaps at 45°, in which case the heave, surge coordinates are best rotated.

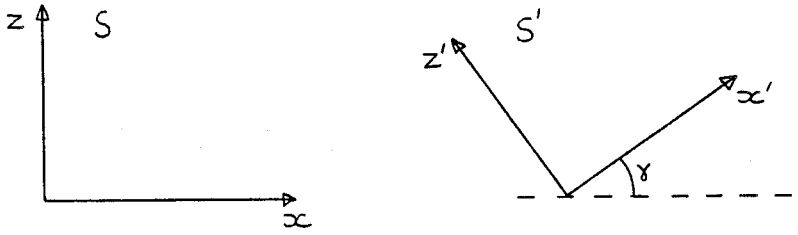

Rotation of the axes from S to S′ is effected by the rotation matrix $\underline{\underline{L}}$

$$\underline{X}' = \underline{\underline{L}}.\underline{X} \qquad \begin{bmatrix} \theta' \\ z' \\ x' \end{bmatrix} = \begin{bmatrix} 1 & 0 & 0 \\ 0 & \cos\gamma & -\sin\gamma \\ 0 & \sin\gamma & \cos\gamma \end{bmatrix} \begin{bmatrix} \theta \\ z \\ x \end{bmatrix} \tag{6.1}$$

The control matrix $\underline{\underline{A}}$ can be rotated into the new coordinate system by using $\underline{\underline{L}}$ twice

$$\underline{\underline{A}}' = \underline{\underline{L}}.\underline{\underline{A}}.\underline{\underline{L}}^{-1} \tag{6.2}$$

And

$$\underline{\underline{A}} = \underline{\underline{L}}^{-1}.\underline{\underline{A}}'.\underline{\underline{L}} \tag{6.3}$$

Rewriting (6.3) in full

$$\underline{\underline{A}} = \begin{bmatrix} 1 & 0 & 0 \\ 0 & \cos\gamma & \sin\gamma \\ 0 & -\sin\gamma & \cos\gamma \end{bmatrix} \begin{bmatrix} A'_{00} & A'_{01} & A'_{02} \\ A'_{10} & A'_{11} & A'_{12} \\ A'_{20} & A'_{21} & A'_{22} \end{bmatrix} \begin{bmatrix} 1 & 0 & 0 \\ 0 & \cos\gamma & -\sin\gamma \\ 0 & \sin\gamma & \cos\gamma \end{bmatrix} \tag{6.4}$$

For the case of diagonal terms in $\underline{\underline{A}}'$ only

$$\underline{\underline{A}} = \begin{bmatrix} p & 0 & 0 \\ 0 & \cos^2\gamma\, h + \sin^2\gamma\, s & \cos\gamma \sin\gamma\, (s-h) \\ 0 & \cos\gamma \sin\gamma\, (s-h) & \sin^2\gamma\, h + \cos^2 s \end{bmatrix} \tag{6.4}$$

In this way mooring lines may be simulated. Figure 6.7 contains predicted efficiency surfaces in a 1.1 second PM spectra as the spring rates of the mooring lines are varied for different angles of rotation. The same values for pitch damping and pitch spring are used throughout.

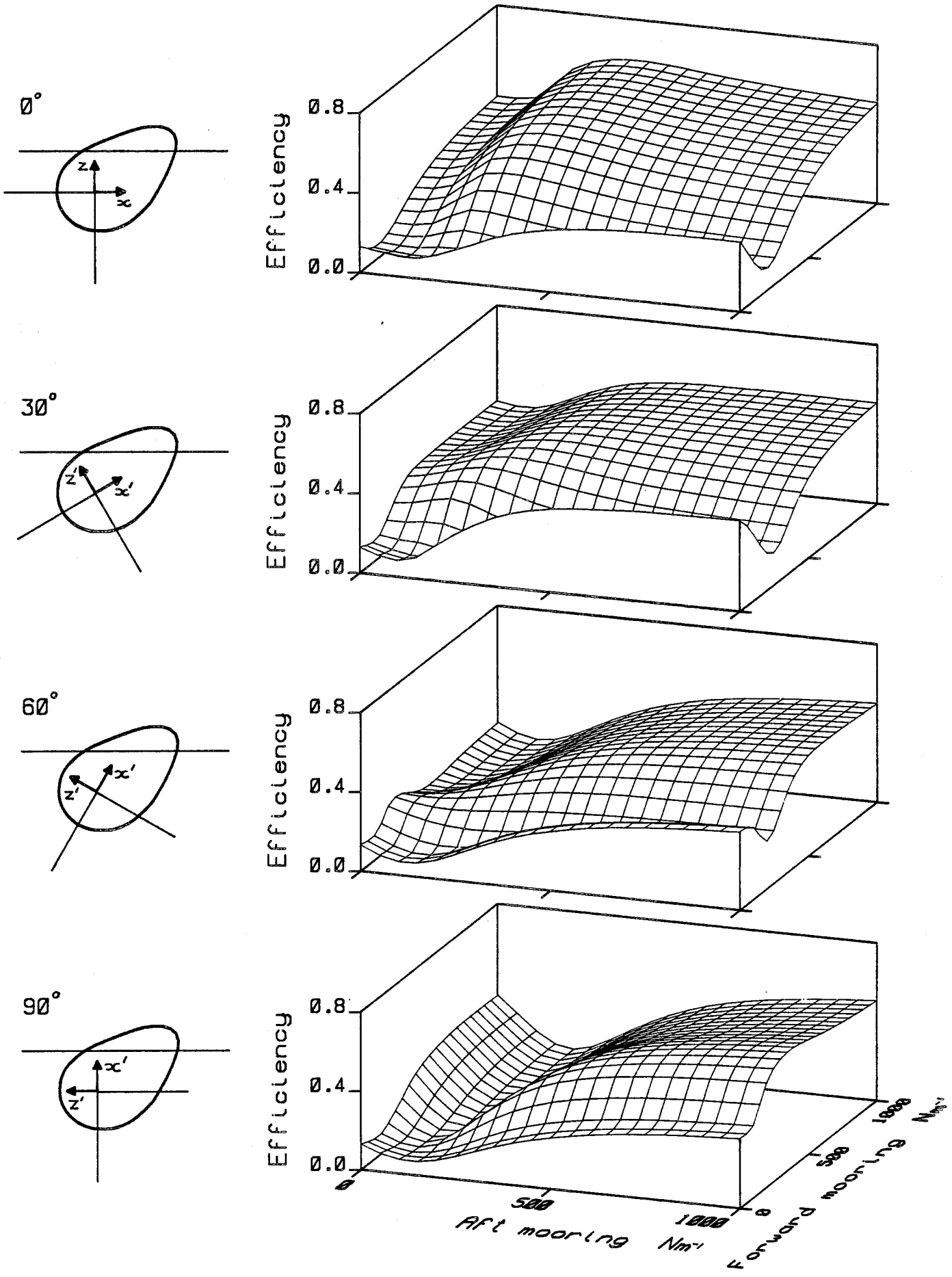

Figure 6.7 Efficiency in 1.1s PM versus mooring spring rates

7) A full-scale application

An upper limit for the efficiency of the duck in a set of sea spectra is presented as a function of scale.

The South Uist '399' spectra

In March 1976 the Institute of Oceanographic Sciences began a wave data collection programme. They deployed a Datawell Waverider buoy in about 42 m of water at site 8 nautical miles to the west of South Uist in the Outer Hebrides. The data collected comprises the surface elevation measured every 3 hours for a period of about 15 minutes. Complementary wind data was also available from meteorological records.

By comparison with the long term annual wind statistics Crabb (1979) selected 399 wave records to represent a typical year and converted them to frequency distributions. Components in each spectra were identified as being due to local wind conditions, wind conditions just before sampling and distant storms.

Using a frequency dependent correction (Mollison 1983), we have modified the raw spectral data to 100 m depth. Each spectrum is described as the sum of Pierson Moskowitz components with spectral width compression factor and angular spreading distribution type. The spectral parameters are set so that if a depth water Pierson Moskowitz is generated the power distribution matches that assumed for 100 m water depth.

A typical South Uist spectrum

In figure 7.1 the amplitude squared distribution is plotted for one of the spectra, number 86. The original spectrum is shown along with that generated from the statistical parameters. The curves show the form of the energy distribution.

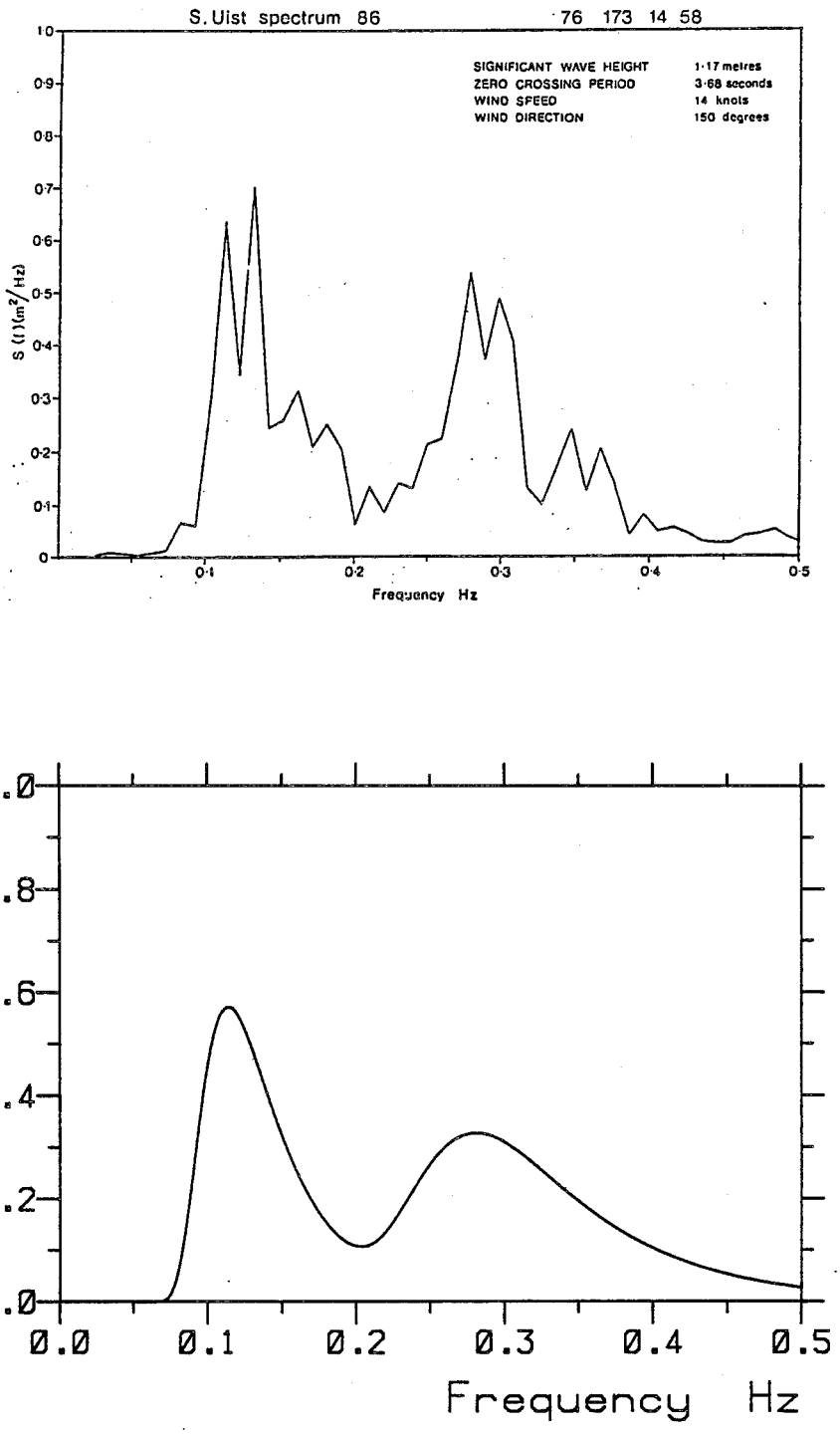

Figure 7.1 South Uist spectrum 86. Measured and fitted

Wave height and available power

The '399' set is taken to represent a typical year and comprise sea states ranging from winter storms to summer calms all with equal weighting.

Figure 7.1 shows the fraction of the year when a particular rms wave height is exceeded. The geometric linearity of the duck depends upon the ratio of wave height to duck size, along with other factors.

Figure 7.2 gives the fraction of time that a given power level is exceeded. The area under the curve is the mean annual incident power, assuming no power limit. Only 25% of the seas have power levels above the mean, but these account for 75% of the annual power.

The seas are arranged in different orders to produce each graph, but the order is only slightly different. The energy period distribution also correlates well with that for power and rms amplitude. Since power depends on period and the square of amplitude, its own distribution is more heavily dominated by the largest seas.

The economic power limit will probably be near the mean annual incident power. Care must be taken to ensure that the high power seas do not distort any initial assessment of duck performance, since when the duck is working at its power limit linear efficiency does not matter.

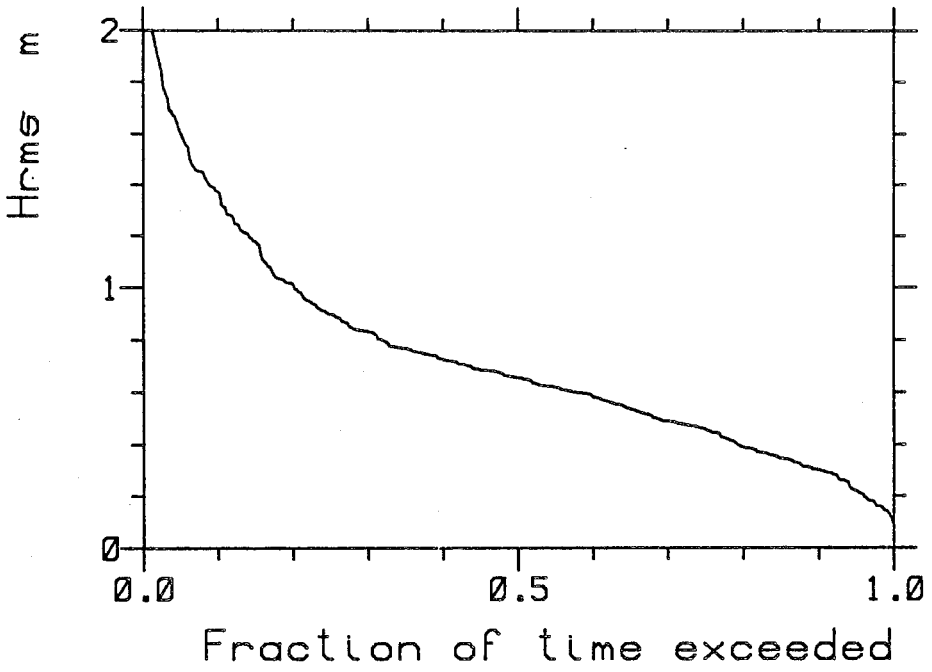

Figure 7.2 Rms amplitude distribution in the '399' spectra

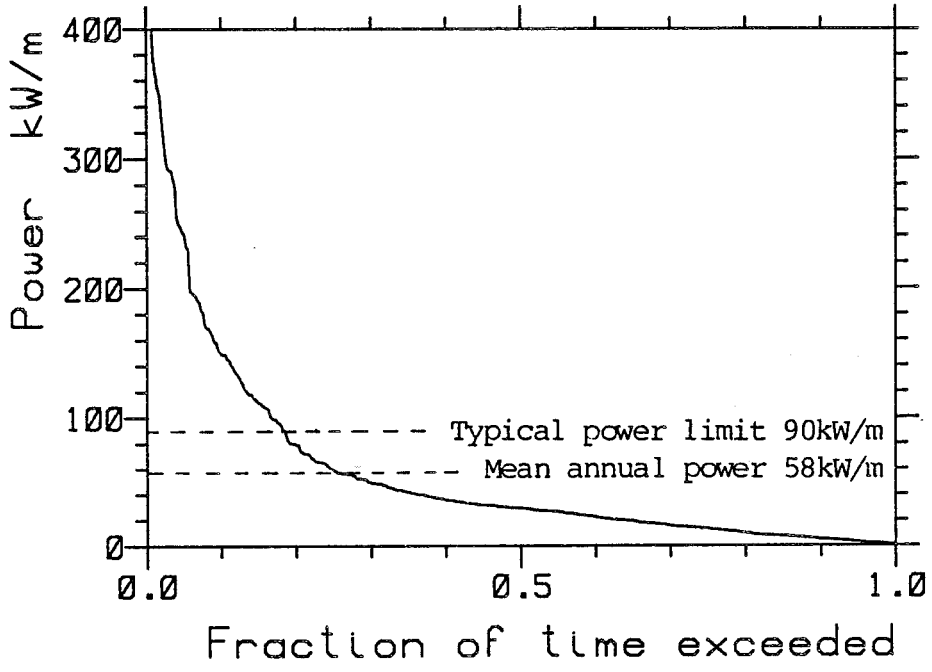

Figure 7.3 Incident power distribution in the '399' spectra

Duck efficiency on the '399' weighted period axis

The '399' weighted period axis is produced by deforming the period axis so that the distance between points is proportional to the power available in the 399 spectra in that interval.

The maximum efficiency curve (figure 6.1) is replotted against full scale period in figure 7.3. Curves are drawn for three different scales, transformed from model scale after dividing frequency by the square root of scale factor. The area under the curve is proportional to the mean annual efficiency, assuming no power limit, linear behaviour and no change of efficiency with angle.

In figure 7.4 the same efficiency curves are plotted assuming an arbitary power limit of 1.5 times the mean incident power. In the production of the weighted period axis all seas with power greater than this limit are disregarded, since it is does not matter what the duck's efficiency is when its power output is limited.

The efficiency curves drawn against the power limited weighted axis give a good idea of how useful a particular efficiency curve might be at full scale. A guess for the best scale factor from this graph is might be around 100.

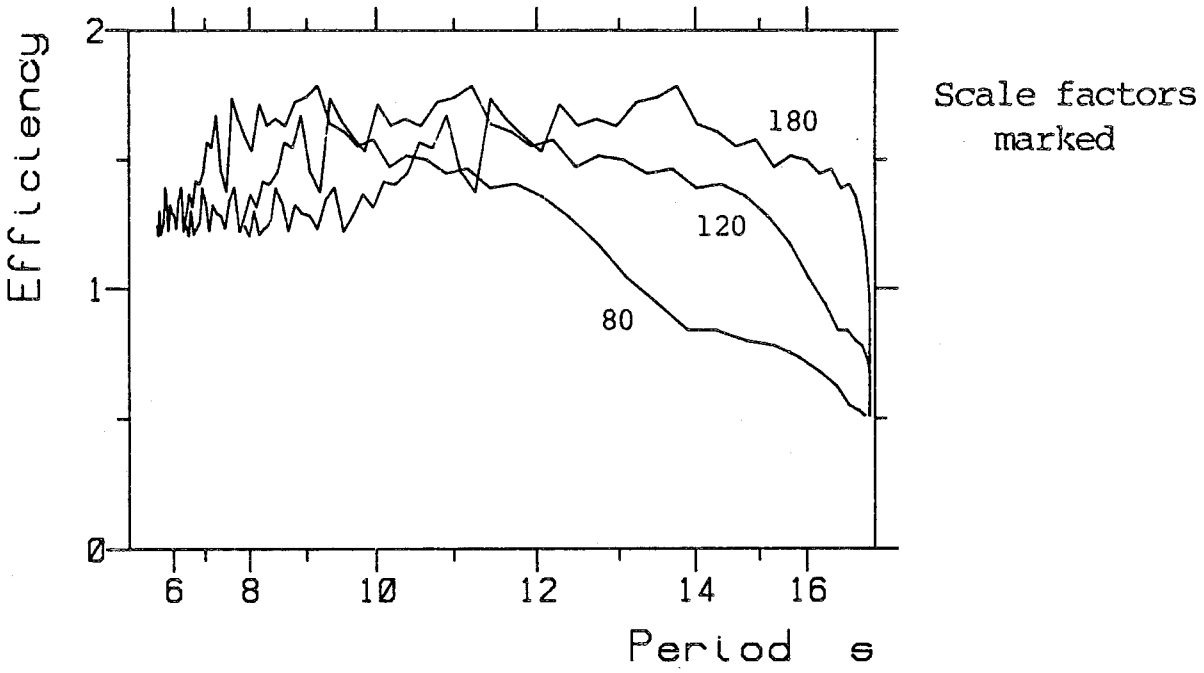

Figure 7.4 Maximum efficiency on the '399' weighted period axis

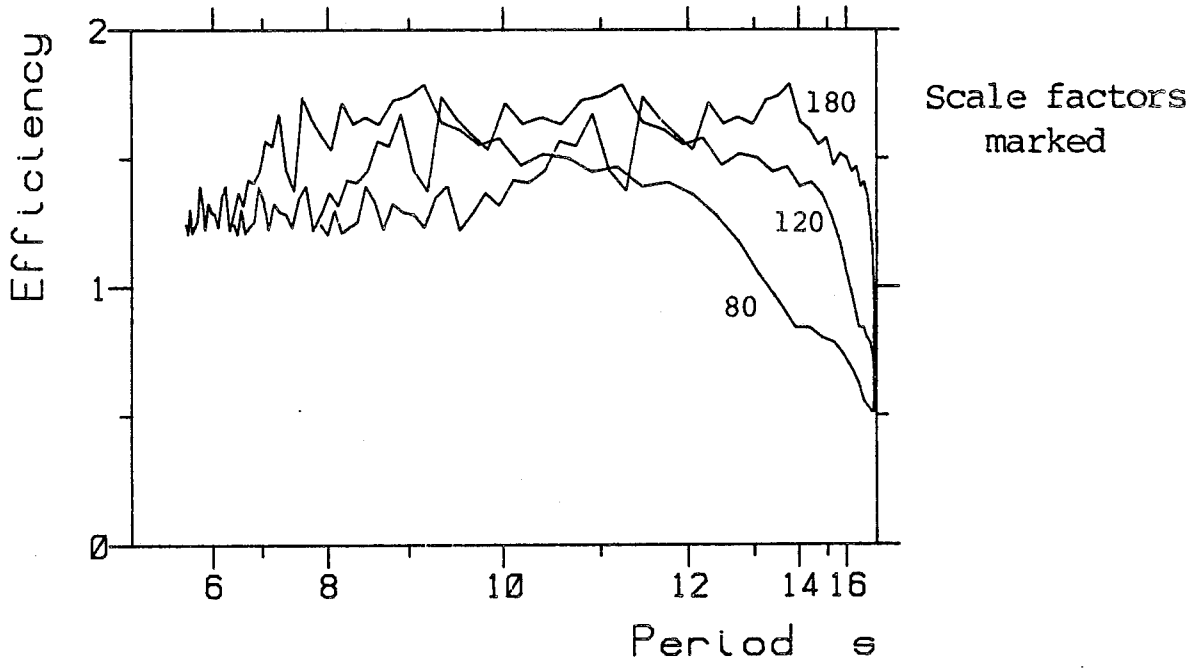

Figure 7.5 Maximum efficiency on the power limited '399' weighted period axis

The effect of scale

In figure 7.5 the mean annual efficiency is plotted against scale factor for three different power limits. The curves are obtained by scaling the linear efficiency curves drawn in figure 6.3 and calculating the extracted power in 46 of the '399' directional spectra.

The 46 spectra selected are those chosen by Rendal, Palmer and Tritton (1981) to reflect the principal characteristics of the 399 and are used because our present '399' data set is incomplete.

The top curve is for the case of no power limit. It assumes device linearity in the heaviest seas and will be wrong for all but the largest scale factors.

The bottom curve is produced assuming a power limit of 90kW/m, 1.5 times the mean incident power, and some short term smoothing of the power output. The imposition of the power limit means that the assumption of linearity only goes badly wrong for scale factors below about 100.

The middle curve assumes a natural power limit per metre which will alter with scale factor to the power 2.5. The limit is .9 W/m at model scale, 90 kW/m when the scale factor is 100. The form of this limit attempts to take account non-linearity when the duck is small.

Scale factor	Diameter (m)	Width (m)	Displacement (tonnes)	Power in width (kW)
100	10	29	2630	1682
120	12	34.8	4545	2018
140	14	40.6	7217	2355
160	16	46.4	10770	2691
180	18	52.2	15340	3028
200	20	58	21040	3364

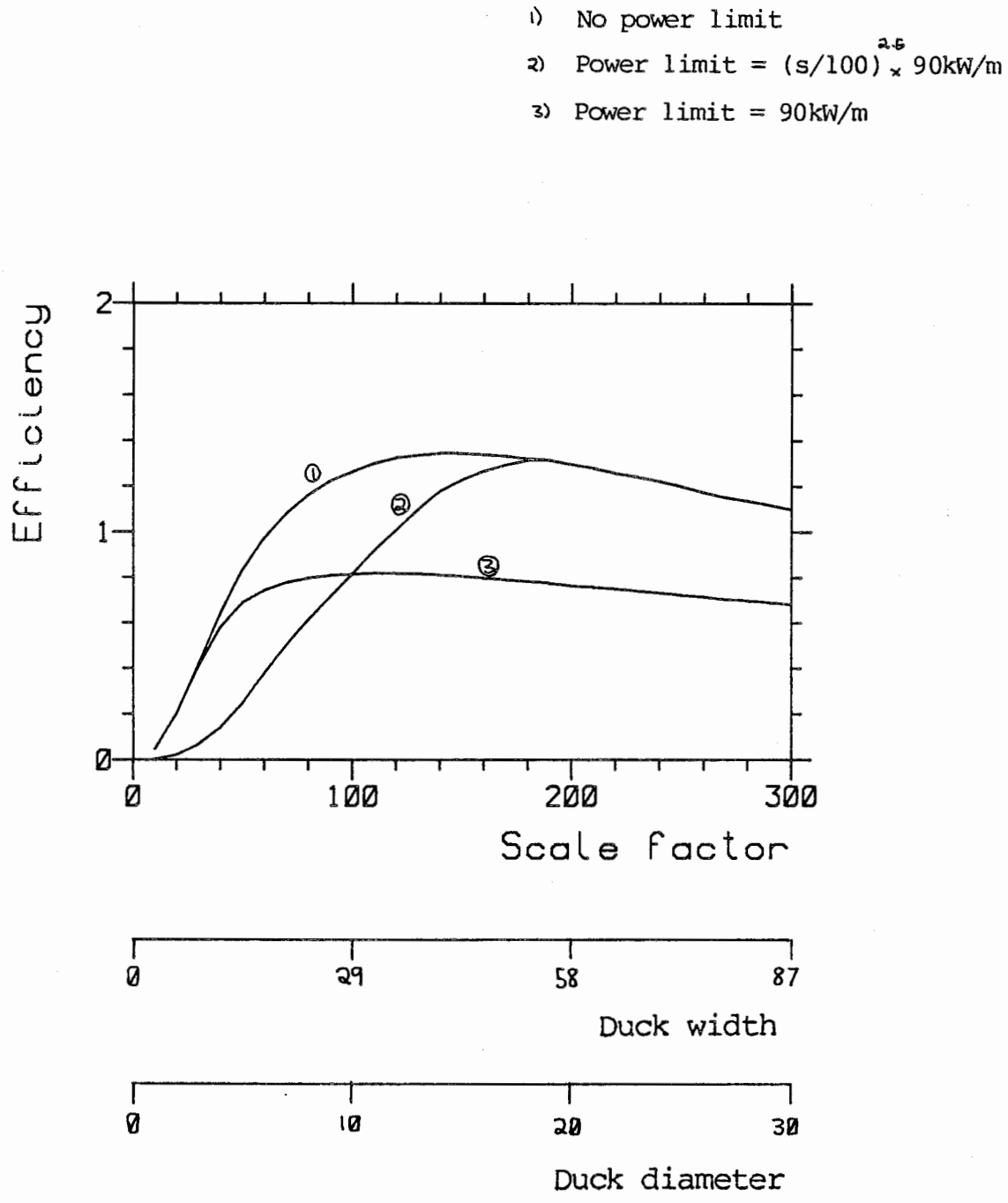

Figure 7.6 Power limited linear efficiency for the '46' set

8) Further work

The limitations of the present work are noted and suggestions made for further work, both theoretical and experimental.

Linearity

In all the experiments described care was taken to ensure the motion was linear, avoiding the question of when this assumption would break down. Unfortunately the 'linear region' is a rather nebulous area with no simply defined boundaries, although some general remarks can be made.

The reasons for departure from linearity divide into three groups; those due to the limits of the rig, the effects of the controller and those associated with the motion in the water.

The current rig has a limit to the force that can be delivered to each mode which is particularly easy to reach in surge. The main linkage translates displacements into rotations introducing a 1% departure from linearity when the motion amplitudes are around 20mm.

The controller can introduce non-linearities by making the duck motion unstable. By including some non-linear terms in the controller the duck system might be made more linear. For example, the hydrostatic spring in pitch is function of angle which could be negated in the controller.

In the presence of waves when the relative motion of the duck and water becomes large, non-linearities can be expected because of effects due to the geometry and viscous losses. The magnitude of the relative motion depends on the controller, being smaller when the duck is close to optimal power absorption and moving with the water. In regular waves the size of the motion is also a function of amplitude, whereas in mixed spectra large motions depend on the phasing of the fronts as well.

At low frequencies the predicted maximum efficiency is much less than the point absorber limit and the radiation resistance is larger than each of two predictions (see figures 6.1, 4.5, 4.6). Further work might establish how these discrepancies would scale.

Theoretical predictions

The radiation impedances can be obtained from hydrodynamic equations. Comparison between theoretical predictions and experimental determination would be a good starting point for the identification of non-linearities.

Duck shape

Only one duck shape was used in this set of experiments. The effects of changes in shape, particularly width and cross-sectional shape, are required if the best device is to be found.

Implementation of the controller

Deciding the best form of the controller required is straightforward in the frequency domain, but it must be implemented in the time domain with knowledge of the past only. The equation of motion could be written as a convolution integral and measurement of the duck response made by impulse methods. The most appropriate digital controller would then be found using the theory of z-transforms.

Scale changes

Some non-linear effects change with scale and could be identified by testing larger models, or by comparison with theoretical predictions. It is particularly important that the limits of scaling are understood if conclusions about full-scale performance are to be made from model tests.

Productivity analysis

The duck shape and the form of the controller can only be optimised if the cost constraints are known, along with the sea conditions where it is to operate. Towards this end a means of predicting performance, given the design of duck and controller and a set of test seas, is required.

Appendix A: List of symbols

a	Incident wave amplitude	$\underline{\underline{A}}$	Control matrix
b	Reflected wave amplitude	B	Buoyancy force
c	Total wave amplitude	C	
d	Distance	D	Damping factor
e		E	
f		F	Duck forces
g	Acceleration due to gravity	G	
h	Water depth	H	Hub depth
i		I	Moment of Inertia
j		J	
k	Wave number	K	
l	Water line length	L	
m	Rotating duck mass	M	Total duck mass
n		N	
o		O	
p		P	Mean power
q		$\underline{\underline{Q}}$	Velocity response matrix
$\underline{r}$	Position vector	$\underline{R}$	Radiation vector
s	Stern radius	S	Spring rate
t	Time	T	Sampling time
$\underline{u}$	Duck velocities	U	Upward force from rig
v		V	
w	Duck width	$\underline{W}$	Force coefficient vector
x	} Coordinates	$\underline{X}$	Duck displacement vector
y		Y	
z		$\underline{\underline{Z}}$	Radiation impedance matrix

α	Wave angle	ν	Frequency
β	Centre of mass angle	ρ	Density of water
γ	Mooring angle	$\underline{\underline{\sigma}}$	Hydrostatic spring matrix
δ	Kronecker delta	τ	Pitch torque
η	Efficiency	ϕ	Phase angle
θ	Pitch angle	ψ	Wave front
λ	Wavelength	ω	Angular frequency
$\underline{\underline{\mu}}$	Duck inertia matrix		

Appendix B: Derivation of the power equation

$$P = \frac{1}{T}\int_0^T \underline{F}(t).\underline{u}(t)\,dt$$

$$= \frac{1}{T}\int_0^T \frac{1}{2}\sum_{n=-\infty}^{\infty}\underline{F}(\omega_n)e^{i\omega_n t}\cdot\frac{1}{2}\sum_{m=-\infty}^{\infty}\underline{u}(\omega_m)e^{i\omega_m t}\,dt$$

$$= \frac{1}{4}\sum_{n=1}^{\infty}\sum_{m=1}^{\infty}\frac{1}{T}\int_0^T (\underline{F}(\omega_n)e^{i\omega_n t} + \underline{F}^*(\omega_n)e^{-i\omega_n t}).(\underline{u}(\omega_m)e^{i\omega_m t} + \underline{u}^*(\omega_m)e^{-i\omega_m t})\,dt$$

$$= \frac{1}{4}\sum_{n=1}^{\infty}\sum_{m=1}^{\infty}\frac{1}{T}\int_0^T \underline{F}(\omega_n).\underline{u}(\omega_m)e^{i(\omega_n+\omega_m)t} + \underline{F}^*(\omega_n).\underline{u}^*(\omega_m)e^{-i(\omega_n+\omega_m)t} + \underline{F}(\omega_n).\underline{u}^*(\omega_m)e^{i(\omega_n-\omega_m)t} + \underline{F}^*(\omega_n).\underline{u}(\omega_m)e^{-i(\omega_n-\omega_m)t}\,dt$$

$$= \frac{1}{4}\sum_{n=1}^{\infty}\sum_{m=1}^{\infty}\left(0 + 0 + \underline{F}(\omega_n).\underline{u}^*(\omega_m) + \underline{F}^*(\omega_n).\underline{u}(\omega_m)\right)\delta_{nm}$$

$$= \frac{1}{4}\sum_{n=1}^{\infty}\underline{F}(\omega_n).\underline{u}^*(\omega_n) + \underline{F}^*(\omega_n).\underline{u}(\omega_n)$$

Appendix C: Analytic maximisation of the extracted power

Recalling the equations of motion (1.7) and control (1.9)

$$\underline{F} = \underline{\underline{Z}}.\underline{u} + \underline{W}a \qquad [1.7]$$

$$\underline{F} = -\underline{\underline{A}}.\underline{u} \qquad [1.9]$$

With $\underline{\underline{A}} = \underline{\underline{B}} + i\underline{\underline{C}}$ $\qquad$ $\underline{\underline{B}}$, $\underline{\underline{C}}$ real

Rearranging (1.7) and (1.9)

$$(\underline{\underline{A}}+\underline{\underline{Z}}).\underline{u} = -\underline{W}a \qquad (9.1)$$

$$\underline{u} = -\underline{\underline{Q}}.\underline{W}a \qquad (9.2)$$

Where $\underline{\underline{Q}} = (\underline{\underline{A}}+\underline{\underline{Z}})^{-1}$ $\qquad$ (9.3)

Recalling the power equation (1.14)

$$4P = \underline{u}^{*}.\underline{F} + \underline{u}.\underline{F}^{*}$$

Substituting for $\underline{F}$ from (1.7) and rearranging

$$\rightarrow \quad 4P = \underline{u}^{*}.\underline{W}\,a + \underline{u}.\underline{W}^{*}a^{*} + \underline{u}^{*}.(\underline{\underline{Z}} + \underline{\underline{Z}}^{*T}).\underline{u} \qquad (9.4)$$

This equation will be differentiated with respect to the real and imaginary parts of the control matrix $\underline{\underline{A}}$. First the derivatives of $\underline{u}$, $\underline{u}^{*}$ are found. In suffix notation equation (9.1) becomes

$$-W_j a = (A_{jk} + Z_{jk})u_k$$

Differentiating with respect to $B_{\alpha\beta}$

$$0 = \delta_{j\alpha}\delta_{k\beta}u_k + (A_{jk} + Z_{jk})\frac{\partial}{\partial B_{\alpha\beta}}u_k$$

Multiplying by Q_{lj}

$$0 = Q_{lj}\delta_{j\alpha}u_\beta + Q_{lj}(A_{jk} + Z_{jk})\frac{\partial}{\partial B_{\alpha\beta}}u_k$$

Substituting for u_β from (9.2) and renaming suffices

$$\frac{\partial}{\partial B_{\alpha\beta}}u_j = Q_{j\alpha}Q_{\beta k}W_k a \qquad \text{and} \qquad \frac{\partial}{\partial B_{\alpha\beta}}u_j^{*} = Q_{j\alpha}^{*}Q_{\beta k}^{*}W_k^{*}a^{*} \qquad (9.5)$$

Similarly the derivatives with respect to $C_{\alpha\beta}$ are found

$$i\frac{\partial}{\partial C_{\alpha\beta}}u_j = Q_{j\alpha}Q_{\beta k}W_k a \qquad \text{and} \qquad i\frac{\partial}{\partial C_{\alpha\beta}}u_j^{*} = -Q_{j\alpha}^{*}Q_{\beta k}^{*}W_k^{*}a^{*} \qquad (9.6)$$

Rewriting (9.4) in suffix notation

$$4P = u_j^* W_j a + u_j W_j^* a^* + u_j^* (Z_{jk} + Z_{kj}^*) u_k$$

Differentiating with respect to $B_{\alpha\beta}$

$$\frac{\partial}{\partial B_{\alpha\beta}} 4P = \frac{\partial}{\partial B_{\alpha\beta}} u_j^* W_j a + \frac{\partial}{\partial B_{\alpha\beta}} u_j W_j^* a^* + \frac{\partial}{\partial B_{\alpha\beta}} u_j^* (Z_{jk} + Z_{kj}^*) u_k + u_j^* (Z_{jk} + Z_{kj}^*) \frac{\partial}{\partial B_{\alpha\beta}} u_k$$

$$= \frac{1}{2} \mathrm{Re}\{ \frac{\partial}{\partial B_{\alpha\beta}} u_j^* W_j a + \frac{\partial}{\partial B_{\alpha\beta}} u_j^* (Z_{jk} + Z_{kj}^*) u_k \}$$

Substituting for $\frac{\partial}{\partial B_{\alpha\beta}} u_j^*$ and u_j and rearranging

$$\frac{\partial}{\partial B_{\alpha\beta}} 2P = \mathrm{Re}\{ Q_{j\alpha}^* Q_{\beta l}^* W_l^* (\delta_{jm} - (Z_{jk} + Z_{kj}^*) Q_{km}) W_m \} |a|^2 \qquad (9.7)$$

Similarly

$$\frac{\partial}{\partial C_{\alpha\beta}} 2P = \mathrm{Im}\{ Q_{j\alpha}^* Q_{\beta l}^* W_l^* (\delta_{jm} - (Z_{jk} + Z_{kj}^*) Q_{km}) W_m \} |a|^2 \qquad (9.8)$$

Combining (9.7) and (9.8)

$$\frac{\partial}{\partial B_{\alpha\beta}} + i \frac{\partial}{\partial C_{\alpha\beta}} 2P = Q_{j\alpha}^* Q_{\beta l}^* W_l^* (\delta_{jm} - (Z_{jk} + Z_{kj}^*) Q_{km}) W_m |a|^2 \qquad (9.9)$$

Or $$\boxed{\mathcal{L}_{\alpha\beta} P = \tfrac{1}{2} (\underline{\underline{Q}}^* . \underline{W}^*)_\beta \, (\underline{\underline{Q}}^{*T} (\underline{\underline{I}} - (\underline{\underline{Z}} + \underline{\underline{Z}}^{*T}) . \underline{\underline{Q}}) . \underline{W})_\alpha \, |a|^2} \qquad (9.10)$$

Where $\underline{\underline{Q}} = (\underline{\underline{A}} + \underline{\underline{Z}})^{-1}$ and $\mathcal{L}_{\alpha\beta} = \frac{\partial}{\partial \mathrm{Re}\{A_{\alpha\beta}\}} + i \frac{\partial}{\partial \mathrm{Im}\{A_{\alpha\beta}\}}$

P is minimised, and the extraced power maximised, when the left hand side of equation (9.10) is zero. One control matrix which satisfies this condition for all $\underline{W}$ is found by setting

$$\underline{\underline{I}} = (\underline{\underline{Z}} + \underline{\underline{Z}}^{*T}) . (\underline{\underline{A}} + \underline{\underline{Z}})^{-1}$$

$$\rightarrow \quad \boxed{\underline{\underline{A}} = \underline{\underline{Z}}^{*T}} \qquad (9.11)$$

But $\underline{\underline{Z}}$ is symmetric, $\underline{\underline{Z}} = \underline{\underline{Z}}^T$, so by substitution into (9.1), etc.

$$\boxed{\begin{aligned} \underline{u} &= -\frac{1}{2} (\mathrm{Re}\{\underline{\underline{Z}}\})^{-1} . \underline{W} a \qquad (9.12) \\ F &= \frac{1}{2} \underline{\underline{Z}}^* . (\mathrm{Re}\{\underline{\underline{Z}}\})^{-1} . \underline{W} a \qquad (9.13) \\ P &= -\frac{1}{8} \underline{W}^* . (\mathrm{Re}\{\underline{\underline{Z}}\})^{-1} . \underline{W} \, |a|^2 \qquad (9.14) \end{aligned}}$$

Appendix D: Wave equations

Monochromatic formulae

$$c = \frac{\omega}{k} \qquad c_g = \frac{d\omega}{dk}$$

$$\omega^2 = gk \tanh(kh)$$

$$P(\omega) = \frac{\rho g^2 |a|^2}{4\omega} \tanh(kh)\left(1 + \frac{2kh}{\sinh(2kh)}\right) \qquad P_N(\omega) \text{ for unit amplitude}$$

$$\phi(\underline{r},t) = iac \frac{\cosh(k(z+h))}{\sinh(kh)} e^{i(\underline{k}.\underline{r} + \omega t)}$$

$$\underline{v} = \underline{\nabla}\phi \qquad \underline{r} = (x,y,z)$$

Spectra

Normalised energy distribution $S(\omega,\alpha)$

$$1 = \int_0^{2\pi}\int_0^{\infty} S(\omega,\alpha)\, d\omega\, d\alpha$$

$$T_e = \int_0^{2\pi}\int_0^{\infty} \frac{2\pi}{\omega} S(\omega,\alpha)\, d\omega\, d\alpha$$

$$\omega_e = \frac{2\pi}{T_e}$$

$$P = \int_0^{2\pi}\int_0^{\infty} P_N(\omega)\, S(\omega,\alpha)\, d\omega\, d\alpha \quad \times 2H_{rms}^2$$

$$= \frac{\rho g^2}{4\pi} H_{rms}^2 T_e \qquad \text{in deep water}$$

Separation of variables

Often the distribution can be split

$$S(\omega,\alpha) = S(\omega)\, \Theta(\omega,\alpha)$$

With $1 = \int_0^{\infty} S(\omega)\, d\omega$ and $1 = \int_0^{2\pi} \Theta(\omega,\alpha)\, d\alpha$

Pierson-Moskowitz spectra

$$\int_0^{\omega} S(\omega')\, d\omega' = e^{-\gamma(\omega_e/\omega)^4} \qquad \text{with } \gamma = .675$$

Angular spreading

COSA: $\Theta(\omega) = C_N \cos^{s}(\alpha - \alpha_o)$ where C_N is the appropriate normalisation constant

CSHA: $\Theta(\omega) = C_N \cos^{2s}(\alpha - \alpha_o)/2$

MITS: $\Theta(\omega, \alpha) = C_N \cos^{2s}(\alpha - \alpha_o)/2$ with $s = s_o (\omega/\omega_o)^{-2.5}$ for $\omega > \omega_o$

$s_o (\omega/\omega_o)^{5}$ for $\omega < \omega_o$

and $s_o = 15.85$

$\omega_o = \omega_e/1.137$

empirical constants

Normal PM

$$H_{mo} = .0136\, T_e^2$$

$T_e = .625\, U_{19.5}$ where $U_{19.5}$ is the wind speed measured 19.5m above the water

the constants are empirical

Compression factor

The spectrum of energy against period is compressed about T_e by transforming the period

$$t' = \frac{t - (1 - C_f)\, T_e}{C_f}$$

References

Budal, K. and Falnes, J.: Marine Science Communications 3, No. 2, (1977) 133-150

Crabbe, J.A.: Synthesis of a directional wave climate. 'Power from Sea Waves', Count, B. ed., Academic Press, London (1980) 41-74

Evans, D.V.: Journal Fluid Mechanics 77 (1976) 1-25

Evans, D.V.: Some theoretical aspects of three-dimensional wave-enrgy absorbers. Proc. 1st Symp. Ocean Wave Energy Utilisation, Gothenberg (1979)

Falnes, J.: Radiation impedance matrix and optimum power absorption for interacting oscillators in surface waves. Applied Ocean Research 2 (1980) 75-80

Nelder J.A. and Mead, R.: A simplex method for functional minimisation, Computer Journal 7 (1965) 308

Newman, J.N.: The interaction of staionary vessels with regular waves. Proc. 11th Symp Naval Hydrodynamics, London (1976) 491-501

Mei, C.C.: Power extraction from water waves. Journal of Ship Research 20 (1976) 63-66

Mollison, D.: Wave energy losses in intermediate depths. Applied Ocean Research 5 (1983) 234-237